




University of
Nottingham
UK | CHINA | MALAYSIA

Synthesis of Potential *Mycobacterium tuberculosis* InhA Inhibitors

Tabrez Ali Saleem
20304530

Supervised by Professor Neil Thomas
2020-2021

The Biodiscovery Institute
School of Chemistry
University of Nottingham

Signature: 

Date: 06/06/2023

Acknowledgements

Throughout my research, I have received a great deal of support and assistance from my colleagues and supervisor. I would like to thank Professor Neil Thomas for the formulation of the methodology and the guidance he had given me throughout my course. I would like to acknowledge Christopher Merrett and Liam Du Ross who have always been happy to help when I had problems during the lab. Finally, I would like to thank my family and friends for lending ears to listen to my problems and helping me find a way to overcome them.

Abbreviations and Acronyms

aq. – Aqueous

AG – Arabinogalactan

δ – Chemical shift

COSY – Correlation spectroscopy

J – Coupling constant

CoA – Coenzyme A

DMAP – *N,N*-dimethyl-4-aminopyridine

DMF – Dimethyl formamide

DMSO – Dimethyl sulfoxide

dt – Double triplet (NMR)

d – Deuterated solvent (NMR)

EDC·HCl – 1-(3-dimethylaminopropyl)-3-ethylcarbodiimide hydrochloride

XDR-TB – Extensively drug resistant tuberculosis

FAS-I – Fatty acid system I

FAS-II – Fatty acid system 2

GOLD – Generic Optimisation for Ligand Docking

Hz – Hertz

HPLC – High Performance Liquid Chromatography

IR – Infrared

MHz – MegaHertz

mDAP – *meso*-diaminopimelic acid

MOM – Methoxymethyl

MDR-TB – Multidrug resistant tuberculosis

m – Multiplet

mAGP – mycolyl-arabinogalactan-peptidoglycan

MurNAc – *N*-acetylmuramic acid

MurNGly – *N*-glycolylmuramic acid

NMR – Nuclear Magnetic Resonance

NAD⁺ – Nicotinamide adenine dinucleotide (oxidised form)

NADH – Nicotinamide adenine dinucleotide (reduced form)

ppm – Parts per million

PG – Peptidoglycan

PDB – Protein Database

s – Singlet

TLC – Thin Layer Chromatography

t – Triplet

TDM – Trehalose 6,6'-dimycolate

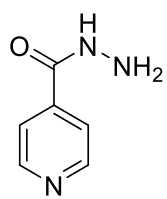
TMM - Trehalose-6-monomycolate

WHO – World Health Organisation

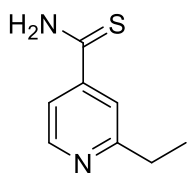
Abstract

Tuberculosis caused by *Mycobacterium tuberculosis* is an infectious disease that predominately affects the lungs. *Mycobacterium tuberculosis* can be prevented or treated by many anti-tuberculosis drugs. Isoniazid **1** is a prodrug that is used in the treatment against *Mycobacterium tuberculosis* and for isoniazid **1** to become potent it requires to be activated by KatG prior to forming the isoniazid-NAD⁺ adduct. However, mutations within the KatG peroxidase results in the resistance of the major anti-tuberculosis drugs, isoniazid **1** and ethionamide **7**.

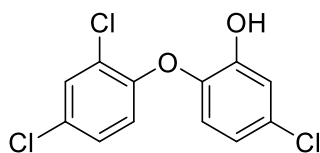
2-*Trans*-enoyl-acyl carrier protein reductase, InhA, plays a key role in the synthesis of long fatty acid chains. The fatty acid chains are not found within other bacteria or mammals which makes it a key aspect for potential anti-tuberculosis drugs. Triclosan **11** has shown unique InhA inhibition as two molecules of triclosan bind to InhA without the need of activation by KatG. A library of new triclosan derivatives were synthesised and the *in silico* docking of the proposed products into InhA was completed with the GOLD docking program. The binding affinity of the proposed compounds and InhA was calculated using the GOLD fitness score. The score indicated that [5-(((2,4-dichlorobenzyl)oxy)methyl)-2-phenoxyphenol] **51** had the lowest binding affinity of 77.18 kcal/mol and [5-(((4-(cyclopropylmethoxy)benzyl)oxy)methyl)-2-phenoxyphenol] **52** having the greatest binding affinity of 86.79 kcal/mol, the binding affinity of the designed products correlate to the potential protein-ligand bond energies with **51** having the weakest bond energies and **52** having strong bond energies. GOLD docking also portrayed successful InhA docking potential with 4-(trifluoromethyl)benzyl **48** and 4-bromobenzyl **50** groups which resulted in the preparation and synthesis of the compounds.



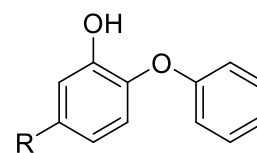
1



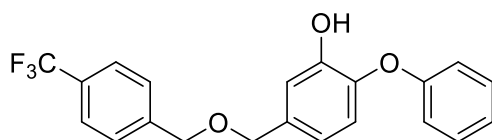
6



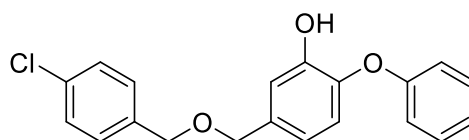
11



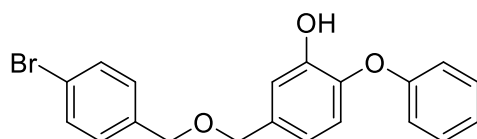
Triclosan Core



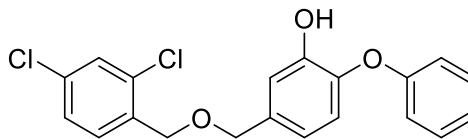
48



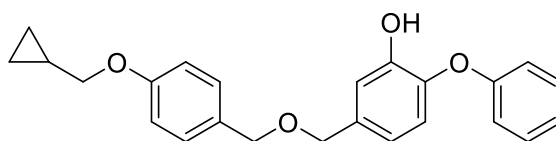
49



50



51



52

Table of Contents

Acknowledgements.....	1
Abbreviations and Acronyms.....	2
Abstract.....	4
Chapter 1: Introduction.....	9
1.1 – Significance of study.....	9
1.2– Tuberculosis.....	10
<i>1.2.1 – What is tuberculosis?</i>	<i>10</i>
<i>1.2.2 – Mycobacterium tuberculosis</i>	<i>11</i>
<i>1.2.3 – Bovine tuberculosis</i>	<i>12</i>
<i>1.2.4 – Active vs Latent tuberculosis</i>	<i>12</i>
<i>1.2.5 – Pulmonary tuberculosis and Extrapulmonary tuberculosis.....</i>	<i>13</i>
<i>1.2.6 – Multidrug-resistant and Extensively drug-resistant tuberculosis</i>	<i>13</i>
1.3 – Mycobacteria.....	14
<i>1.3.1 – Mycobacterium Structure</i>	<i>14</i>
<i>1.3.2 – Peptidoglycan.....</i>	<i>15</i>
<i>1.3.3 – Arabinogalactan.....</i>	<i>16</i>
<i>1.3.4 – Mycolic Acids.....</i>	<i>17</i>
<i>1.3.5 – Mycolic Acid Biosynthesis.....</i>	<i>19</i>
1.4 – Targets and Treatment of Tuberculosis.....	22
<i>1.4.1 – Current treatment for tuberculosis</i>	<i>22</i>
<i>1.4.2 – Drug Targets of Anti-tuberculosis Drugs</i>	<i>22</i>

1.4.3 – Mechanism of Action for Isoniazid	23
1.4.4 – Mutations in <i>InhA</i> and <i>katG</i>	25
1.4.5 – Other inhibitors of <i>InhA</i>	27
1.5 – Design of triclosan derivatives	32
1.5.1 – Di-triclosan Compounds	32
1.5.2 – Design and docking of triclosan analogues	35
1.6 – Aims and objectives	36
1.6.1 – Aims	36
1.6.2 – Objectives	36
Chapter 2: Results and Discussions	37
2.1 – Discussion	37
2.1.1 – Docking and synthesis of triclosan analogues	37
2.1.2 – Synthesis of Scaffold	41
2.1.3- Synthesis of R group – 4-(cyclopropylmethoxy)benzyl chloride	44
2.1.4 – Synthesis of Final Products	46
2.2 – Future Work	48
Chapter 3: Experimental	51
3.1- Chemicals and General procedures	51
3.1.1 – Chemicals and Analytical techniques	51
3.1.2 – General Procedure A: Ether synthesis	52
3.1.3 – General Procedure B: Methoxy methyl ether deprotection	52
3.2 – Synthetic pathway for (3-(methoxymethoxy)-4-phenoxyphenyl)methanol, 32	53

3.3 – Synthetic pathways of R Group	56
3.4 – R Group Coupling to (3-(methoxymethoxy)-4-phenoxyphenyl)methanol, 33	58
3.5 – MOMCl Deprotection	61
References.....	64
Appendix	69
Spectroscopic Data:	69
<i>IR Data:</i>	90

Chapter 1: Introduction

1.1 – Significance of study

Tuberculosis is a bacterial disease of mammals primarily caused by a bacterium called *Mycobacterium tuberculosis*. The bacterium causes many symptoms within humans with the most prevailing symptoms being breathlessness and chest pains. Tuberculosis is also documented to attack bones and cause skeletal deformities.¹

According to the World Health Organisation (WHO) an estimated 10 million people were infected and fell ill with tuberculosis in 2019 with a total of 1.4 million deaths within that year.² Around 14.5% of the tuberculosis deaths in 2019 were the result of HIV coinfection with tuberculosis.² However, deaths caused by tuberculosis are seen to be on a steady decline with about 2% each year and 9% reduction between 2015 to 2019.² Even with this steady decline in deaths per year, tuberculosis is seen as an important threat to future human health due to an increasing prevalence of multidrug resistant (MDR-TB) and extremely drug resistant (XDR-TB) forms. MDR-TB is classified as being resistant towards two or more first-line anti-tuberculosis drugs whilst XDR-TB is defined as resistant to two or more first-line drugs including isoniazid **1**, rifampicin **2**, pyrazinamide **3**, and ethambutol **4**, as well as one or more injectable second-line drugs, such as amikacin **5**, and fluoroquinolone, such as ciprofloxacin **6** (**Figure 1**).³

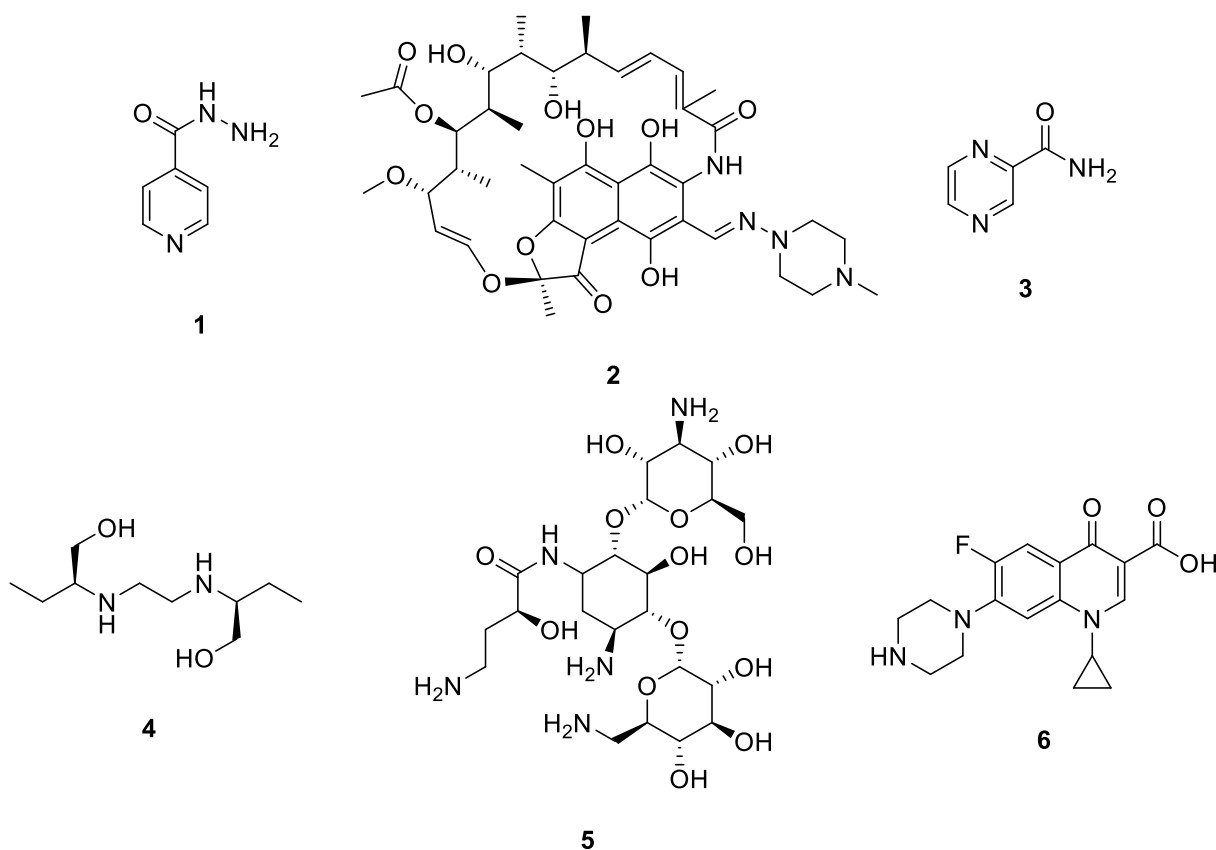


Figure 1: Chemical structure of the first line drugs; Isoniazid **1**, Rifampicin **2**, Pyrazinamide **3**, and Ethambutol **4**. As well as the chemical structure of Amikacin **5** a second-line drug and Ciprofloxacin **6** a fluoroquinolone.

1.2– Tuberculosis

1.2.1 – What is tuberculosis?

First identified as ‘phthisis’, tuberculosis is a bacterium-based infection that is passed through the air from one person to another through droplets. Infection occurs when a person inhales a droplet containing tubercle bacilli.⁴ Once inhaled, the tubercle bacillus develops and multiplies exponentially causing pulmonary tuberculosis disease or extrapulmonary tuberculosis disease.⁵ On the other hand, when the macrophages ingest the tubercle bacilli and they are potent enough to form a granuloma to contain the bacilli, the tubercle bacilli are unable to multiply. Once this occurs the bacterium is either ingested and decomposed with no infection, or the tubercle bacilli become inactive and are viable for future activation which is commonly known as latent tuberculosis infection.⁶

The risk of developing tuberculosis disease increases the weaker the immune system, this is a major factor for coinfection for tuberculosis. The coinfection between *Mycobacterium tuberculosis* and HIV is the strongest known factor for the progression of tuberculosis disease. As HIV infection is directly related to the death of many CD4+ T cells, the potency of the immune response of the host is decreased.⁷ As the immune response to *Mycobacterium tuberculosis* is controlled by T lymphocytes, a decline in the immune response results in a greater infection rate of active tuberculosis.⁸ The coinfection of COVID-19 and *Mycobacterium tuberculosis* has also been seen in a few clinical cases. COVID-19 is an infectious disease that causes respiratory illnesses, and the coinfection was shown to accelerate the progression of both *Mycobacterium tuberculosis* and COVID-19 infection resulting in the death of the patients.^{9, 10} The effects of COVID-19 to *Mycobacterium tuberculosis* are still unknown due to both positive and negative evidence for the coinfection being obtained.^{9, 10}

1.2.2 – *Mycobacterium tuberculosis*

Mycobacterium tuberculosis is an aerobic pathogenic bacterial species in the genus *Mycobacterium* and the causative agent of tuberculosis disease. *Mycobacterium tuberculosis* has an unusually high content of lipids and mycolic acids within their cell wall which makes *Mycobacterium* impervious to common bacteriological staining. As *Mycobacterium tuberculosis* does not retain any Gram staining, Ziehl-Neelsen or acid-fast stains are used.¹¹ Therefore, *Mycobacterium* is classed as an acid-fast Gram-positive bacteria due to the lack of an outer cell membrane.¹¹

In humans, the most common types of mycobacterial disease include both *Mycobacterium tuberculosis* and *Mycobacterium leprae*, causing tuberculosis and leprosy respectively.¹² Some mycobacteria are identified as saprophytes; these mycobacteria live on decaying organic matter. Whereas, other mycobacteria are obligate parasites resulting in a species that is unable to reproduce outside a host.¹² *Mycobacterium tuberculosis* and *Mycobacterium bovis* are some of the major obligate parasites known to cause major diseases to humans and cattle.¹³⁻¹⁵

1.2.3 – Bovine tuberculosis

Bovine tuberculosis is an infectious disease which is caused by *Mycobacterium bovis*. First indicated as a cattle independent disease, bovine tuberculosis has provided evidence to be transmitted between species, often from animals to humans.¹⁶ *Mycobacterium bovis* is a member of the *Mycobacterium tuberculosis complex* and the causative agent of bovine tuberculosis in cattle. Transmission of *Mycobacterium bovis* can generally occur due to the consumption of contaminated dairy products.¹⁷ When *Mycobacterium bovis* passes through the species barrier the symptoms are seen like those who are infected with *Mycobacterium tuberculosis*.¹⁸ However, *Mycobacterium bovis* can be differentiated, in clinical settings, using biochemical or genetic tests. Many clinical trials and tests have estimated that 5 – 10% of global tuberculosis may be due to *Mycobacterium bovis* with many cases resulting in extrapulmonary infection.^{19, 20}

Mycobacterium bovis is intrinsically resistant to pyrazinamide and drug-resistant strains of *Mycobacterium tuberculosis* which resulted in the preparation of vaccines.²¹ The *Mycobacterium bovis* bacillus Calmette-Guerin (BCG) vaccine has been widely used for the control of bovis tuberculosis. In cattle, *Mycobacterium bovis* BCG has provided many successful tests with various degrees of protection towards *Mycobacterium bovis*. However, *Mycobacterium bovis* BCG interferes with the detection of tuberculosis by the means of a tuberculosis skin test.²² *Mycobacterium bovis* BCG is also undertaking many clinical tests for many immunotherapies of cancer due to its potential antitumour behaviour.^{23, 24}

1.2.4 – Active vs Latent tuberculosis

Mycobacterium tuberculosis infected individuals are classified as either having active tuberculosis or latent tuberculosis. Tuberculosis disease becomes active when the immune response of the host cannot stop the replication and the growth of *Mycobacterium tuberculosis*. When *Mycobacterium*

tuberculosis is actively multiplying within the lungs and spreads to the other parts of the body, many clinical symptoms are observed.²⁵ With the initial replication and growth of primary *Mycobacterium tuberculosis* causing active tuberculosis disease, latent tuberculosis infection can also progress into active tuberculosis disease.

1.2.5 – Pulmonary tuberculosis and Extrapulmonary tuberculosis

Active tuberculosis is split into two clinical manifestations which are pulmonary tuberculosis and extrapulmonary tuberculosis. Pulmonary tuberculosis refers to tuberculosis disease within the lungs, whereas extrapulmonary tuberculosis refers to the disease involving organs other than the lungs. Extrapulmonary tuberculosis includes many organs resulting in a range of tuberculosis sites such as skeletal tuberculosis (Pott's disease), genitourinary tuberculosis, abdominal tuberculosis, lymphadenitis, pleuritis and meningitis.²⁶

Pulmonary tuberculosis is stated as the only form of infection of tuberculosis that can be transmitted.²⁷ So when a person is infected with *Mycobacterium tuberculosis* and both pulmonary and extrapulmonary tuberculosis sites are affected, this is known as miliary tuberculosis. Miliary tuberculosis enters the category of pulmonary tuberculosis as the disease can be spread.^{27, 28}

1.2.6 – Multidrug-resistant and Extensively drug-resistant tuberculosis

When *Mycobacterium tuberculosis* becomes resistant to isoniazid **1**, the mutation in *Mycobacterium tuberculosis* can result in resistance towards many other first-line anti-tubercular drugs causing MDR-TB.^{2, 3, 29} Isoniazid **1** is seen to attack the biosynthetic pathway of mycolic acids within mycobacteria and the mutations within the mycobacteria would cause resistance to isoniazid **1**. This mutation would also cause cross-resistance with other anti-tuberculosis drugs such as ethionamide **7** (**Figure 2**). Ethionamide **7** is another major anti-tuberculosis drug that inhibits the biosynthetic pathway of

mycolic acids within mycobacteria.^{2, 3, 29, 30} Second-line injectable drugs such as amikacin **5** (**Figure 2**) are used in the treatment of MDR-TB, however in the rare case in which MDR-TB *Mycobacterium tuberculosis* become resistance to the injectable second line drug or fluoroquinolone such as ciprofloxacin **6** (**Figure 2**) this is known as XDR-TB.

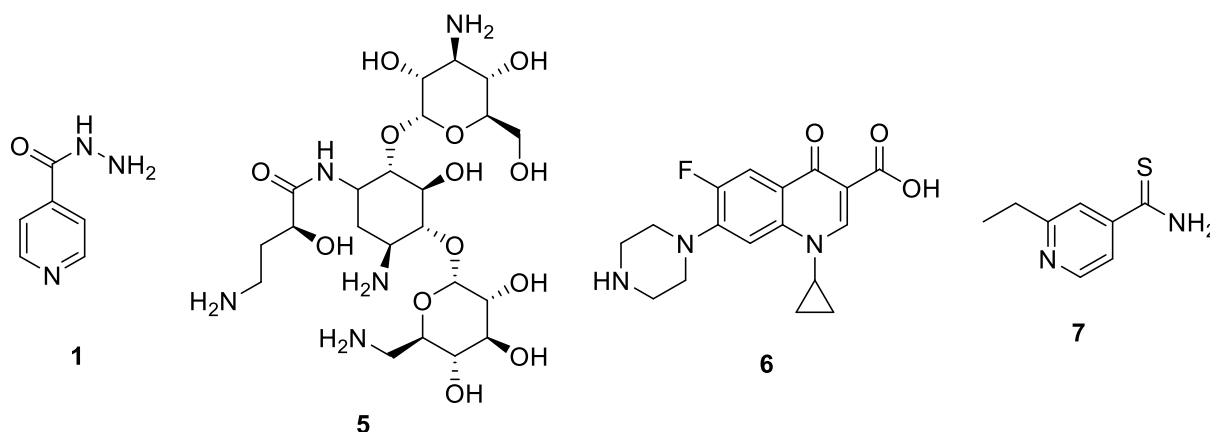


Figure 2: Chemical structure of the major anti-tuberculosis drugs that *Mycobacterium tuberculosis* has shown resistance to; Isoniazid **1**, Amikacin **5**, Ciprofloxacin **6** and Ethionamide **7**

1.3 – Mycobacteria

1.3.1 – Mycobacterium Structure

Mycobacteria are GC rich, rod-shaped bacilli that are termed acid-fast Gram-positive prokaryotes due to their ability to retain the colour of a stain after an acid wash and the lack of the outer membrane.³¹ The high lipid and mycolic acid content within the mycobacterial cell wall makes it unique when compared to other prokaryotes.¹¹

The complex cell wall (**Figure 3**) is composed of three distinctive layers; cross-linked polymers of peptidoglycan, highly branched arabinogalactan polysaccharide and long-chain mycolic acids. These components of the cell wall are vital for the support and growth of the bacterium which also provides a dense barrier to antibiotics.^{32, 33} The lipid and carbohydrate layers not only act as a permeability barrier but these layers also act important roles in survival and pathogenesis.³³

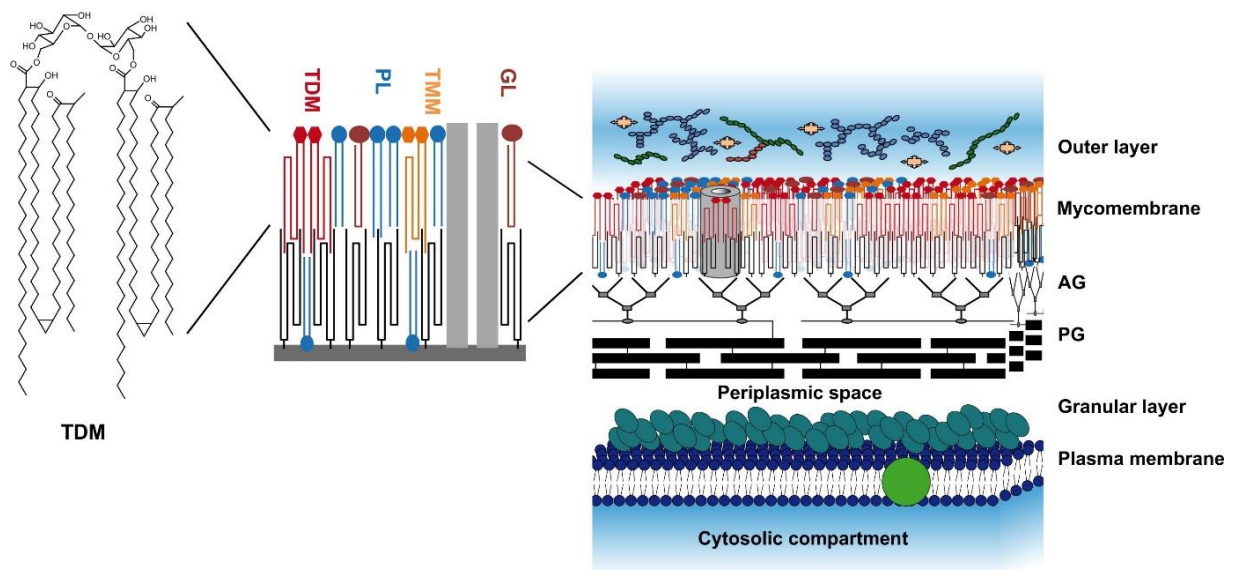


Figure 3: Model of the mycobacterial cell wall showing the distinctive layers of the cell wall identifying the key aspects that make it unique from other prokaryotic cell walls.³⁴

The mycolyl-arabinogalactan-peptidoglycan (mAGP) complex is essential for *Mycobacterium tuberculosis* survival and also providing a stable and robust structure to support the mycomembrane.¹¹

The inner leaflet between both mAGP and the mycomembrane is composed of free lipids such as trehalose 6,6'-dimycolate (TDM), trehalose-6-monomycolate (TMM), glycolipids and phospholipids.³⁴⁻

³⁶ The granular layer, located between the plasma membrane and the mAGP complex, is composed of penicillin-binding proteins, lipoproteins and lipoteichoic acids.^{34, 37}

1.3.2 – Peptidoglycan

The bacterial cell is surrounded by a rigid cell wall containing peptidoglycan. As a crucial structural component, peptidoglycan provides structural strength and counteracts the osmotic pressure of the cytoplasm.³³ Peptidoglycan is a heteropolymer made of long chains of glycan strands that are crosslinked with short peptide bridges. The glycan strands are composed of *N*-acetylglucosamine (GlcNAc) and *N*-acetylmuramic acid (MurNAc) residues linked by β -1,4 glycosidic bonds (**Figure 4**).^{11, 38}

Adjacent glycan strands are cross-linked *via* short peptide bridges with the sequence L-alanyl- γ -D-isoglutamyl-*meso*-diaminopimelate-D-alanyl-D-alanine linking to D-lactoyl of each MurNAc residue.³⁹

Adjacent glycan strands within the peptide are cross-linked between D-Ala and *meso*-diaminopimelic acid (mDAP).³⁸⁻⁴⁰

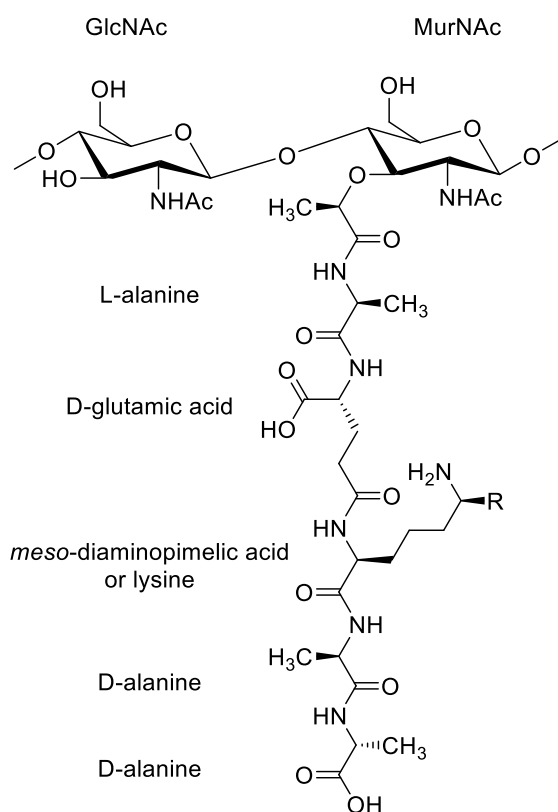


Figure 4: Representation of a monomer unit of peptidoglycan showing the β -1,4 glycosidic bond between N-acetylglucosamine (GlcNAc) and N-acetylmuramic acid (MurNAc) residues.

1.3.3 – Arabinogalactan

Situated above the peptidoglycan layer, to which it is covalently bonded, is the arabinogalactan layer (**Figure 3**). Providing major structural support, arabinogalactan is a branched polysaccharide composed of both galactose and arabinose in furanoid form.³⁷ In many mycobacterial species, including *Mycobacterium tuberculosis*, an approximate of 10% MurNAc residues within the peptidoglycan layer are covalently bonded to arabinogalactan via α -l-rhamnopyranose-(1 \rightarrow 3)- α -d-GlcNAc-(1 \rightarrow P) linker unit.^{37, 41} The main body of the arabinogalactan layer is composed of β -D-galactofuranose residue with alternating β (1 \rightarrow 5) and β (1 \rightarrow 6) linkages.⁴² Arabinofuranose residues are linked to the galactofuranose residues forming branches. The initial connection of arabinofuranose to the main body is formed *via* α (1 \rightarrow 5) linkages. Furthermore, the branch is extended with more

arabinofuranose residues connected with $\alpha(1\rightarrow5)$ and $\alpha(1\rightarrow3)$ linkages.⁴² The terminating ends and penultimate residues of arabinofuranose are classed as the anchoring points for the mycolic acids.⁴³

1.3.4 – Mycolic Acids

The cell envelope of *Mycobacterium tuberculosis* is a lipid-rich bilayer composed of mycolic acids, glycolipids, and phospholipids (**Figure 3**). Mycolic acids are major constituents of the lipid bilayer providing both structural support and selective permeability.³⁴ Specifically, within *Mycobacterium tuberculosis* the mycolic acid contributes towards the protection of the tubercle bacillus from oxidative stress, obtained by the cyclopropyl rings, making the bacterium less susceptible to antibiotics.^{44, 45} Mainly found attached covalently to peptidoglycan-arabinogalactan complex, mycolic acids have constituents on the outermost layer of the lipid bilayer including trehalose 6,6'-dimycolate (TDM), trehalose-6-monomycolate (TMM), glucose monomycolate, glycerol monomycolate and free mycolic acids (**Figure 3**).^{34, 45-47} These mycolic acids have unique properties that make the mycobacteria more resistant to chemical damage and dehydration. They also limit the effectiveness of hydrophilic antibiotics and biocides.^{34, 45-47}

Mycolic acids are composed of long β -hydroxylated strands with shorter α -alkyl sidechains.⁴⁸ In *Mycobacterium tuberculosis*, the mycolic acids are characterized with hydrophobic fatty acids (merochain) (C_{54} to C_{63}) and α -side chains (C_{22} to C_{24}) (**Figure 5**).⁴⁹ With this characterization, three distinct structure classes are found within *Mycobacterium tuberculosis* which are alpha-, methoxy- and keto mycolic acids (**Figure 5**).^{34, 50} The most abundant form of mycolic acids are α -mycolic acids, these are calculated to be approximately 70% of all mycolic acids residues whereas keto- and methoxy-mycolic acids are the minor components contributing to 10 to 15% of the lipid bilayer.^{44, 49} There are many structural differences seen between the mycolic acid residues such as the length and functional groups, these are dependent on the lipid homeostasis of the membrane and its ability to adjust the lipid composition.^{34, 44} The main difference in mycolic acids found within *Mycobacterium tuberculosis*

is the length of the mycolic acid chains. The oxygenated mycolic acids, methoxy- and keto-mycolic acids contain four to eight carbons more with specified functional groups located on the merochain distal section when compared to α -mycolic acids cyclopropyl group.³⁴

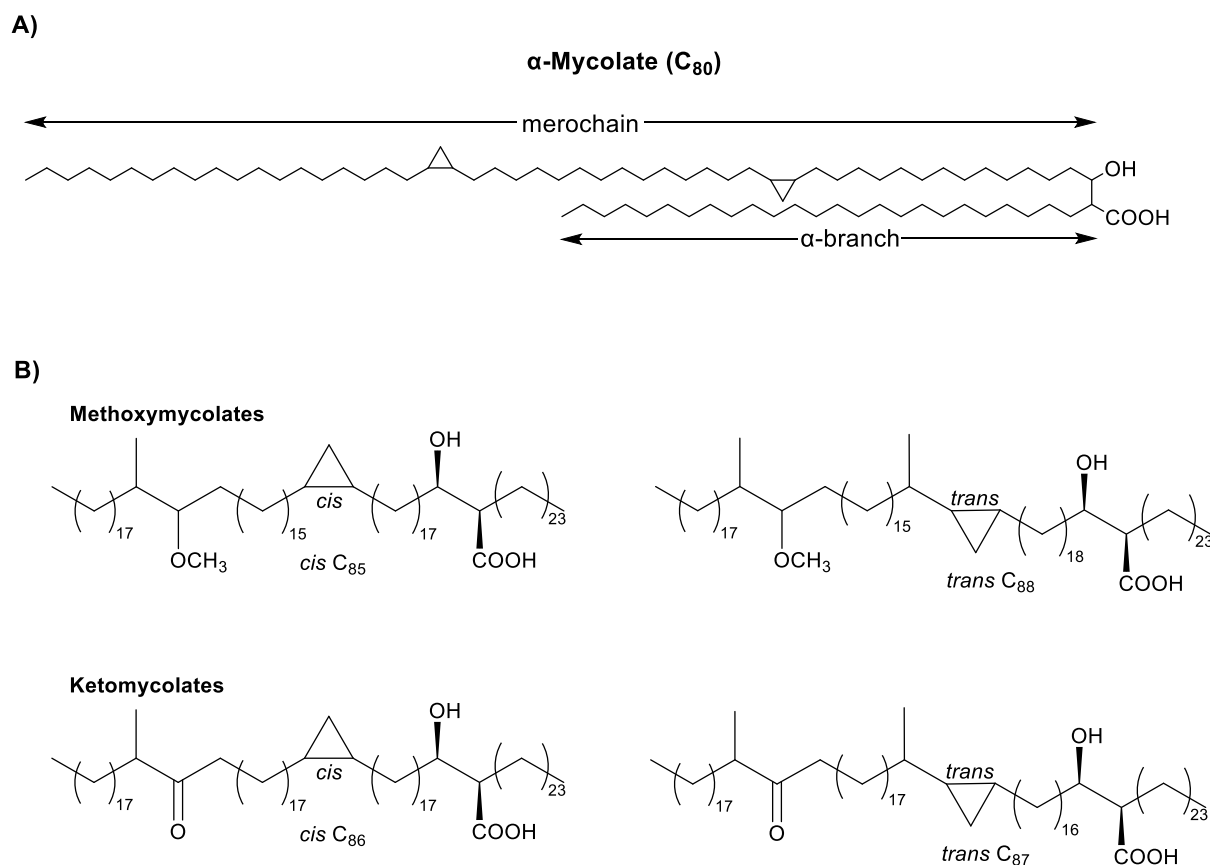


Figure 5: Chemical representation of **A)** α -mycolic acid, and **B)** *cis/trans* methoxy-mycolic acids and *cis/trans* keto-mycolic acids.

The most predominant mycolic acid, α -mycolic acid is a *cis,cis*-dicyclopropyl fatty acid with both cyclopropyl constituents in the *cis* configuration located on the merochain of the mycolic acid. Whereas, both methoxy-mycolic acid and keto-mycolic acid have singular cyclopropyl rings on the proximal region of the merochain either in the *cis*-configuration or *trans*-configuration (**Figure 5**). The proximal section of the merochain is responsible for the functionality of the mycolic acid which also affects the cell wall viscosity.⁵¹ The oxygenated mycolic acids have a *trans* configuration on the proximal cyclopropyl ring or *trans* configurations with unsaturation's within this part of the mycolate chain which in return increases the rigidity of the meromycolate chain.⁵¹

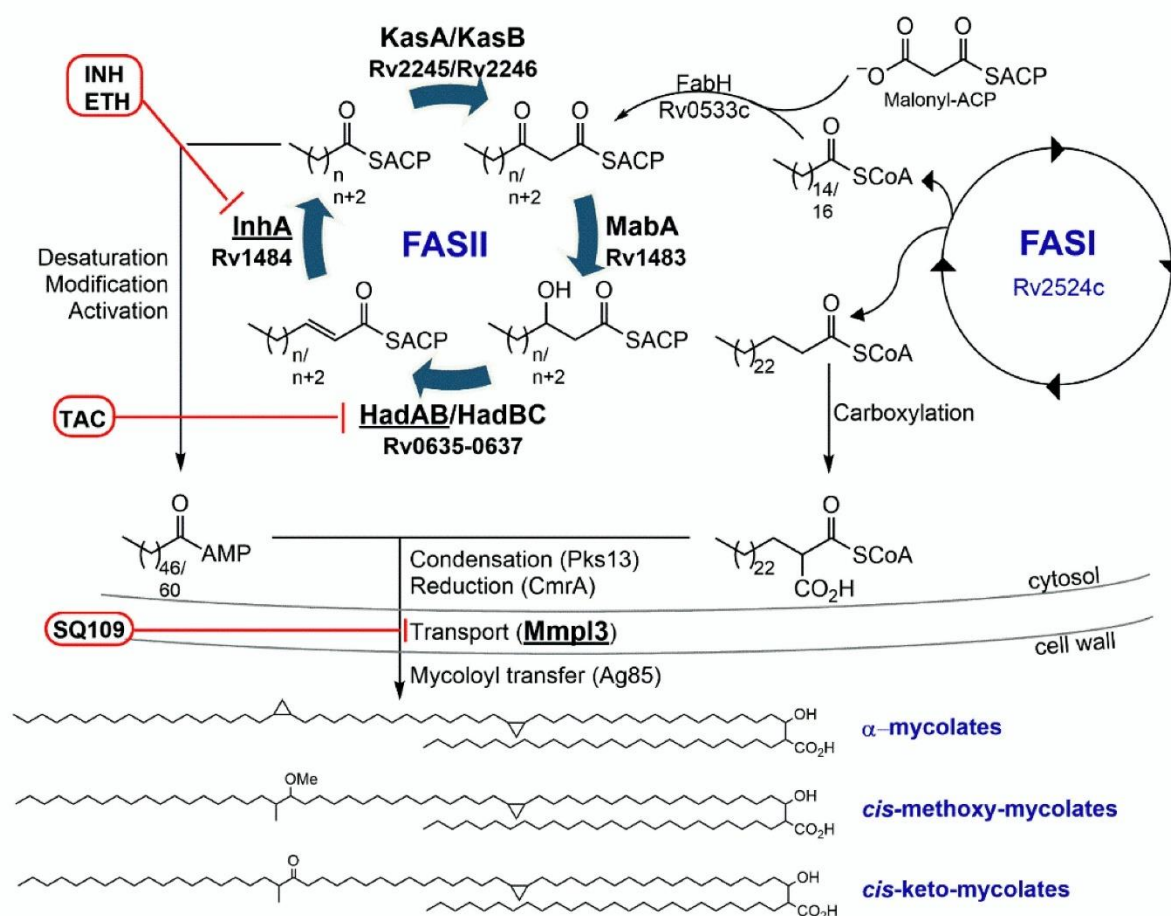
The distal section of the mycolate chain is the key to the interaction of mycolic acids with extractable lipids.⁵¹ Since keto-mycolic acid and methoxy-mycolic acid have *cis* configurations with the oxygen functions on the distal section of the merochain, this disrupts the tight local packaging of the mycolic acid chains. This allows the extractable lipids to enter the inner leaflet in which the extractable lipids associate with the arabinogalactan-linked mycolates.^{44, 51} However, a *cis*-cyclopropyl group in the distal region of the merochain is a highly resistant mycobacterium against hydrogen peroxide.^{44, 45, 51} In addition, the interaction of peripheral cell surface molecules is promoted by the oxygenated molecules, mainly keto-mycolates, as they are very active hydrogen bond acceptors.^{52, 53}

1.3.5 – Mycolic Acid Biosynthesis

The survival of *Mycobacterium tuberculosis* is reliant upon the almost impermeable mycolic acid lipid bilayer. As a vital part for the survival of *Mycobacterium tuberculosis*, the mycolic acid biosynthetic pathway was researched for the synthesis of potential anti-tuberculosis drugs.

The biosynthetic pathway of mycolic acid starts with fatty acid synthase type I (FAS-I) that results in the elongation of the fatty acid alkyl chain, with the assistance of coenzyme A (CoA) derivatives.^{34, 44} FAS-I elongation corresponds to the α -branch within the mycolic acid chain. Fatty acid synthase type II (FAS-II) is responsible for the further elongation of the fatty acids at the base of the merochain. The products synthesised by FAS-I and FAS-II are the substrates used for a Claisen condensation reaction to yield a mycolic acid (**Scheme 1**).^{34, 44}

Scheme 1: Process of the biosynthesis of mycobacterial mycolic acids



FAS I system and FAS II system are type I and type II fatty acid synthases responsible for the elongation of the mycolates.^{34, 54}

The mycobacterial FAS-I system consists of a single coding gene (Rv2524c) with the synthetic cycle consisting of seven domains that correspond to the catalytic activities of the synthetic pathway.^{34, 51} The domains are organized in a specific order: acyltransferase, enoyl reductase, dehydratase, malonyl/palmitoyl transferase, acyl carrier protein, ketoacyl reductase, and ketoacyl synthase with the intermediated synthesised remaining enzyme bound.⁵¹ Within the slow-growing *Mycobacterium tuberculosis*, FAS-I catalyses the synthesis of C₁₆-C₁₈ acyl-CoAs from acetyl-CoA with malonyl-CoA as an extender unit. This can be re-entered into the FAS-I system in which the alkyl chain is further elongated to C₂₄-C₂₆ acyl-CoA.^{34, 51} The C₂₄-C₂₆ CoA is then carboxylated producing the α-branch of the mycolic acid (**Scheme 1**).

FAS-I and FAS-II systems are connected by the enzyme β -ketoacyl-ACP synthase III (FabH, Rv0533) which catalyses the reaction between malonyl-ACP with the FAS-I product (C_{16} - C_{18} acyl-CoA) producing β -ketoacyl-ACP at the start of the FAS-II system. β -ketoacyl-ACP is then reduced by the NADPH dependant β -ketoacyl-ACP reductase (MabA, Rv1483) producing a β -hydroxyacyl-ACP intermediate which is dehydrated by HadAB and HadBC, Rv0635-Rv0636 and Rv636-Rv637 respectively, producing *trans*-2-enoyl-ACP.³⁴ The *trans*-2-enoyl-ACP is then reduced by the NADH-dependant reductase enzyme (InhA, Rv1484) in which produces an acyl-ACP (**Scheme 1**).³⁴ If the fatty acid chain is not the desired length for the merochain of the mycolic acid the acyl-ACP can be further elongated by the β -ketoacyl-ACP synthase (KasA or KasB, Rv2245 or Rv2246) in return re-enters the FAS-II system.³⁴ When the FAS-II system synthesises the desired length of the acyl-ACP chain, the chain undergoes further modifications in which unsaturation and functional groups are added to the chain producing the different merochains (alpha-, methoxy- and keto-).³⁴ It is shown that for α -mycolic acids the coding gene PcaA encodes the formation of the proximal *cis*-cyclopropane ring and MmaA2 encodes for the distal cyclopropyl ring with CmaA1, CmaA2, MmaA2 and PcaA used for catalysing the reactions.^{34, 51, 54, 55}

After the formation of products from the FAS-I system and the FAS-II system, the products undertake a Claisen condensation reaction. In the Claisen condensation, a carbon-carbon bond is formed between the activated meromycolic chain, the activated FAS-II product catalysed by the FaD32 gene, and the α -branch (FAS-I product).³⁴ Catalysed by the Pks13 gene, the Claisen condensation reaction between the two products produce a mycolic β -ketoester which is reacted with a trehalose sugar. The product is then reduced producing trehalose monomycolate (TMM).³⁴ TMM is transported through the plasma membrane via the transporter gene MmpL3. TMM can either be transferred to arabinogalactan initiating the formation of mAGP or TMM can be used in the formation of the outer membrane trehalose-6,6'-dimycolate (TDM) which protects the bacilli from the immune response by reducing antibiotic effectiveness (**Scheme 1**).^{34, 54}

1.4 – Targets and Treatment of Tuberculosis

1.4.1 – Current treatment for tuberculosis

Current treatment for *Mycobacterium tuberculosis* consists of isoniazid **1** in combination with other anti-tuberculosis drugs, due to *Mycobacterium tuberculosis* gaining resistance to the individual drugs. The drugs commonly used in combination with isoniazid **1** are rifampicin **2**, pyrazinamide **3**, and/or ethambutol **4**.⁵⁶ However, when *Mycobacterium tuberculosis* becomes resistant to the first-line drugs many second-line drugs are used, even though second-line drugs have adverse side effects.^{3, 57}

1.4.2 – Drug Targets of Anti-tuberculosis Drugs

InhA is an enoyl-ACP reductase that is a key component for the preparation of the meromycolate chain for mycolic acids in return is an essential step for the elongation cycle of the FAS-II system.^{34, 44, 51} The enoyl-ACP reductase has been the target for the most potent anti-tuberculosis drug, isoniazid **1**.⁵⁷ Due to InhA being involved in fatty acid synthesis this makes InhA a validated target in the treatment of tuberculosis. Isoniazid **1** has shown the formation of NAD⁺ adducts that inhibits the NADH dependant enoyl-ACP reductase of the FAS-II system.³⁴

Rifampicin **2**, pyrazinamide **3**, and ethambutol **4**, do not attack the biosynthetic pathway of the mycolic acid but are still effective anti-tuberculosis drugs. Rifampicin **2** acts by binding to the β -subunit of bacterial RNA polymerase. Since, the β -subunit of RNA polymerase is responsible for transcription and expression of mycobacterial genes, the binding of rifampicin results in the inhibition of bacterial transcription which inevitably leads to cell death.⁵⁸ In addition, pyrazinamide **3** is activated to form pyrazinoic acid which increases pH levels and binds to ribosomal proteins (RpsA) and inhibits translation.⁵⁹ However, activated pyrazinamide inhibits the synthesis of fatty acids, particularly the

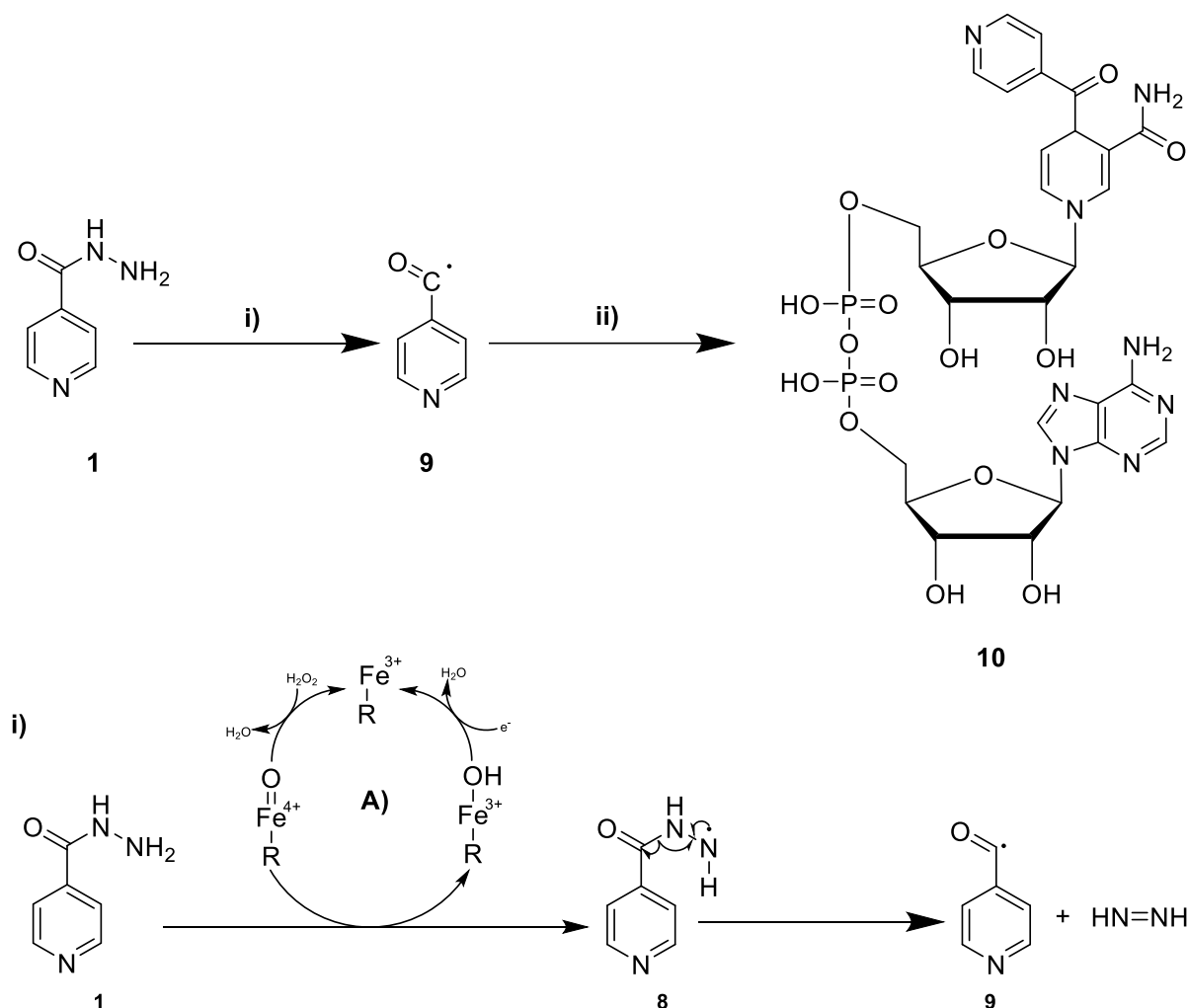
FAS-I system, which confuses the mechanism of action for pyrazinamide **3** due to the inhibition properties with both ribosomal proteins and the fatty acid system.^{59, 60}

Finally, ethambutol **4** is the first-line drug that has shown evidence for the prevention of cell wall formation. Ethambutol **4** inhibits the arabinosyltransferases preventing the formation of arabinogalactan and lipoarabinomannan.⁶¹ Decreased concentrations of arabinogalactan and lipoarabinomannan reduce the number of mycolic acid binding sites which causes increased accumulation of mycolic acids in the form of TMM and TDM as extractable fatty acids. A key feature of decreased number of mycolic acid-arabinogalactan bonds is a decreased rigidity of the cell wall resulting in increased permeability of the cell wall.^{43, 61, 62}

1.4.3 – Mechanism of Action for Isoniazid

Isoniazid **1** requires activation before becoming therapeutically effective. The activation of isoniazid **1** is achieved by a catalyse-peroxidase mycobacterial enzyme called katG. The catalyse-peroxidase activity of the katG does not only activate isoniazid **1** but also creates mutations in katG contributing to isoniazid resistance.^{63, 64} When isoniazid passively diffuses through the mycobacterial cell envelope it is activated by katG to form an acyl radical **9** which later forms an isoniazid-NAD adduct **10** by reacting with NADH (**Scheme 2**). The isoniazid-NAD adduct **10** is a slow, tight-binding competitive inhibitor of InhA which prevents the synthesis of mycolic acids at the FAS-II system of the biosynthetic pathway.^{63, 65, 66}

Scheme 2: Mechanism of action for isoniazid



*i) Activation of isoniazid **1** using a catalytic Fe^{3+} complex of KatG to form the hydrazinyl radical product **8** and a heme-oxyferryl by-product. ii) Formation of Isoniazid-NAD adduct **10** using isonicotinic acyl radical **9**.*

In the activation of isoniazid using katG (**Scheme 2i**), isoniazid **1** is converted into the isonicotinic acyl radical **9** via a hydrazinyl radical intermediate **8**. During the peroxidase cycle, katG is seen to be in its ferric state (Resting enzyme) that reacts with hydrogen peroxide, or a hydrogen peroxide equivalent, to form the oxyferryl iron-protoporphyrin IX, a Fe^{3+} complex (**Scheme 2iA**).⁶⁴ The Fe^{4+} complex is reduced when reacted with isoniazid **1** to form the hydrazinyl radical product **8** and the heme-oxyferryl by-product (Fe^{3+} compound, **Scheme 2i**). The hydrazinyl radical formed from this reaction undertakes a rearrangement which forms the active isonicotinic acyl radical **9** whereas the catalytic Fe^{3+} by-

product is further reduced to produce the KatG resting enzyme. When obtained the isonicotinic radical covalently bonds to NADH forming the isoniazid-NAD adduct **10** that is an inhibitor of InhA. The NAD-dependant enoyl acyl-ACP reductase, InhA, is vital for the elongation of the fatty acids chains during the FAS-II system in which the chains can reach a length of up to 56 carbons.⁶⁷ The inhibition of isoniazid-NAD adduct **10** to NAD-dependant InhA leads to the disruption of the mycolic acid biosynthesis leading to cell death.

Isoniazid-resistant strains of *Mycobacterium tuberculosis* occur with mutations in both InhA and KatG. InhA mutations cause low-level isoniazid resistance, so lower doses of isoniazid **1** will remain ineffective but high doses may be effective towards *Mycobacterium tuberculosis*, whereas katG mutations result in high-level isoniazid resistance leaving isoniazid **1** ineffective towards the treatment of *Mycobacterium tuberculosis*.²⁹

1.4.4 – Mutations in InhA and katG

Drug-resistance is reliant on mutations within genes that encode drug targets or drug mechanisms that affect the impact of tuberculosis therapy. When *Mycobacterium tuberculosis* gains resistance the lack of treatment and the use of inappropriate treatment can increase the population of drug-resistant strains.⁶⁸ Resistance in *Mycobacterium tuberculosis* against isoniazid **1** is a result of mutations within InhA and the katG gene.²⁹ The katG gene mutations are more frequent when compared to InhA mutations. KatG mutations are found in 42% to 95% of clinical isolates whereas InhA mutations occurring within 6% to 43% of clinical isolates with only 10% of *Mycobacterium tuberculosis* isolates containing both mutations.^{29, 67, 68}

Low-level resistance to isoniazid **1** occurs with mutations within the regulatory region of InhA.²⁹ C15T mutation within InhA which is cysteine to threonine amino acid change in the InhA regulatory region. This mutation results in the overexpression of InhA by increasing the InhA mRNA level which leads to

the titration of isoniazid **1**.⁶⁷ Studies have demonstrated that greater amounts of isoniazid **1** can be used in the treatment of MDR-TB and XDR-TB without the risk of toxicity.²⁹

Prevention of isoniazid activation (katG mutation) is the most frequent form of resistance within *Mycobacterium tuberculosis*. With over 300 mutations within katG, the 315 codon mutation rules as the most prevalent form of katG mutations which confer high-level isoniazid resistance.^{29, 68, 69} The most common nucleotide change within the katG 315 codon is AGC to ACC (serine to threonine) occurring among 93.4% of clinical isolates (**Table 1** – in red).⁶⁸ AGC to AAC (serine to asparagine) is the second most common 315 codon mutation which occurs in 3.6% of clinical isolates.⁶⁸ The S315T (AGC to ACC) mutation causes subtle changes within the isoniazid binding site preventing the binding ability of the drug rendering the drug inactive. The addition of the extra methyl group in the S315T mutation increases the steric hindrance of the active site. The increase of steric hindrance results in reduced acceptability to the heme site, from 6 Å to 4.7 Å.⁷⁰ Whilst reducing the acceptability of the heme site leads to the loss of activation of isoniazid **1** it does not decrease the catalase-peroxidase activity of katG.⁷⁰ Within clinical tests it is shown that the S315T mutation is associated with MDR-TB, resulting in other InhA inhibitors being synthesised.

Amino acid	Nucleotide	Total Number	%
Threonine			95.3
	ACC	4208	93.4
	ACA	73	1.6
	ACG	7	0.2
	ACT	7	0.2
Asparagine			3.6
	AAC	161	3.6
Isoleucine			0.5
	ATC	23	0.5

Arginine			0.4
	AGA	8	0.2
	CGC	5	0.1
	AGG	4	0.1
Glycine			0.2
	GGC	9	0.2
Total		4505	100

Table 1: Amino acid and nucleotide mutation frequency of *katG315* isolates with the most common mutation highlighted in red.⁶⁸

1.4.5 – Other inhibitors of *InhA*

Inhibition of mycobacterial *InhA* is one of the most effective pathways in tuberculosis treatment shown by the anti-mycobacterial activity of isoniazid **1**. The resistance to isoniazid **1** has caused the synthesis of many analogues and some such as ethionamide **7** (Figure 6) have become major second-line drugs.⁶⁷ Others such as triclosan **11** and thiolactomycin **12** (Figure 6) have been used in active treatment against MDR-TB and XDR-TB.^{71, 72}

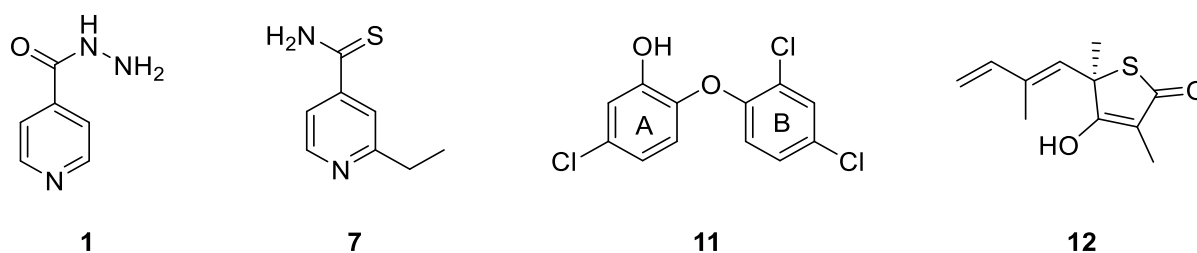


Figure 6: Chemical structures of targets that inhibit *InhA*; isoniazid **1**, ethionamide **7**, triclosan **11**, and thiolactomycin **12**.

Ethionamide **7** is a major second-line prodrug that is an analogue of isoniazid **1** which has shown less activity towards *Mycobacterium tuberculosis* when compared to isoniazid **1**. However, ethionamide **7** has shown activity against isoniazid-resistant *Mycobacterium tuberculosis* strains.⁶⁷ Ethionamide **7** has a similar mechanism of action as isoniazid in which the prodrug is activated by the *EthA* gene.

The active ethionamide species creates an ethionamide-NAD adduct, by reacting with NAD^+ , that inhibits InhA solely leading to mycolic acid biosynthesis inhibition.^{29, 67} Even though ethionamide **7** is a major second-line drug that's effective against MDR-TB, *Mycobacterium tuberculosis* can obtain mutations within InhA and EthA making it resistant towards ethionamide **7**.^{29, 67} Cross-resistance from isoniazid **1** with ethionamide **7** is evident as the target for ethionamide **7** is InhA therefore, mutations within the promoter region of *inhA*, caused by isoniazid resistance, causes resistance to ethionamide **7**.^{2, 3, 29, 30}

Unlike isoniazid **1** and ethionamide **7**, triclosan **11** does not require activation to obtain inhibitory effects. Therefore, triclosan would remove the need for activation by KatG which avoids pre-existing resistance. The development of potential inhibitors that bypass the KatG mediated resistance and bind directly to InhA would be key for current and future research.⁷² With many drugs binding one molecule in the active site of InhA, triclosan **11** is unusual as two molecules of triclosan bind to the active site of InhA. It has been shown that lower concentrations of triclosan **11** inhibit InhA and higher concentrations of triclosan **11** disrupt the bacterial protein synthesis.^{73, 74} Inspection of the crystal structure shows that the distance between the two triclosan molecules within the binding site of InhA is $\sim 4.2 \text{ \AA}$ (**Figure 7**).⁷⁴ This suggests that possible modifications within triclosan may develop into potent anti-tubercular drugs that could bypass the KatG mediated resistance and bind directly to InhA. Modifications of triclosan would occur in ring B (**Figure 6**) due to hydrogen bonds forming between the OH on ring A of triclosan and InhA. Triclosan scaffolding is obtained from these features resulting in many potential potent InhA inhibitors (**Table 2**).^{74, 75}

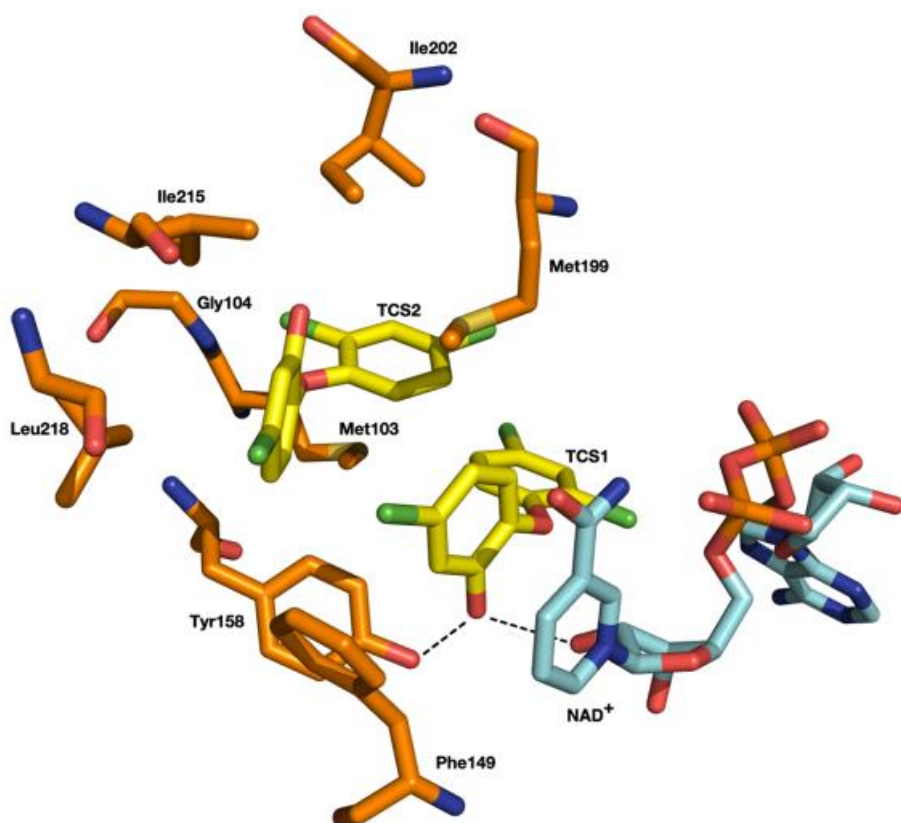


Figure 7: Xray structure showing two triclosan molecules bond to the InhA active site. Triclosan is shown by the yellow carbons, residues are shown by the orange carbons, NAD⁺ is shown by the teal carbons and Hydrogen bonds are indicated with the dashed black lines. (PDB: 1P45).⁷⁴

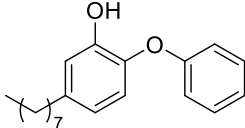
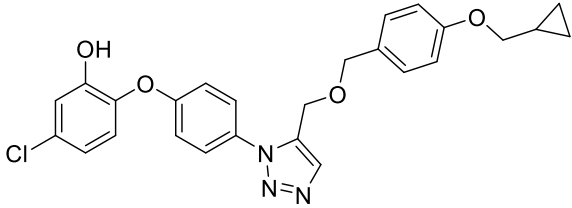
Triclosan analogues as potential InhA Inhibitors	Mycobacterial IC ₉₉ /MIC ₉₉ (μM)	InhA IC ₅₀ /MIC ₅₀ (μM)	Organism tested
 13	6.6 ± 1.7	0.005 ± 0.003	Lab grown <i>Mycobacterium bovis</i>
 14	12.9 ± 5.0	>50	Lab grown <i>Mycobacterium bovis</i>

Table 2: Triclosan analogues, potential anti-tuberculosis drugs tested against lab grown *Mycobacterium bovis* with concentration of the inhibitor when 50% inhibition was achieved and the concentration of the inhibitor when 99% of inhibition is achieved.⁷⁴

Triclosan analogue **13** has shown potency within whole-cell assays with an MIC₉₉ value of 6.6 μ M with triclosan analogue **14** showing MIC₉₉ values of 12.9 μ M. This suggests that the potency of **14** is lower at a whole-cell assay when compared to **13** due to **13** requiring a smaller concentration to inhibit the mycobacterium. With **13** having a low mycobacterial IC₉₉ and InhA IC₅₀, when compared to triclosan **14**, **13** can inhibit both mycobacterium and InhA with lower concentrations. It was concluded that **14** may have a secondary target within mycobacterium resulting in a larger concentration needed for InhA inhibition.⁷⁴

Other InhA inhibitors have emerged from further studies with analogues from specific functional groups. Analogues from the thiadiazole group (highlighted in blue, **Table 3**) have indicated many anti-tuberculosis activities. Thiadiazole analogues from **Table 3** indicate a low concentration for the inhibition of *Mycobacterium tuberculosis*. The inhibition concentration of InhA for **16** is 2 nM and the InhA IC₅₀ value for **15** is 7 nM which suggests that a lower concentration of **16** can bind tightly with InhA and decrease the activity of InhA within the biosynthetic pathway of mycolic acids when compared to **15**.

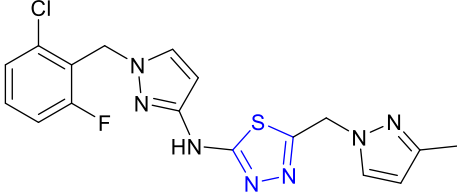
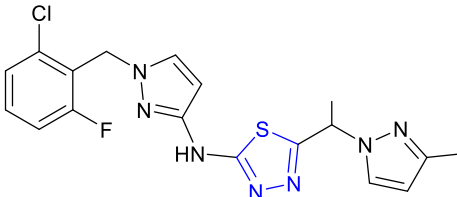
Inhibitors	<i>Mycobacterium tuberculosis</i> IC/MIC (μ M)	InhA IC ₅₀ /MIC (nM)	Organism tested
 <p style="text-align: center;">15</p>	≤ 1	7	Mouse – <i>Mycobacterium tuberculosis</i> infected
 <p style="text-align: center;">16</p>	1	2	Mouse – <i>Mycobacterium tuberculosis</i> infected

Table 3: Potential InhA drugs using a thiadiazole core tested against *Mycobacterium tuberculosis* infected organism with concentration of the inhibitor at which 50% of inhibition is achieved.⁶⁵

In addition, the thiadiazoles, indicated in **Table 3**, have shown that lower concentrations are required for InhA and mycobacterium inhibition when compared to triclosan analogues, shown in **Table 2**. The triclosan and thiadiazole analogues are compared due to the structure of InhA within *Mycobacterium bovis* and *Mycobacterium tuberculosis* being identical. The triclosan analogue **13** (**Table 2**) has an InhA IC₅₀ of 5 nM whereas the thiadiazole analogues have InhA IC₅₀ of 2 nM and 7 nM which indicates that both triclosan and thiadiazole analogues have the potential to become potent anti-tubercular drugs.

1.5 – Design of triclosan derivatives

1.5.1 – Di-triclosan Compounds

Observed within the 1P45 crystal structure (**Figure 7**) the triclosan molecules occupy two different regions within the active site of InhA. Therefore, the first step of design was to identify any current research that observed molecules that contained a linker between both triclosan molecules. Research conducted by Neil Thomas group shows the two triclosan fragments connected through a triazole linker (**Figure 8**).⁷⁴

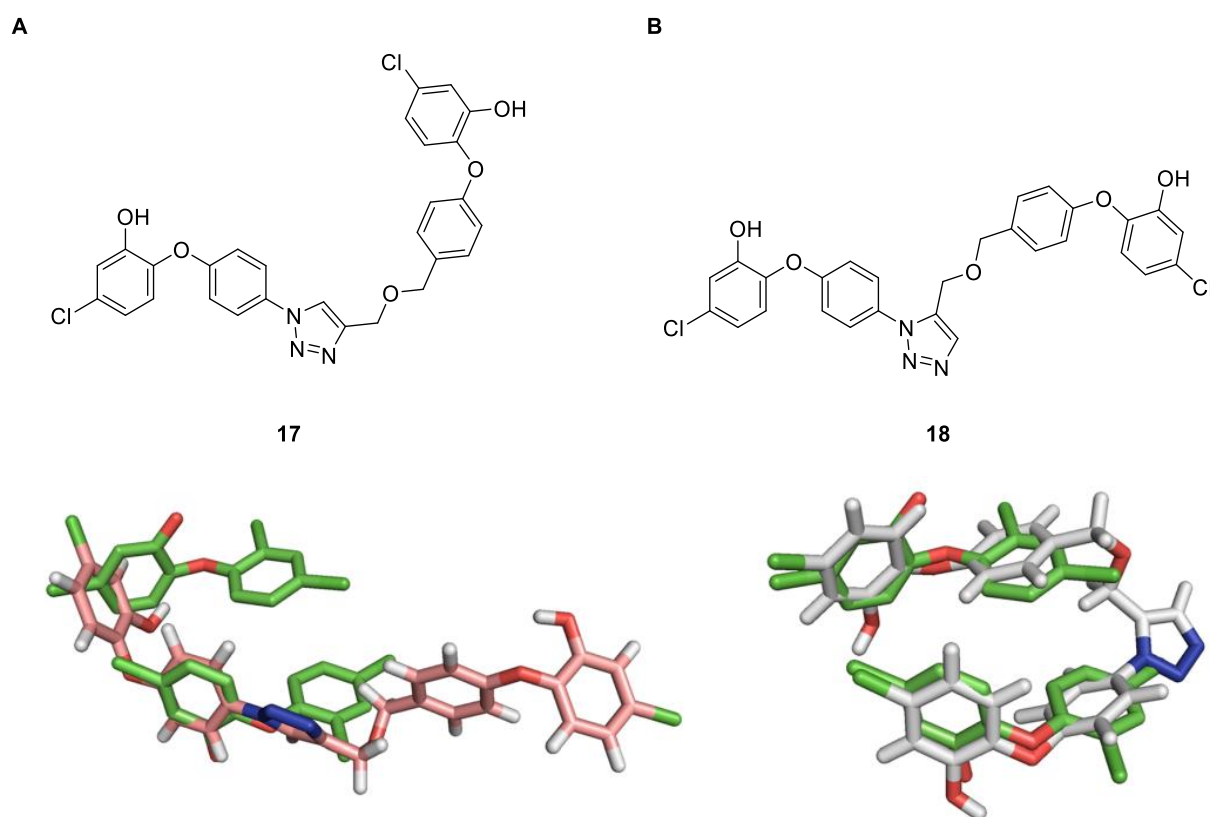


Figure 8: The structures of two triclosan-triazole molecules and their docking overlapped with two triclosan moieties found in the active site (PDB: 1P45). A) 1,4-triazole analogue, B) 1,5-triazole analogue.⁷⁴

A 1,4-triazole and 1,5-triazole linker was designed and were docked into InhA active site (PDB: 1P45). The 1,5-triazole structure (**Figure 8B**) occupied both spaces of triclosan and contained similar binding modes. It was also observed that the 1,5-triazole structure conserved the important H-bonding network seen within the triclosan binding (**Figure 7**). However, the 1,4-triazole structure (**Figure 8A**)

did not generate a suitable structure that occupied both triclosan moieties within InhA active site. As 1,5-triazole linker showed desirable docking, a range of compounds bearing a single aromatic ring attached through a 1,5-triazole motif was designed (**Figure 9**).⁷⁴

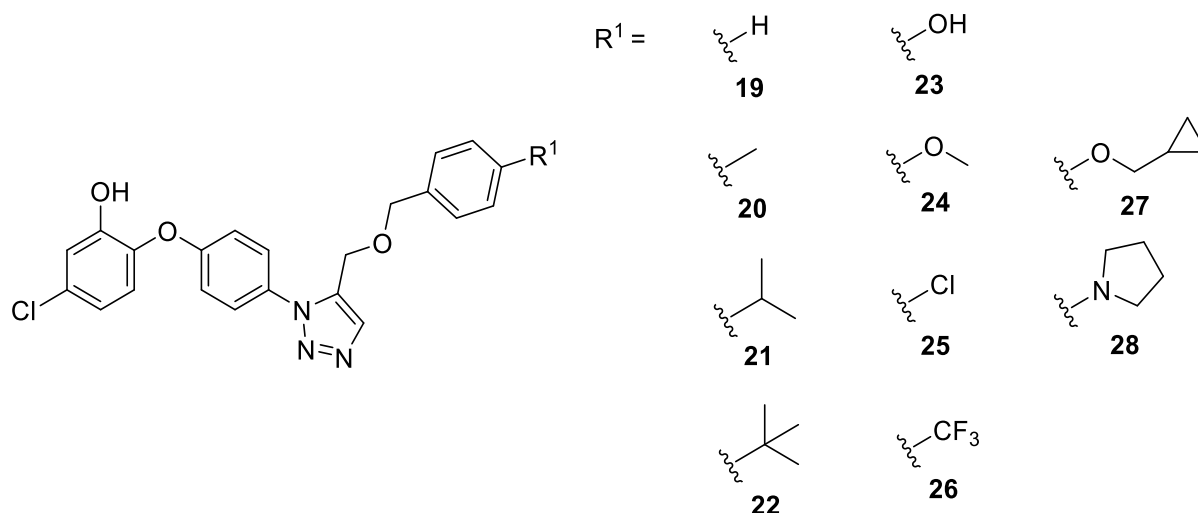


Figure 9: Compounds with a single aromatic ring and attached through a 1,5-triazole linker.⁷⁴

Functional groups can determine the intrinsic reactivity of the molecule and be responsible for the overall properties of the molecule. Therefore, R groups with different electronic and steric properties would affect the overall properties of the drugs and how the binding would occur within the associated binding site. R groups observed within **Figure 9** have a range of steric effects and electronic effects which would differentiate the docking and inhibitory activities of the 1,5-triazole molecule.

The inhibitory activities were observed for compounds **18** – **28** with initial screening performed at 50 μ M with 150 nM of InhA from *Mycobacterium tuberculosis*. Changing hydrogen to methyl to isopropyl (**19** \rightarrow **20** \rightarrow **21**) shows increased inhibition (**Table 4**) whereas the introduction to larger bulky groups, such as ^tBu on **22** results in reduced enzyme inhibition suggesting a clash between the bulky group and protein.⁷⁴ This is supported by the smaller more flexible R groups on **24**, **26** and **28** which show a moderate inhibition.⁷⁴

Compound	Gold Fitness Score	Inhibition (%)
18	87.7	100
19	65.2	12
20	73.5	38
21	77.8	72
22	74.0	6
23	69.0	13
24	76.7	44
25	73.2	0
26	75.6	47
27	80.7	11
28	83.6	42

Table 4: Inhibitory data for 1,5-triazole compounds tested using an isolated enzyme assay conducted at 50 μ M.⁷⁴

The whole cell evaluation for the 1,5-triazole compounds (**18 – 28**) were calculated and measured against the isolated enzyme activity.⁷⁴ The growth inhibition for the compounds were assessed against *Mycobacterium bovis* at a fixed concentration of 40 μ M (**Table 5**). The isolated assay potency for **18** towards InhA, shown in **Table 4**, does not correlate against the whole cell potency (**Table 5**). This was assumed to be the inability for the compound to pass through the dense mycobacterial wall.⁷⁴ However, compound **27** shows the greatest whole cell potency with 99% growth inhibition at 40 μ M. Overall, it is observed that the compounds containing larger and bulkier R groups show the greatest inhibition and docking studies (**Table 4** and **Table 5**). However, the rigid 1,5-triazole linker within the compound limits flexibility of the compound and the design of a drug without the linker would alter the movement of the drugs and effect the inhibitory activities.

Compound	Inhibition (%)	cLogP
18	20	5.80
19	3	5.11
20	6	5.43
21	15	5.89
22	20	6.11
23	0	4.37
24	40	5.03
25	4	5.61
26	19	6.09
27	99	6.07
28	23	5.95
Triclosan	70	4.98

Table 5: Inhibition data for the 1,5-triazole compounds tested against *Mycobacterium bovis* at 40 μ M.⁷⁴

1.5.2 – Design and docking of triclosan analogues

As seen within the 1,5-triazole compounds (**18** – **28**) the rigidity and large bulky groups resulted in reduced enzyme inhibition and whole cell potency.⁷⁴ Therefore, the removal of the 1,5-triazole group results in the flexibility for bulky R groups which may result in greater inhibition. Retaining the OH functional group on ring A would allow the molecule to retain the hydrogen bonding network that is important amongst all potent direct InhA inhibitors. Therefore, a range of compounds bearing a single aromatic ring attached to a triclosan core without a 1,5-triazole motif were designed (**48** – **52**) (**Figure 10**).

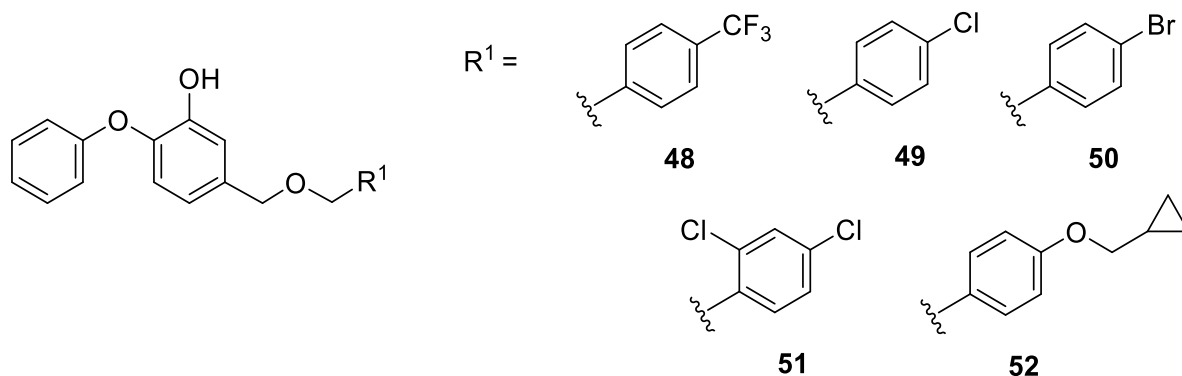


Figure 10: Proposed products designed without a 1,5-triazole linker group that would be docked into GOLD docking program.

1.6 – Aims and objectives

1.6.1 – Aims

The aim of this research project was to synthesise triclosan derivatives that will then be evaluated for their potential to be used for future anti-tuberculosis treatment.

1.6.2 – Objectives

The key objectives of this research were:

- To synthesise the desired triclosan derivatives containing different R groups at the *meta*-positions of benzene A of the triclosan core (**Figure 11**).

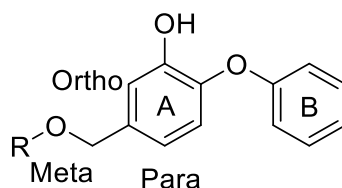


Figure 11: Chemical structure of triclosan analogue with modifications occurring within the benzene A ring

- The use of analytical techniques to indicate the purity of the synthesised products.
- To use a computational docking program to calculate the potential binding of the putative inhibitor to InhA.

Chapter 2: Results and Discussions

2.1 – Discussion

2.1.1 – Docking and synthesis of triclosan analogues

The triclosan analogues designed (**Figure 10**) were docked *in silico* to InhA using GOLD docking in which the GOLD fitness score was calculated (**Table 6**). Observed by the docking studies compounds **48** – **52**, having smaller R groups indicate desirable GOLD fitness scores whereas larger and bulkier R groups, **51**, show a lower GOLD fitness score (**Table 6**). This may be due to the chlorines on the benzene ring as chlorines cause greater steric hindrance due to the size so the hydrogen bonds from the amino acid to the putative inhibitor are less likely to form. It is also seen that **48** (**Figure 12**), **49** (**Figure 13**), and **50** (**Figure 14**) form hydrogen bonds with serine and threonine side chains whereas the hydrogen bond calculated for **51** was with the valine amide backbone (**Figure 15**). The R group that indicated the greatest whole cell potency for the 1,5-triazole compound **27** also shown the greatest GOLD fitness score with the removal of the rigid triazole linker **52**. This may be due to the angular strain within the cyclopropyl ring becoming more stable when inhibiting InhA, shown within the docking of **52** (**Figure 16**) as the phenylalanine residues of InhA (Phe41 and Phe97) have a greater attraction towards the cyclopropyl ring within **52**.

Compound	GOLD Fitness Score	Protein-Ligand hydrogen bond energy	Protein-Ligand Van der Waals energy
48	81.12	8.06	54.41
49	80.54	0.98	58.08
50	83.39	10.02	54.44
51	77.18	4.57	54.22
52	86.79	0.81	63.91

Table 6: The *in silico* docking of the proposed products into InhA using GOLD docking program

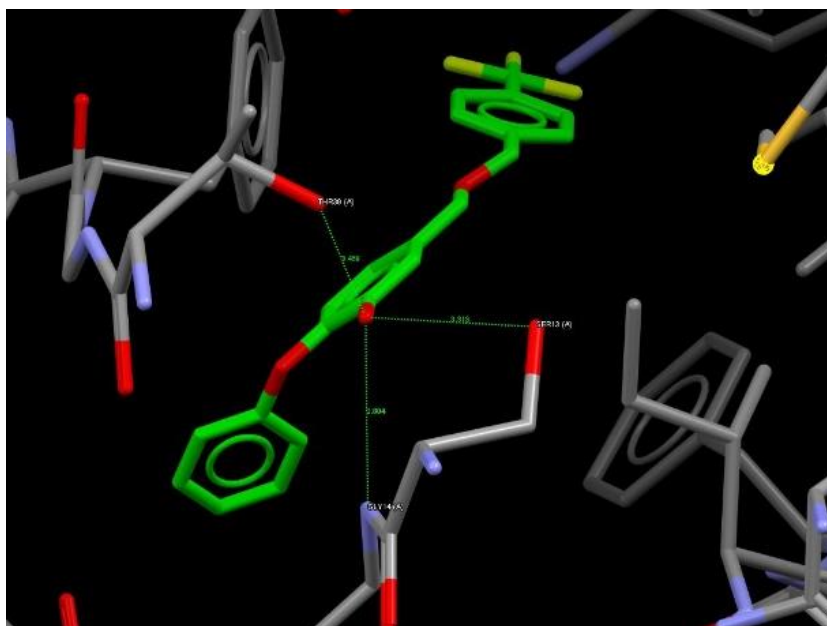


Figure 12: GOLD Docking of **48** within InhA (PDB: 1P45), Ligand-protein hydrogen bonds with protein residues; Ser13, Thr39 and Gly14

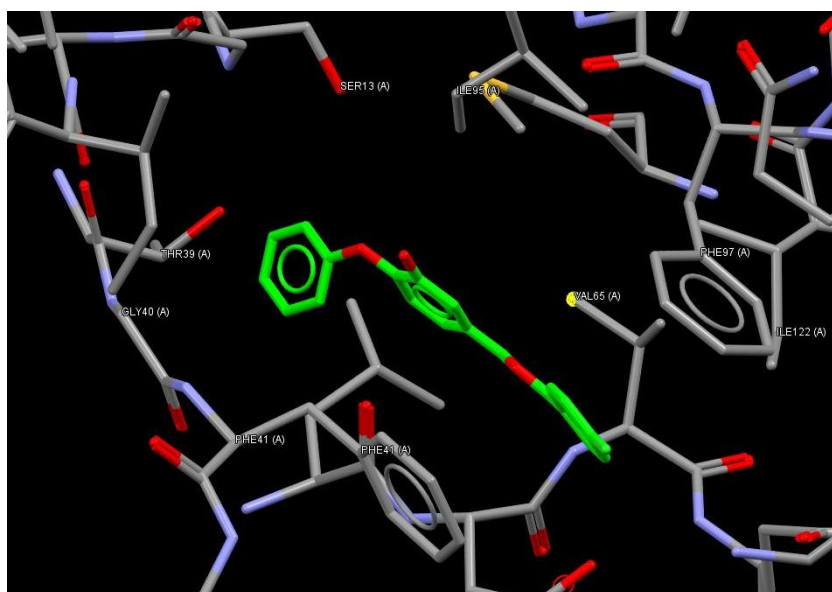


Figure 13: GOLD Docking of **49** within InhA (PDB: 1P45), Ligand-protein hydrogen bonds with protein residues; Ser13 and Thr39

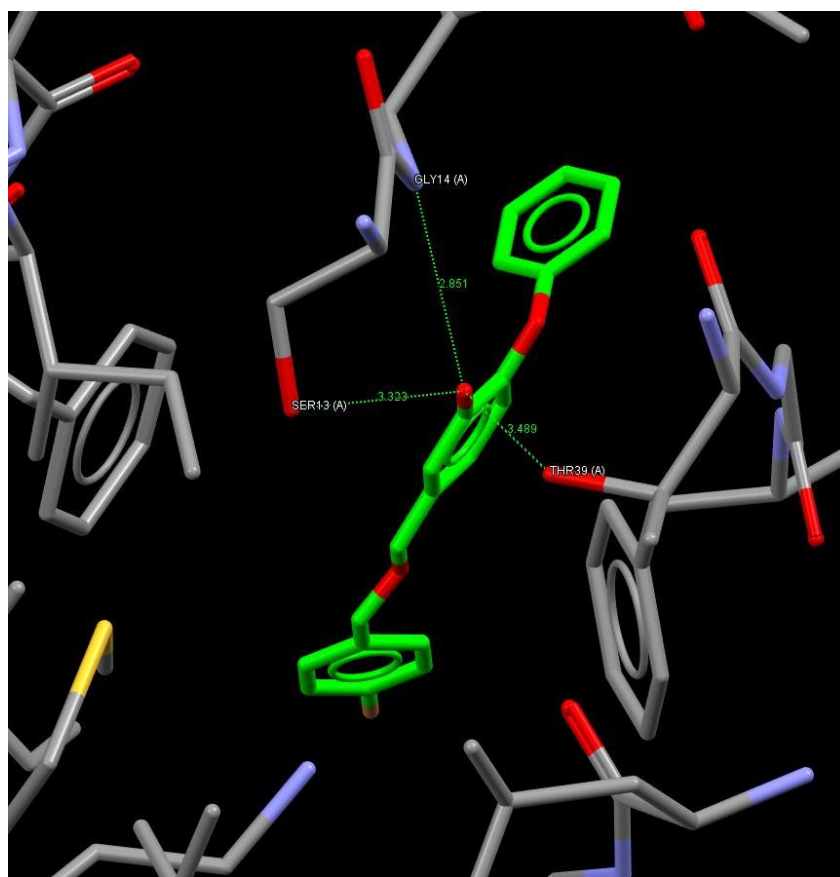


Figure 14: GOLD Docking of **50** within InhA (PDB: 1P45) and the ligand-protein hydrogen bonds with protein residues; Ser13, Thr39 and Gly14

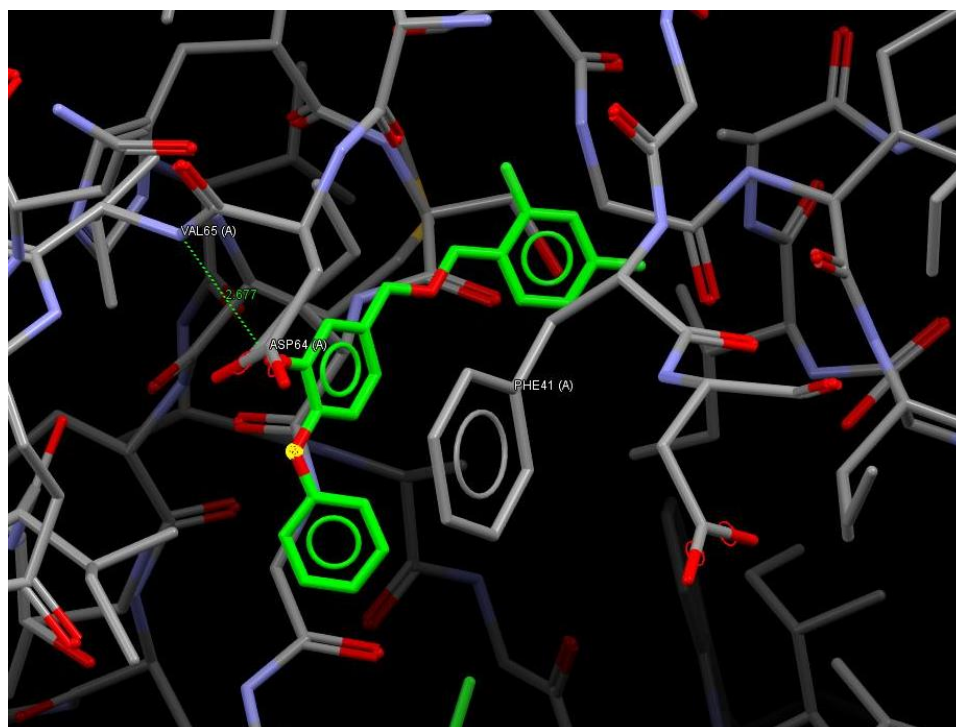


Figure 15: GOLD Docking of **51** within InhA (PDB: 1P45) the docking of **50** in InhA with Hydrogen bond between ligand-protein at Val65 protein residue.

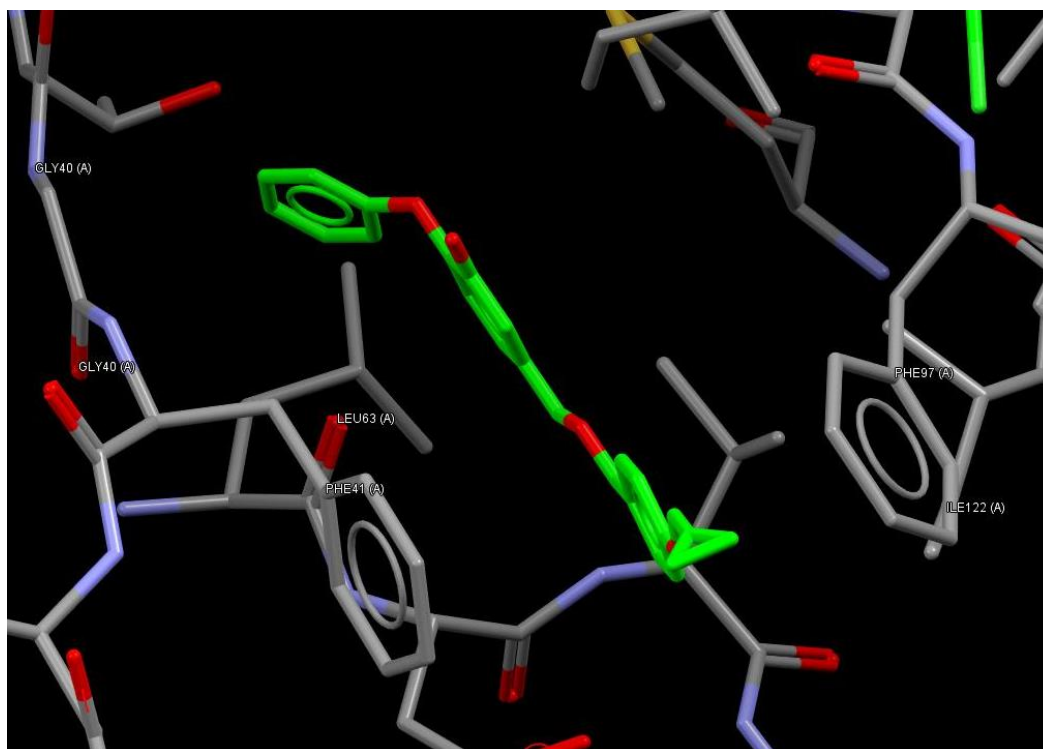
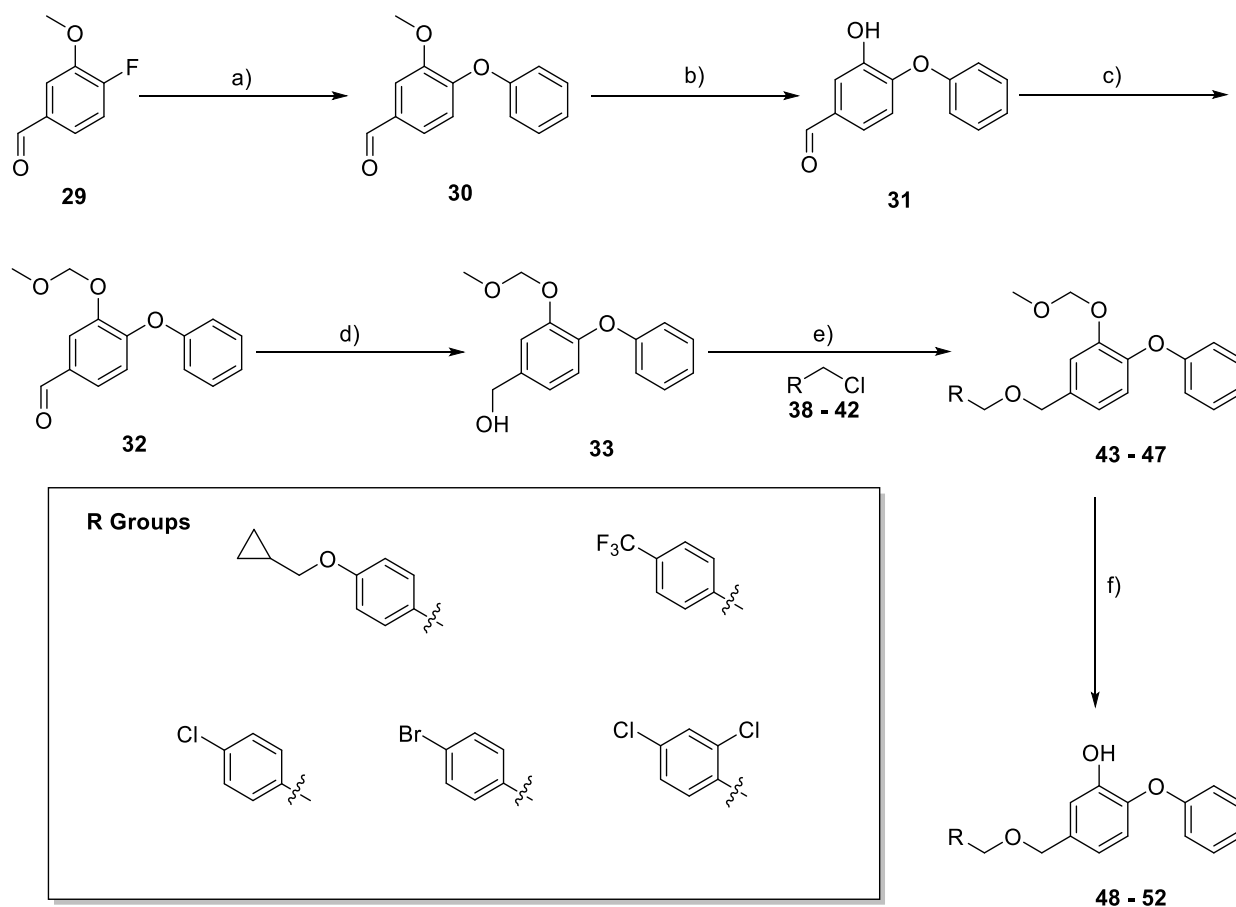


Figure 16: GOLD Docking of **52** within InhA (PDB: 1P45) with Van der Waal forces present between **51** and Phe41 and Phe97 residues.

The GOLD docking shows successful docking into InhA so the proposed products **48** – **52** were synthesised. The synthesis started with the preparation of the triclosan scaffold **33** through a range of methodologies. Then the non-commercial R group 4-(cyclopropylmethoxy)benzyl chloride **38** was synthesised and added to the scaffold through a nucleophilic substitution reaction. This was similar for the addition of the other R groups; 4-trifluoromethylbenzyl chloride **39**, 4-bromobenzyl chloride **41**, and 2,4-dichlorobenzyl chloride **42**. After the addition of the R groups (**38** – **42**) the alcohol was deprotected leaving the final and proposed compounds **48** – **52** (Scheme 3).

Scheme 3: Reaction synthesis



a) Phenol, K_2CO_3 , DMF, 130 °C, 18 h, 76%; b) HBr, AcOH, 113 °C, 36 h, 49%; c) MOMCl, iPr_2NEt , CH_2Cl_2 , 18 h, 86%; d) $NaBH_4$, MeOH, 0 °C \rightarrow r.t., 4h, 91%; e) R-Cl, DMF, NaH, 0 °C, 1 hr; f) HCl, MeOH, 70 °C, 2-3 hrs.

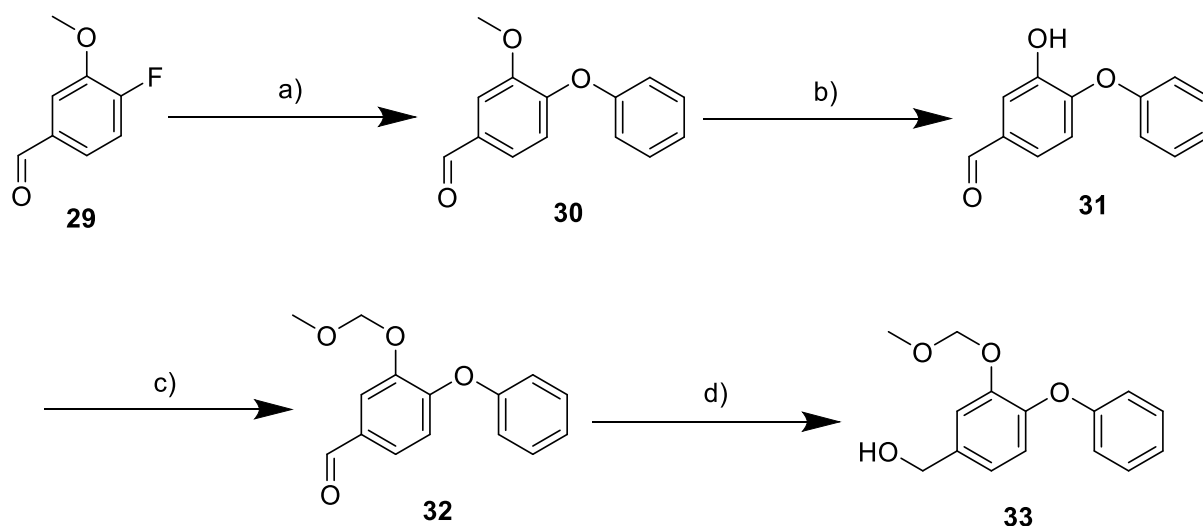
The synthetic pathway of the proposed products without the 1,5-triazole linker unit, starting with the synthesis of the triclosan core **33** and ending with the potential *InhA* inhibitors **48 – 52**.

2.1.2 – Synthesis of Scaffold

The synthesis of the diphenyl ether unit of the triclosan scaffold, (3-(methoxymethoxy)-4-phenoxyphenyl)methanol **33**, was overall a high yielding procedure which produced a pure product. The biaryl ether synthesis (**Scheme 4a**) consisted of the reaction between phenol and 4-fluoro-3-methoxybenzaldehyde **29**. The purification step for this reaction consisted of flash column chromatography with a hexane/EtOAc solution with EtOAc having a gradient of 0 \rightarrow 30% which was altered from the original hexane/EtOAc 15% solution.⁷⁴ The percentage of EtOAc was altered due to the spectroscopic analysis indicating the presence of starting material after purification with flash

column chromatography. The mobile phase was changed to a gradient elution as a gradient elution provides the ability to modify the retention times in the separation between the starting materials and products. Therefore, resulting in a defined retention time between the product and starting materials/impurities.

Scheme 4. Synthesis of InhA inhibitor scaffold



a) Phenol, K_2CO_3 , DMF, 130 °C, 18 h, 76%; b) HBr, AcOH, 113 °C, 36 h, 49%; c) MOMCl, iPr_2NEt , CH_2Cl_2 , 18 h, 86%; d) $NaBH_4$, MeOH, 0 °C \rightarrow r.t., 4h, 91%

The demethylation of 3-methoxy-4-phenoxybenzaldehyde **30** to produce 3-hydroxy-4-phenoxybenzaldehyde **31** (Scheme 4b) was repeated many times with varying equivalents of the reactants.^{74, 76, 77} The highly stable aryl methyl ether on 3-methoxy-4-phenoxybenzaldehyde **30** creates a problem for the removal of the methyl group which was seen as the completed reaction produced a low yield of 49%. The demethylation of the aryl methyl ether with the use of a hydrobromic acid catalyst and glacial acetic acid at high temperatures is not compatible with many aromatic structures and is seen to produce unwanted side reactions and low yields.⁷⁷ As the demethylation is known to produce low-yielding reactions the number of equivalents for both AcOH and HBr (aq.) was increased from 17 and 3 eq. to 66 and 16 eq. respectively. The change in equivalents allowed the reaction yield to get closer to the literature yield of 47%.⁷⁴ In addition to the low-yielding reaction, the product was

observed to decompose under light which resulted in the need for the reaction to be conducted in the absence of light and was conducted in an inert atmosphere. Conducting the reaction under strict reaction conditions prevented the hydrobromic acid from readily fuming. The prevention of this is important for the reaction as hydrobromic acid fumes would alter the concentration of hydrobromic acid within the solution resulting in an incomplete reaction. Keeping the reaction under strict conditions produced a high purity product which was shown within the spectroscopic data.

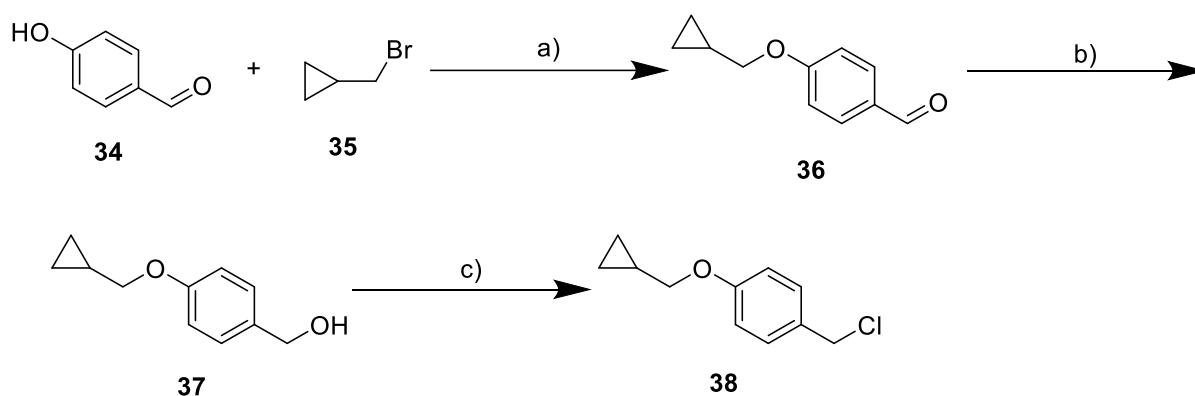
After the demethylation of 3-methoxy-4-phenoxybenzaldehyde **30**, the functional group that remained on 3-hydroxy-4-phenoxybenzaldehyde **31** was an alcohol group. The alcohol group required protection with a MOM protecting group (**Scheme 4c**) as this would prevent the alcohol group from reacting with the proposed R groups. The MOM protecting group was selected due to its simple protection and deprotection reactions which was shown with an 86% yield produced from the reaction procedure. Furthermore, the protection of the alcohol group on 3-hydroxy-4-phenoxybenzaldehyde **31** would allow chemoselectivity in the compound. The reaction between MOMCl and 3-hydroxy-4-phenoxybenzaldehyde **31** was successful which is shown within the NMR spectroscopy obtained.

The reduction of the aldehyde to a primary alcohol creates a site that allows nucleophilic substitution to occur. Therefore, the reduction of 3-(methoxymethoxy)-4-phenoxybenzaldehyde **32** to make (3-(methoxymethoxy)-4-phenoxyphenyl)methanol **33** (**Scheme 4d**) was required to produce a highly pure product with a high yield as the product would later react with the designated R groups (**38 – 42**). This was achieved as the reaction between 3-(methoxymethoxy)-4-phenoxybenzaldehyde **32** and NaBH₄ in MeOH to synthesise (3-(methoxymethoxy)-4-phenoxyphenyl)methanol **33** produced a yield of 91% with NMR data showing high purity. As the NMR showed a pure compound with little to no impurities, (3-(methoxymethoxy)-4-phenoxyphenyl)methanol **33** was carried forward for further reactions.

2.1.3- Synthesis of R group – 4-(cyclopropylmethoxy)benzyl chloride

Due to 4-(cyclopropylmethoxy) chloride **38** not being commercially available the synthesis of the R group 4-(cyclopropylmethoxy) chloride **38** required a various range of synthetic pathways steps starting with the synthesis of 4-(cyclopropylmethoxy)benzaldehyde **36** (Scheme 5). The synthesis of 4-(cyclopropylmethoxy)benzaldehyde **36** was predicted as a highly successful reaction as bromine on bromomethyl cyclopropane **35** is a good leaving group allowing the addition of 4-hydroxybenzaldehyde **34** to make 4-(cyclopropylmethoxy)benzaldehyde **36**. During the reaction procedure the residue after reduced pressure evaporation was recrystallised with ethanol. This produced a pure product and didn't require any further purification which was seen in the NMR data obtained.

Scheme 5: Synthetic pathway of the R Group 4-(cyclopropylmethoxy)benzyl chloride **38**



a) K_2CO_3 , Acetone, 55 °C, 24 hrs, 93%; b) $NaBH_4$, MeOH, 0 °C, 1 hr, 82%; c) $SOCl_2$, Et_2O , r.t, 2 hrs, 92%

After 4-(cyclopropylmethoxy)benzaldehyde **36** was synthesised and portrayed as pure the aldehyde group on 4-(cyclopropylmethoxy)benzaldehyde **36** was reduced to an alcohol to produce (4-(cyclopropylmethoxy)phenyl)methanol **37** (Scheme 5b). The reduction of the aldehyde would allow a site for the SN_2 reaction between the alcohol and thionyl chloride. As the reduction reaction of 4-(cyclopropylmethoxy)benzaldehyde **36** to make (4-(cyclopropylmethoxy)phenyl)methanol **37** is an essential step for the preparation of 4-(cyclopropylmethoxy)benzyl chloride **38**, the product had to be pure with good yield to be considered for further reaction with thionyl chloride. The purity and success

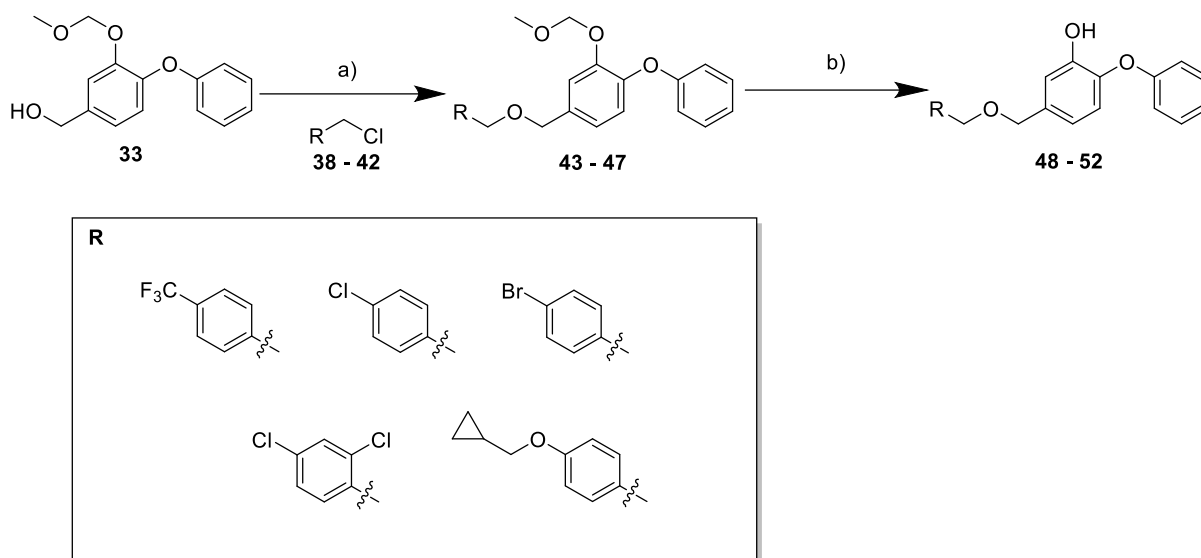
of the reduction reaction for 4-(cyclopropylmethoxy)benzaldehyde **36** to make (4-(cyclopropylmethoxy)phenyl)methanol **37** was indicated within the NMR data, with the ^{13}C NMR and ^1H NMR portraying successful aldehyde reduction.

The synthesis of 4-(cyclopropylmethoxy)chloride **38** was first attempted as a Appel reaction, as a Appel reaction is an important reaction for the conversion of a primary alcohol group to an alkyl halide in the presence of triphenylphosphine and carbon tetrahalide. However, this was not completed as the reaction pathway used toxic halogenating agents and the synthesis using both triphenylphosphine and carbon tetrachloride would produce an organophosphorus biproduct which must be separated from the organic compound. The synthetic pathway selected was the reaction between thionyl chloride and (4-(cyclopropylmethoxy)benzyl) methanol **37** (**Scheme 5c**).⁷⁸ In this reaction, the nucleophilic oxygen atom displaces the chloride ion from thionyl chloride to form a protonated alkyl chlorosulfite intermediate which releases SO_2 and HCl , thus resulting in a highly flammable reaction. The product 4-(cyclopropylmethoxy)benzyl chloride **38** was assumed to decompose within the silica medium of the column when purified within flash column chromatography, which proved to be correct after successful 2D TLC showing the decomposition of the product. As the desired product decomposed on the silica medium, recrystallisation was identified as an alternative method of purification. However, the product showed high solubility in many solvents and showed no signs of crystallisation when cooled and during the addition of a second solvent. Therefore, the reaction was repeated under strict conditions such as keeping the reaction under an inert atmosphere and keeping the reaction protected from light. In addition, the reaction progress was monitored thoroughly through TLC and mass spectra for the formation of the product and the consumption of starting material. Keeping the reaction monitored allowed the formation of the product and prevented the formation of any by-products resulting in a highly pure crude material. As the desired peaks for a successful reaction were obtained within the NMR with no residual solvent being present, the product was used within the coupling step with (3-(methoxymethoxy)-4-phenoxyphenyl)methanol **29** to synthesize **47** without further purification.

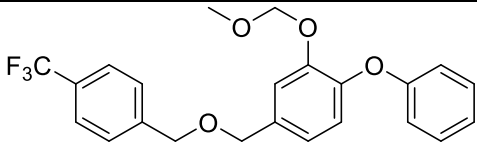
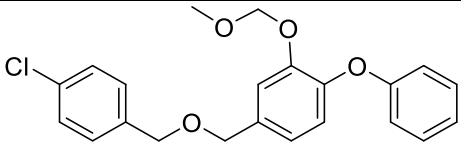
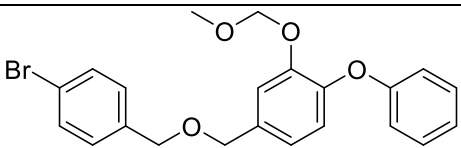
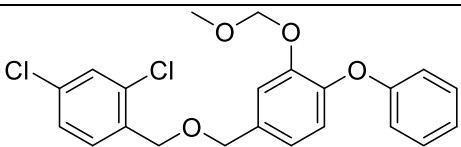
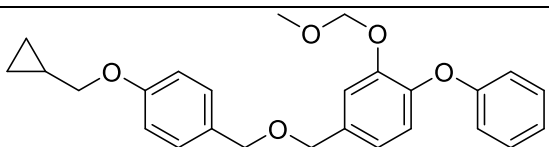
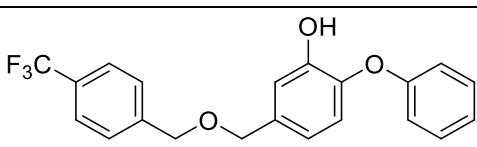
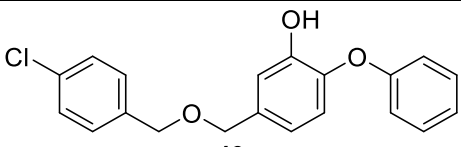
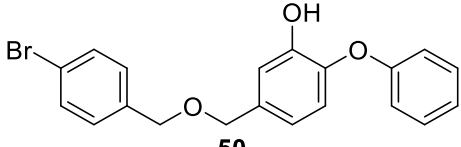
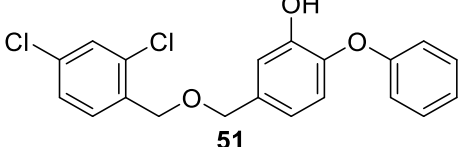
2.1.4 – Synthesis of Final Products

The synthesis of the final compounds started with the coupling between (3-(methoxymethoxy)-4-phenoxyphenyl)methanol **33** and the different benzyl chlorides (**38 – 42**) (**Scheme 6a**). The coupling of each group undertook the same reaction procedure and conditions with the MOM protecting group allowing selective substitution with the *meta*-OH group. After successful coupling the MOM protecting group was removed via a deprotection reaction (**Scheme 6b**) and the purity of the products was measured via reverse-phase semi-preparative HPLC with HRMS. However, for products **44** and **49** this was not completed as the R group was not delivered from the supplier in time for the experiment.

Scheme 6: Synthesis of final products



a) *R*-Cl, DMF, NaH, 0 °C, 1 hr; b) HCl, MeOH, 70 °C, 2-3 hrs

Final Product	Percentage Yield
 <p>43</p>	65%
 <p>44</p>	0%
 <p>45</p>	98%
 <p>46</p>	91%
 <p>47</p>	68%
 <p>48</p>	20%
 <p>49</p>	0%
 <p>50</p>	35%
 <p>51</p>	36%

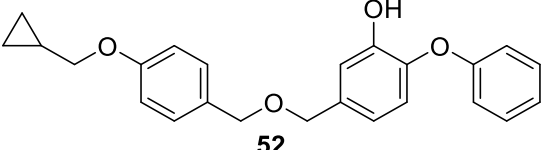
 <p style="text-align: center;">52</p>	<p>6%</p>
--	-----------

Table7: The tabulated results for the final products and percentage yields.

The deprotection of the compounds brings back the alcohol functional group which is important for the final product as potential InhA inhibitors. The alcohol functional group on the final compounds **48** – **52** allows the possibility of hydrogen bonding between InhA and the compounds. This is an important step due to the GOLD docking showing successful docking into InhA with high hydrogen bonding.

The low yield obtained from the deprotection occurred during the purification with HPLC. With HPLC having many advantages as a purification method HPLC, a key disadvantage observed within my research was the decomposition of products within the column. Also assisting with the low yield was human error and loss of product in transfer between glassware.

2.2 – Future Work

The research project has shown the synthesis and *in silico* binding affinities of triclosan derivatives to InhA. The binding of the products to InhA should be calculated by not only computational means but also measured through controlled lab inhibition with InhA. This would help identify the inhibition properties of the products in controlled setting and the inhibition can be compared to the computational results. Also, decomposition of the product and stability can be tested. The inhibition of a *M. tuberculosis* or *M. bovis* cell may also become a factor as the drug has to pass through the lipid membrane to enter the cytoplasm and inhibit InhA. Therefore, further tests of the inhibition of whole cells could be analysed. The synthesis of 4-(((4-chlorobenzyl)oxy)methyl)-2-(methoxymethoxy)-1-phenoxybenzene **49** wasn't completed due to the unavailability of starting material. Therefore, if the product was synthesised with purity and yield measurements, a controlled lab inhibition could be obtained for the product as the computational docking within InhA shows great potential.

Future compounds that could be tested may include both triclosan analogues and thiadiazole analogues as they both bind to similar regions of InhA causing inhibition. Since both triclosan and thiadiazoles have great anti-tuberculosis abilities, it would be beneficial for the analysis of producing compounds containing a thiadiazole group (**Figure 17**) and to analyse if any adaptations of the combined groups cause greater or worse anti-tuberculosis abilities.

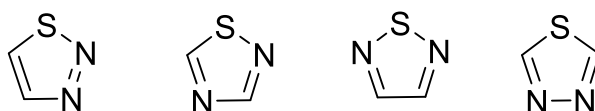


Figure 17: Chemical structure of thiadiazole and its different structural configurations

As the compounds produced with my research project contained functional group on one aromatic ring of the triclosan scaffold (**Figure 18**). The implementation of functional groups on aromatic ring B (**Figure 18**) may increase the effects of inhibition as both aromatic groups would interact with *InhA*. This may create a mimic of triclosan **11** and as triclosan has the greatest potential as a *InhA* inhibitor the effects of this would be beneficial to be calculated within GOLD docking and whole cell inhibition.

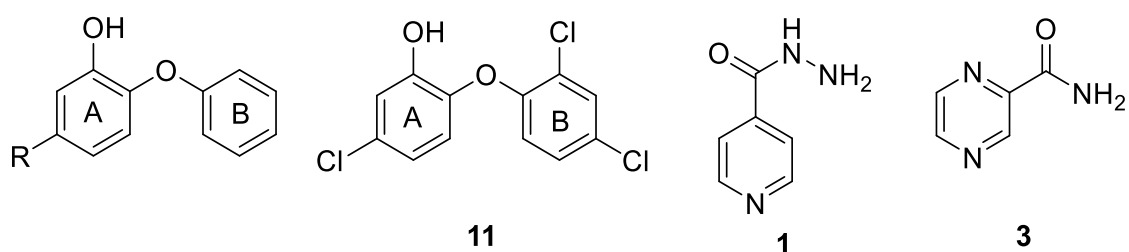


Figure 18: Generalised structure of the synthesised products within the research compared to triclosan **11**, isoniazid **1** and pyrazinamide **3**

Furthermore, it is observed that most first line drugs used for tuberculosis treatment contain nitrogen within the final compound, such as isoniazid **1** and pyrazinamide **3**. Therefore, the inclusion of a nitrogen atom in the form of pyridine or pyrazine could be beneficial as generally nitrogen containing products are known to have antimicrobial and antiviral effects.^{79, 80} The observation of the differences between using benzene within the scaffold and pyridine within the scaffold could provide many branches for future research. This could have a positive impact on the future of tuberculosis research

as current anti-tuberculosis drugs such as isoniazid **1** and pyrazinamide **3** have a pyridine ring and a pyrazine ring respectively.

Chapter 3: Experimental

3.1- Chemicals and General procedures

3.1.1 – Chemicals and Analytical techniques

For all anhydrous reactions, glassware was dried at 100 °C for 24 hours. Reactions were carried out under an atmosphere of nitrogen, unless otherwise noted. Reactions carried out in the absence of light were stated. Commercially available reagents were used throughout, without purification unless otherwise stated. Anhydrous solvents were purchased from Acros and used as supplied. Petroleum ether refers to the fraction with bp 40-60 °C. All aqueous solutions were prepared using deionised water. All chemicals were purchased from Sigma Aldrich, Fisher Scientific, Iduron Ltd, Pepceuticals Ltd or Karebay Biochem Inc, and used without further purification. Analytical thin layer chromatography was carried out on aluminium-backed plates coated with Merck Kieselgel 60 GF254.

NMR spectra analyses at the School of Chemistry, University of Nottingham and Biodiscovery institute, University of Nottingham were recorded at 298 K using Bruker AV400 (400 MHz ^1H frequency, 101 MHz ^{13}C frequency, 376 MHz ^{19}F frequency, equipped with a cryoprobe). Chemical shifts are quoted in parts per million (ppm), referenced to residual chloroform, CDCl_3 (7.26 ppm for ^1H NMR, 77.16 ppm for ^{13}C NMR) and dimethylsulfoxide, $\text{DMSO}-d_6$ (2.50 ppm for ^1H NMR, 39.51 ppm for ^{13}C NMR) as internal standards and coupling constants, J , are quoted in Hz. Multiplicities are as follows: s – singlet, m – multiplet, d – doublet, t – triplet, q – quartet; **Under reduced pressure** refers to the use of a Büchi Rotavapor with a water bath at 40 °C; **TLC plates** were visualised under UV light (254 or 365 nm) and / or stained with the appropriate staining solution (Potassium permanganate). **Mass Spectrometric** analyses at the School of Chemistry, University of Nottingham were recorded on a Bruker MicroTOF II mass spectrometer using electrospray ionization (ESI). m/z values are reported in Daltons; **HPLC** analysis used an Eclipse XDB-C18 column (9.4 × 150 mm; 5 μm) where Buffer A is H_2O (0.1% formic acid), and Buffer B is Acetonitrile. Flow rate 2 mL min^{-1} . Percentage is given as a composition of Buffer B. Variable wavelength detector set at 254 nm, 0 - 20 mins (70 → 100%).

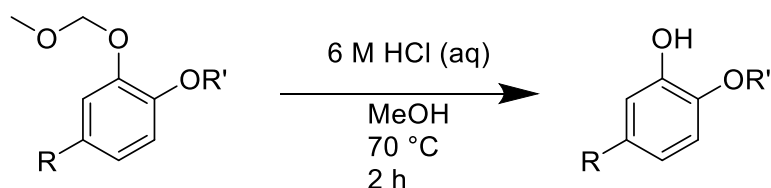
Standard PPE was used whilst carrying out all experimental synthesis; lab coats, gloves, goggles, and the use of a fume hood was required. The experimental pathways and COSHH risk assessment were checked by Professor Neil Thomas.

3.1.2 – **General Procedure A: Ether synthesis**



The alcohol derivative (1 eq) was dissolved in anhydrous DMF (3 mL per mmol⁻¹) and cooled to 0 °C. NaH (60% dispersion in mineral oil, 2 eq) was added portion-wise and the reaction mixture was stirred for 1 h. Alkyl halide derivative (1.5 eq) was added dropwise, and the solution was allowed to warm to r.t. and stirred for a further 18 h. The reaction was quenched by the addition of H₂O before being extracted with EtOAc. The combined organic layers were then washed sequentially with saturated aqueous NaHCO₃, H₂O and brine (100 mL). The organic layer was dried over MgSO₄, filtered and concentrated under reduced pressure before purification by flash column chromatography.

3.1.3 – **General Procedure B: Methoxy methyl ether deprotection**

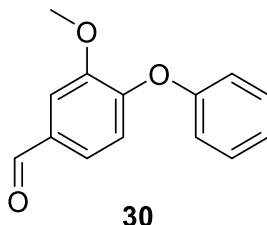


Methoxy methyl ether derivative (1 eq) was dissolved in MeOH followed by the addition of 6 M HCl (aq) (6 eq). The reaction mixture was then heated to reflux and stirred for 2 h before being allowed to cool to r.t. before being concentrated under reduced pressure. The crude material was diluted with saturated aqueous NaHCO₃ and then extracted with EtOAc (3 X 30 mL). The combined organic

layers were then dried over MgSO_4 , filtered and concentrated under reduced pressure before purification by semi-preparative reverse-phase high-performance liquid chromatography.

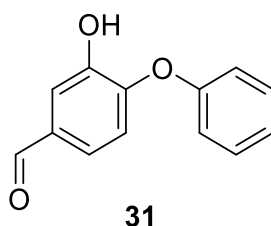
3.2 – Synthetic pathway for (3-(methoxymethoxy)-4-phenoxyphenyl)methanol, 32

3-Methoxy-4-phenoxybenzaldehyde, 30



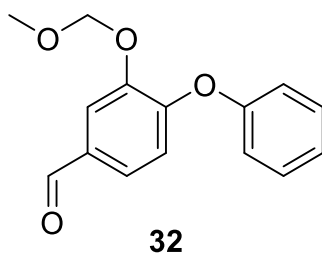
Phenol (1.14 g, 12.1 mmol) was dissolved in DMF (0.6 mL mmol^{-1}) and 4-flouro-3-methoxybenzaldehyde **29** (1.69 g, 11.0 mmol) and K_2CO_3 (1.67 g, 12.1 mmol) were added sequentially. The reaction mixture was then heated and refluxed for 18 h. The reaction was monitored via TLC, Hexane:EtOAc (0 \rightarrow 30%, r_f = 0.3). Once the reaction had reached completion the reaction was allowed to cool to room temperature before being diluted with H_2O (20 mL) and EtOAc (20 mL). The aqueous layer was extracted with EtOAc (3 X 20 mL). The organic layers were washed sequentially with saturated aqueous NaHCO_3 , H_2O and Brine (30 mL each) and dried over MgSO_4 . The dried organic solution was concentrated under reduced pressure, before being purified via flash column chromatography, the mobile phase used was Hexane:EtOAc (0 \rightarrow 30%), producing a pale-yellow oil (1.89 g, 8.28 mmol, 76%). **^1H NMR** (400 MHz, Chloroform- d) δ 9.90 (s, 1H, COH aldehyde), 7.53 (d, J = 1.9 Hz, 1H, ArH), 7.42 – 7.34 (m, 3H, ArH), 7.21 – 7.15 (m, 1H, ArH), 7.08 – 7.02 (m, 2H, ArH), 6.92 (d, J = 8.2 Hz, 1H, ArH), 3.96 (s, 3H, CH_3). **^{13}C NMR** (101 MHz, Chloroform- d) δ 190.9 (C=O aldehyde), 155.8 (ArC), 152.2 (ArC), 151.0 (ArC), 132.3 (ArC), 129.9 (ArCH), 125.7 (ArCH), 124.4 (ArCH), 119.4 (ArCH), 117.8 (ArCH), 110.6 (ArCH), 56.2 (OCH_3).

3-Hydroxy-4-phenoxybenzaldehyde, **31**



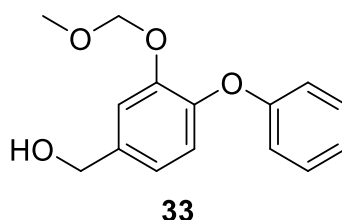
Keeping the reaction protected from light, 3-methoxy-4-phenoxybenzaldehyde **30** (1.8 g, 7.90 mmol) was dissolved in a solution of AcOH (30 mL) followed by the addition of 33% w/w HBr (23.08 mL, 132 mmol). The reaction mixture was then brought to reflux and stirred for 36 h. The reaction progress was monitored with mass spec and TLC, Hexane:EtOAc (20:3, *r_f* = 0.3). Once the reaction had reached completion, the mixture was cooled to room temperature and was poured into cold water (50 mL) with continuous stirring. The solution was then extracted with EtOAc (3 X 50 mL) and the organic layers were combined, washed with saturated NaHCO₃ solution, dried over anhydrous MgSO₄ and evaporated under reduced pressure. The crude product was obtained and purified via flash column chromatography, Hexane:EtOAc (0 → 15% EtOAc) producing a bright yellow oil (0.874 g, 4.08 mmol, 49%). ¹H NMR (400 MHz, Chloroform-*d*) δ 10.01 (s, 1H COH aldehyde), 7.71 (d, *J* = 2.0 Hz, 1H, ArH), 7.60 – 7.55 (m, 2H, ArH), 7.50 (d, *J* = 10.3 Hz, 1H, ArH), 7.39 (t, *J* = 7.4 Hz, 1H, ArH), 7.25 (d, *J* = 7.7 Hz, 2H, ArH), 7.03 (d, *J* = 8.3 Hz, 1H, ArH). ¹³C NMR (101 MHz, Chloroform-*d*) δ 190.9 (CO aldehyde), 154.8 (ArC), 149.9 (ArC), 147.2 (ArC), 132.5 (ArC), 130.3 (ArC), 125.2 (ArC), 123.6 (ArC), 119.8 (ArC), 116.3 (ArC), 116.1 (ArCO phenol).

3-(Methoxymethoxy)-4-phenoxybenzaldehyde, **32**



3-Hydroxy-4-phenoxybenzaldehyde **31** (0.8 g, 3.734 mmol) was dissolved in CH₂Cl₂ (20 mL) before the addition of DIPEA (1.95 mL, 11.203 mmol) and MOMCl (0.43 mL, 5.602 mmol). The reaction mixture was allowed to stir for 18 h. The reaction mixture was then diluted with 1 M HCl (20 mL) and extracted with EtOAc (3 × 25 mL). The combined organic layers were then dried over MgSO₄ and concentrated under reduced pressure. Purification was completed via flash column chromatography, Petroleum ether/EtOAc, (3:1 rf = 0.4), gave the title compound, **32**, as a light-yellow oil (0.83 g, 3.21 mmol, 86%). ¹H NMR (400 MHz, Chloroform-*d*) δ 9.89 (s, 1H, COH aldehyde), 7.74 (d, *J* = 1.9 Hz, 1H, ArH), 7.47 (dd, *J* = 8.3, 1.9 Hz, 1H, ArH), 7.39 – 7.32 (m, 2H, ArH), 7.18 – 7.13 (m, 1H, ArH), 7.06 – 7.00 (m, 2H, ArH), 6.96 (d, *J* = 8.3 Hz, 1H, ArH), 5.27 (s, 2H, CH₂), 3.47 (s, 3H, CH₃). ¹³C NMR (101 MHz, Chloroform-*d*) δ 190.8 (CO aldehyde), 156.0 (ArC), 152.7 (ArC), 148.5 (ArC), 132.4 (ArC), 129.9 (ArC), 125.8 (ArC), 124.3 (ArC), 119.1 (ArC), 118.8 (ArC), 116.9 (ArC), 95.4 (OCH₃O), 56.5 (OCH₃).

(3-(Methoxymethoxy)-4-phenoxyphenyl)methanol, **33**

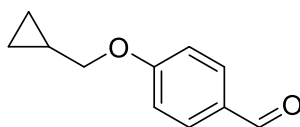


3-(Methoxymethoxy)-4-phenoxybenzaldehyde **32** (1.0 g, 3.87 mmol) was dissolved in MeOH (10 mL) and cooled to 0 °C. Once cooled, NaBH₄ (0.29 g, 7.74 mmol) was added portion-wise and the mixture was allowed to reach room temperature and stirred for 4 h. The reaction was monitored via TLC (Hexane:EtOAc, 3:1, rf = 0.35). Once the reaction had reached completion the mixture was diluted with H₂O (20 mL) before being extracted with CH₂Cl₂ (3 X 20 mL). The combined organic layers were collected and dried over MgSO₄, filtered and concentrated before purification via flash column chromatography (Hexane:EtOAc, 3:1). The product obtained was a pale-yellow oil (0.92 g, 3.53 mmol, 91%). ¹H NMR (400 MHz, DMSO-*d*₆) δ 7.34 – 7.27 (m, 2H, ArH), 7.22 (d, *J* = 1.8 Hz, 1H, ArH), 7.04 – 6.96

(m, 3H, ArH), 6.87 – 6.81 (m, 2H, ArH), 5.13 (s, 2H, CH₂), 4.49 (d, *J* = 5.7 Hz, 2H, CH₂), 3.25 (s, 3H, CH₃), OH peak observed at 3.33 ppm. ¹³C NMR (101 MHz, DMSO-*d*₆) δ 158.6 (ArC), 148.9 (ArC), 143.5 (ArC), 140.6 (ArC), 130.1 (ArC), 122.5 (ArC), 122.3 (ArC), 120.9 (ArC), 116.4 (ArC), 115.8 (ArC), 94.8 (OCH₂O), 62.9 (COH alcohol), 56.1 (OCH₃).

3.3 – Synthetic pathways of R Group

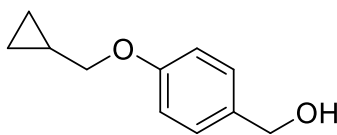
4-(Cyclopropylmethoxy)benzaldehyde, 36



36

4-Hydroxybenzaldehyde (150 mg, 1.42 mmol) was dissolved in acetone (20 mL) before (bromomethyl)cyclopropane (250 mg, 1.85 mmol) and potassium carbonate (157 mg, 1.42 mmol) were added sequentially. The solution was brought to reflux and stirred for 24 h. Following this time, the reaction mixture was filtered and evaporated under reduced pressure. The residue was then taken up in ethanol (10 mL) and evaporated under reduced pressure to afford the title compound as a pale-yellow oil (232 mg, 1.23 mmol, 93%): ¹H NMR (400 MHz, CDCl₃) δ 9.89 (1H, s, COH), 7.92-7.78 (2H, m, ArH), 7.05-6.97 (2H, m, ArH), 3.91 (2H, d, *J* = 6.9 Hz, CH₂), 1.38-1.23 (1H, m, CH), 0.77-0.61 (m, 2H, CH₂), 0.45-0.33 (2H, m, CH₂). ¹³C NMR (101 MHz, CDCl₃) δ 190.8 (C=O), 164.1 (ArC), 132.0 (2 × ArCH), 129.8 (ArC), 114.8 (2 × ArCH), 73.1 (CH₂), 10.1 (CH), 3.3 (2 × CH₂).

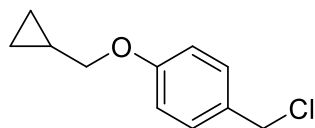
4-(Cyclopropylmethoxy)phenyl)methanol, **37**



37

4-(Cyclopropylmethoxy)benzaldehyde **36** (230 mg, 1.31 mmol) was dissolved in MeOH (5 mL) and the solution was cooled to 0 °C in an ice/water bath. Once the solution had cooled NaBH₄ (99 mg, 2.61 mmol) was added and was stirred at 0 °C for 1 h. Once the reaction had reached completion the mixture was then quenched with aqueous saturated brine (10 mL) and extracted with EtOAc (3 X 10 mL). The organic layers were combined and washed with brine (10 mL) and dried over MgSO₄ and concentrated under reduced pressure to obtain a pale yellow oil (190 mg, 1.07 mmol, 82%): ¹H NMR (400 MHz, Chloroform-*d*) δ 7.31 – 7.26 (m, 2H, ArH), 6.92 – 6.87 (m, 2H, ArH), 4.61 (s, 2H, CH), 3.80 (d, *J* = 6.9 Hz, 2H, CH alkyl), 1.35 – 1.20 (m, 1H, CH alkyl), 0.71 – 0.56 (m, 2H, CH alkyl), 0.35 (dt, *J* = 6.1, 4.6 Hz, 2H, CH alkyl), OH-proton not observed. ¹³C NMR (101 MHz, DMSO-*d*₆) δ 158.0 (ArC), 134.8 (2 × ArCH), 128.3 (ArC), 114.5 (2 × ArCH), 72.4 (CH₂), 63.0 (COH), 10.7 (CH), 3.5 (2 X CH₂).

4-(Cyclopropylmethoxy)benzyl chloride, **38**



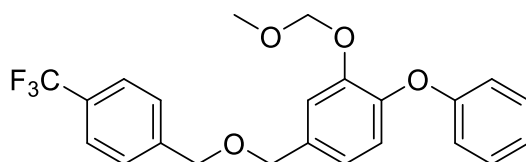
38

(4-(Cyclopropylmethoxy)benzyl)methanol **37** (189 mg, 1.07 mmol) was dissolved in Et₂O (3 mL). Then SOCl₂ (0.15 mL, 2.07 mmol) was added dropwise at room temperature and was stirred at room temperature for 2 h. The reaction progress was monitored via TLC (Hexane:EtOAc, 9:1, *r_f* = 0.6). After the reaction had reached completion, the solution was diluted with EtOAc (10 mL) and washed with

water (3 X 10 mL). The organic layer was dried with MgSO₄, filtered and concentrated under reduced pressure to give a pale-yellow oil (192 mg, 0.976 mmol, 92%): ¹H NMR (400 MHz, DMSO-*d*₆) δ 7.37 – 7.31 (m, 2H, ArH), 6.95 – 6.88 (m, 2H, ArH), 4.72 (s, 2H, CH), 3.82 (d, *J* = 7.0 Hz, 2H CH alkyl), 1.29 – 1.12 (m, 1H CH alkyl), 0.63 – 0.49 (m, 2H CH alkyl), 0.39 – 0.24 (m, 2H CH alkyl). ¹³C NMR (101 MHz, DMSO-*d*₆) δ 159.1 (ArC), 130.8 (2 X ArCH), 129.9 (ArC), 114.9 (2 X ArCH), 72.5 (CH₂), 46.8 (CCI), 10.6 (CH), 3.5 (2 X CH₂).

3.4 – R Group Coupling to (3-(methoxymethoxy)-4-phenoxyphenyl)methanol, **33**

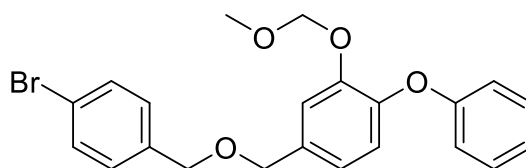
2-(Methoxymethoxy)-1-phenoxy-4-(((4-(trifluoromethyl)benzyl)oxy)methyl)benzene, **43**



43

The title compound was synthesised according to **General Procedure A** from compound **33** (50 mg, 0.200 mmol), 4-(trifluoromethyl)benzyl chloride **39** (56 mg, 0.300 mmol) and NaH (60% dispersion in mineral oil, 0.015 g, 0.400 mmol). Purification was performed by flash column chromatography (Hexane/EtOAc, 3:1, *r_f* = 0.6) to yield a colourless oil (52.6 mg, 0.134 mmol, 65%): ¹H NMR (400 MHz, DMSO-*d*₆) δ 7.72 (d, *J* = 8.2 Hz, 2H, ArH), 7.63 – 7.55 (m, 2H, ArH), 7.43 (d, *J* = 8.1 Hz, 1H, ArH), 7.35 – 7.25 (m, 2H, ArH), 7.04 (d, *J* = 6.7 Hz, 2H, ArH), 6.89 – 6.83 (m, 1H, ArH), 5.15 (s, 1H, CH₂), 4.66 (t, *J* = 6.4 Hz, 2H, CH₂ ether), 4.56 (s, 1H, CH₂ ether), 3.25 (s, 2H, CH₃). ¹³C NMR (101 MHz, DMSO-*d*₆) δ 157.9 (ArC), 148.5 (ArC), 143.9 (ArC), 143.3 (ArC), 135.5 (ArC), 129.7 (ArC), 127.9, (ArC) 127.4 (ArC), 125.2 (ArC), 124.8 (CF), 122.2 (ArC), 121.7 (ArC), 116.5 (ArC), 116.1 (ArC), 94.5 (OCH₂O), 71.3 (CH₂), 70.6 (CH₂), 55.7 (OCH₃). ¹⁹F NMR (377 MHz, DMSO-*d*₆) δ -60.91 (CF₃).

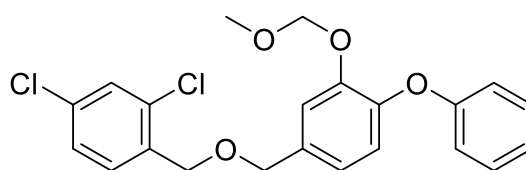
4-(((4-Bromobenzyl)oxy)methyl)-2-(methoxymethoxy)-1-phenoxybenzene, 45



45

The title compound was synthesised according to **General Procedure A** from compound **33** (0.1 g, 0.384 mmol), 4-bromobenzyl chloride **41** (0.12 g, 0.576 mmol) and NaH (60% dispersion in mineral oil, 0.03 g, 0.768 mmol). Purification was performed by flash column chromatography (Hexane/EtOAC, 3:1, r_f = 0.4) to yield a colourless oil (194 mg, 0.452 mmol, 98%): $^1\text{H NMR}$ (400 MHz, $\text{DMSO-}d_6$) δ 7.61 – 7.49 (m, 1H, ArH), 7.36 – 7.29 (m, 2H, ArH), 7.31 – 7.22 (m, 1H, ArH), 7.07 – 6.99 (m, 2H, ArH), 6.89 – 6.83 (m, 1H, ArH), 5.14 (s, 1H, CH_2), 4.52 (d, J = 6.2 Hz, 2H, CH_2 ether). $^{13}\text{C NMR}$ (101 MHz, $\text{DMSO-}d_6$) δ 157.9 (ArC), 148.5 (ArC), 137.8 (ArC), 135.6 (ArC), 131.2 (ArC), 129.7 (ArC), 129.7 (ArC), 122.2 (ArC), 121.7 (ArC), 116.1 (ArC), 94.5 (OCH_2O), 71. (CH_2), 70.6 (CH_2), 55.6 (OCH_3), 45.2 (CBr).

2,4-Dichloro-1-(((3-(methoxymethoxy)-4-phenoxybenzyl)oxy)methyl)benzene, 46



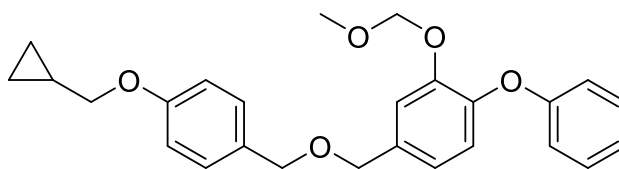
46

The title compound was synthesised according to **General Procedure A** from compound **33** (0.1 g, 0.384 mmol), 2,4 – dichlorobenzyl chloride **42** (0.11 g, 0.576 mmol) and NaH (60% dispersion in mineral oil, 0.03 g, 0.768 mmol). Purification was performed by flash column chromatography (Hexane/EtOAC, 3:1, r_f = 0.6) to yield a pale-yellow oil (161 mg, 0.384 mmol, 91%). $^1\text{H NMR}$ (400 MHz, $\text{DMSO-}d_6$) δ 7.61 (d, J = 2.1 Hz, 1H, ArH), 7.56 (d, J = 8.3 Hz, 1H, ArH), 7.45 (dd, J = 8.3, 2.1 Hz, 1H, ArH),

7.35 – 7.24 (m, 3H, ArH), 7.08 – 6.98 (m, 3H, ArH), 6.89 – 6.82 (m, 2H, ArH), 5.14 (s, 2H, CH₂), 4.59 (d, $J = 10.2$ Hz, 4H, CH₂ ether), 3.25 (s, 3H, CH₃), 1.98 (s, 1H, CH). ¹³C NMR (101 MHz, DMSO-*d*₆) δ 158.3 (ArC), 148.9 (ArC), 144.5 (ArC), 135.8 (ArC), 135.4 (ArC), 133.4 (ArC), 131.3 (ArC), 130.1 (ArC), 129.1 (ArC), 127.8 (ArC), 122.7 (ArC), 117.1 (ArC), 116.6 (ArC), 94.9 (OCH₂O), 72.0 (CH₂), 68.6 (CH₂), 60.2 (OCH₃), 56.1 (CCl), 43.4 (CCl).

4-(((4-(Cyclopropylmethoxy)benzyl)oxy)methyl)-2-(methoxymethoxy)-1-phenoxybenzene,

47

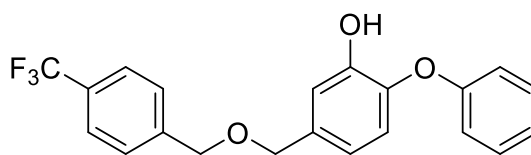


47

The title compound was synthesised according to **General Procedure A** from compound **33** (0.1 g, 0.384 mmol), 4-(cyclopropylmethoxy)benzyl chloride **38** (0.11 g, 0.576 mmol) and NaH (60% dispersion in mineral oil, 0.03 g, 0.768 mmol). Purification was performed by flash column chromatography (Hexane/EtOAc, 3:1, $r_f = 0.5$) to yield a yellow oil (115 mg, 0.273 mmol, 68%). ¹H NMR (400 MHz, Chloroform-*d*) δ 7.36 – 7.25 (m, 5H, ArH), 7.11 – 6.87 (m, 7H, ArH), 5.19 (s, 2H, CH₂), 4.53 (d, $J = 11.1$ Hz, 4H, CH₂ ether), 3.83 (d, $J = 6.9$ Hz, 2H, CH₂ether), 3.43 (s, 3H, CH₃), 1.36 – 1.25 (m, 1H, CH), 0.70 – 0.64 (m, 2H, CH₂), 0.40 – 0.36 (m, 2H, CH₂). ¹³C NMR (101 MHz, Chloroform-*d*) δ 158.7 (ArC), 148.8 (ArC), 145.3 (ArC), 135.3 (ArC), 130.1 (ArC), 129.5 (ArC), 122.5 (ArC), 122.2 (ArC), 121.4 (ArC), 117.1 (ArC), 114.5 (ArC), 95.3 (OCH₂O), 72.8 (CH₂), 72.0 (CH₂), 71.4 (CH₂), 56.3 (OCH₃).

3.5 – MOMCl Deprotection

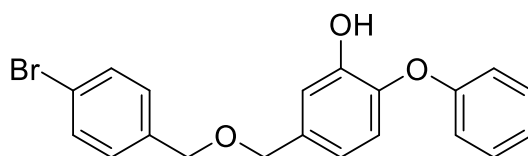
2-Phenoxy-5-(((4-(trifluoromethyl)benzyl)oxy)methyl)phenol, 48



48

The title compound was synthesised according to **General Procedure B** from compound **43** (0.06 g, 0.143 mmol) and 6 M HCl (aq) (0.029 mL, 0.860 mmol). Purification was performed by semi-preparative reverse-phase high-performance liquid chromatography to yield the title compound as a brown solid (11 mg, 0.0294 mmol, 20%) and after NMR analysis the product stayed in a clear oil state. **¹H NMR** (400 MHz, Chloroform-*d*): δ 7.60 (d, J = 8.1 Hz, 2H, ArH), 7.47 (d, J = 8.0 Hz, 2H, ArH), 7.33 (dd, J = 8.5, 7.5 Hz, 2H, ArH), 7.11 (t, J = 7.4 Hz, 1H, ArH), 7.06 (d, J = 1.6 Hz, 1H, ArH), 7.03 – 6.99 (m, 2H, ArH), 6.86 – 6.80 (m, 2H, ArH), 4.60 (s, 2H, CH₂ ether), 4.50 (s, 2H, CH₂ ether). **¹³C NMR** (101 MHz, Chloroform-*d*): δ 156.7 (ArCOH), 147.5 (ArC), 143.1 (ArC), 142.4 (ArC), 134.6 (ArC), 129.9 (ArC), 127.7 (ArC), 125.4 (ArC), 125.3 (ArC), 123.7 (CF), 120.0 (ArC), 118.7 (ArC), 118.0 (ArC), 115.6 (ArC), 72.1 (CH₂), 71.3 (CH₂). **¹⁹F NMR** (377 MHz, Chloroform-*d*): δ -62.49 (CF₃). **HPLC** Rt: ~10 Mins

5-(((4-bromobenzyl)oxy)methyl)-2-phenoxyphenol, 50

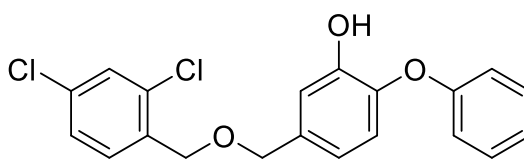


50

The title compound was synthesised according to **General Procedure B** from compound **45** (0.19 g, 0.443 mmol) and 6 M HCl (aq) (0.10 mL, 2.66 mmol). Purification was performed by semi-preparative reverse-phase high-performance liquid chromatography to yield the title compound as a pink solid (59.4 mg, 0.154 mmol, 35%): **¹H NMR** (400 MHz, Chloroform-*d*) δ 7.46 (d, J = 8.4 Hz, 2H, ArH), 7.32

(dd, $J = 8.6, 7.5$ Hz, 2H, ArH), 7.22 (s, 1H, ArH), 7.11 (t, $J = 7.4$ Hz, 1H, ArH), 7.04 (d, $J = 1.7$ Hz, 1H, ArH), 7.00 (dd, $J = 8.7, 1.0$ Hz, 2H, ArH), 6.86 – 6.78 (m, 2H, ArH), 4.50 (s, 2H, CH₂ ether), 4.47 (s, 2H, CH₂ ether). ¹³C NMR (101 MHz, Chloroform-*d*) δ 156.7 (ArCOH), 147.4 (ArC), 142.9 (ArC), 137.2 (ArC), 134.7 (ArC), 131.5 (ArC), 129.9 (ArC), 129.4 (ArC), 123.7 (ArC), 121.5 (ArC), 119.9 (ArC), 118.7 (ArC), 117.9 (ArC), 115.6 (ArC), 71.7 (CH₂), 71.3 (CH₂), 1.0 (CBr). HPLC Rt ~10 mins. Melting point: 61 - 62 °C

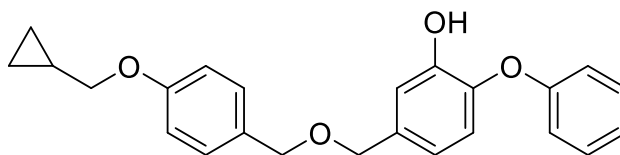
2,4-dichloro-1-(((3-(methoxymethoxy)-4-phenoxybenzyl)oxy)methyl)benzene, 51



51

The title compound was synthesised according to **General Procedure B** from compound **46** (0.16 g, 0.382 mmol) and 6 M HCl (aq) (0.09 mL, 2.29 mmol). Purification was performed by semi-preparative reverse-phase high-performance liquid chromatography to yield the title compound as brown/pink oil (52 mg, 0.139 mmol, 36%). ¹H NMR (400 MHz, Chloroform-*d*) δ 7.51 (d, $J = 8.3$ Hz, 1H, ArH), 7.38 (ddd, $J = 13.9, 6.7, 2.0$ Hz, 3H, ArH), 7.29 (dd, $J = 8.3, 2.1$ Hz, 1H, ArH), 7.18 – 7.10 (m, 2H, ArH), 7.07 – 7.02 (m, 2H, ArH), 6.88 (d, $J = 1.7$ Hz, 2H, ArH), 4.62 (d, $J = 21.6$ Hz, 4H, CH₂ ether). ¹³C NMR (101 MHz, Chloroform-*d*) δ 156.7 (ArCOH), 147.4 (ArC), 143.1 (ArC), 134.7 (ArC), 134.6 (ArC), 133.7 (ArC), 133.4 (ArC), 129.9 (ArC), 129.9 (ArC), 129.0 (ArC), 127.1 (ArC), 123.7 (ArC), 119.9 (ArC), 118.7 (ArC), 118.0 (ArC), 115.6 (ArC), 72.4 (CH₂), 68.7 (CH₂). HPLC Rt ~12 min

4-(((4-(cyclopropylmethoxy)benzyl)oxy)methyl)-2-(methoxymethoxy)-1-phenoxybenzene,
52



52

The title compound was synthesised according to **General Procedure B** from compound **47** (0.1 g, 0.238 mmol) and 6 M HCl (aq) (0.05 mL, 1.43 mmol). Purification was performed by semi-preparative reverse-phase high-performance liquid chromatography to yield the title compound as a yellow oil (5 mg, 0.0133 mmol, 6%). **¹H NMR** (400 MHz, Chloroform-*d*) δ 7.40 – 7.34 (m, 2H, ArH), 7.33 – 7.29 (m, 2H, ArH), 7.17 – 7.11 (m, 1H, ArH), 7.09 (d, *J* = 1.8 Hz, 1H, ArH), 7.06 – 7.02 (m, 2H, ArH), 6.94 – 6.89 (m, 2H, ArH), 6.88 – 6.85 (m, 2H, ArH), 5.59 (s, 1H, ArOH), 4.50 (d, *J* = 15.1 Hz, 4H, CH₂ ether), 3.83 (d, *J* = 6.9 Hz, 2H, CH₂ ether), 0.71 – 0.63 (m, 2H, CH alkane), 0.37 (dt, *J* = 6.1, 4.6 Hz, 2H, CH alkane). **HPLC** Rt ~10 mins.

References

- (1) Smith, I. Mycobacterium tuberculosis Pathogenesis and Molecular Determinants of Virulence. *Clin. Microbiol. Rev.* **2003**, *16*, 463-496.
- (2) World Health, O. *Global Tuberculosis Rep. 2019*; World Health Organization, 2019.
- (3) Seung, K. J.; Keshavjee, S.; Rich, M. L. Multidrug-Resistant Tuberculosis and Extensively Drug-Resistant Tuberculosis. *Cold Spring Harbor Perspect. Med.* **2015**, *5*, a017863-a017863.
- (4) Mishra, A.; Surolia, A. Mycobacterium tuberculosis: Surviving and Indulging in an Unwelcoming Host: HISTORY OF TUBERCULOSIS IN MANKIND. *IUBMB life* **2018**, *70*, 917-925.
- (5) Delogu, G.; Sali, M.; Fadda, G. The biology of mycobacterium tuberculosis infection. *Mediterr. J. Hematol. Infect. Dis.* **2013**, *5*, e2013070-e2013070.
- (6) Rao, M.; Ippolito, G.; Mfinanga, S.; Ntoumi, F.; Yeboah-Manu, D.; Vilaplana, C.; Zumla, A.; Maeurer, M. Latent TB Infection (LTBI) – Mycobacterium tuberculosis pathogenesis and the dynamics of the granuloma battleground. *Int. J. Infect. Dis.* **2019**, *80*, S58-S61.
- (7) Vijayan, K. V.; Karthigeyan, K. P.; Tripathi, S.; Hanna, L. E. Pathophysiology of CD4+ T-Cell depletion in HIV-1 and HIV-2 infections. *Front. Immunol.* **2017**, *8*, 580-580.
- (8) Gambon-Deza, F.; Carracedo, M. P.; Mota, T. C.; Santiago, J. M. Lymphocyte populations during tuberculosis infection: V beta repertoires. *Infect. Immun.* **1995**, *63*, 1235-1240.
- (9) Bandyopadhyay, A.; Palepu, S.; Bandyopadhyay, K.; Handu, S. COVID-19 and tuberculosis co-infection: a neglected paradigm. *Monaldi Arch. Chest Dis.* **2020**, *90*.
- (10) Rădulescu, A. Tuberculosis and Covid-19 Co-Infection – Clinical Characteristics. *Acta Med. Transilv.* **2021**, *26*, 17-19.
- (11) Alderwick, L. J.; Harrison, J.; Lloyd, G. S.; Birch, H. L. The Mycobacterial Cell Wall—Peptidoglycan and Arabinogalactan. *Cold Spring Harbor Perspect. Med.* **2015**, *5*, a021113.
- (12) Howard, S. T.; Byrd, T. F. The rapidly growing mycobacteria: saprophytes and parasites. *Microbes Infect.* **2000**, *2*, 1845-1853.
- (13) Collins, F. M. Mycobacterial disease, immunosuppression, and acquired immunodeficiency syndrome. *Clin. Microbiol. Rev.* **1989**, *2*, 360-377.
- (14) Brudey, K.; Driscoll, J. R.; Rigouts, L.; Prodinger, W. M.; Gori, A.; Al-Hajj, S. A.; Allix, C.; Aristimuño, L.; Arora, J.; Baumanis, V. Mycobacterium tuberculosis complex genetic diversity: Mining the fourth international spoligotyping database (SpolDB4) for classification, population genetics and epidemiology. *BMC Microbiol.* **2006**, *6*, 23-23.
- (15) Prozorov, A. A.; Danilenko, V. N. Mycobacteria of the tuberculosis complex: Genomics, molecular epidemiology, and evolution trends. *Biol. Bull. Rev.* **2011**, *1*, 483-495.
- (16) Etymologia: M. bovis. *Emerg. Infect. Dis.* **2015**, *21* (3), 443-443.
- (17) Grange, J. M. Mycobacterium bovis infection in human beings. *J. Tuberc. Res.* **2001**, *81*, 71-77.
- (18) Lan, Z.; Bastos, M.; Menzies, D. Treatment of human disease due to Mycobacterium bovis: a systematic review. *Eur. Respir. J.* **2016**, *48*, 1500-1503.
- (19) Dankner, W. M.; Davis, C. E. Mycobacterium bovis as a Significant Cause of Tuberculosis in Children Residing Along the United States-Mexico Border in the Baja California Region. *J. Pediatr.* **2000**, *105* (6), e79-e79. DOI: 10.1542/peds.105.6.e79.
- (20) Michel, A. L.; Müller, B.; van Helden, P. D. Mycobacterium bovis at the animal–human interface: A problem, or not? *Vet. Microbiol.* **2010**, *140*, 371-381.
- (21) Ueyama, M.; Chikamatsu, K.; Aono, A.; Murase, Y.; Kuse, N.; Morimoto, K.; Okumura, M.; Yoshiyama, T.; Ogata, H.; Yoshimori, K. Sub-speciation of Mycobacterium tuberculosis complex from tuberculosis patients in Japan. *J. Tuberc.* **2013**, *94* (1), 15-19.
- (22) Buddle, B. M.; Parlane, N. A.; Keen, D. L.; Aldwell, F. E.; Pollock, J. M.; Lightbody, K.; Andersen, P. Differentiation between Mycobacterium bovis BCG-vaccinated and M. bovis-infected cattle by using recombinant mycobacterial antigens. *Clin. Diagn. Lab. Immunol.* **1999**, *6*, 1-5.

- (23) Rentsch, C. A.; Birkhäuser, F. D.; Biot, C.; Gsponer, J. R.; Bisiaux, A.; Wetterauer, C.; Lagranderie, M.; Marchal, G.; Orgeur, M.; Bouchier, C. Bacillus Calmette-Guérin Strain Differences Have an Impact on Clinical Outcome in Bladder Cancer Immunotherapy. *Eur. Urol.* **2014**, *66*, 677-688.
- (24) Magno, C.; Melloni, D.; Galì, A.; Mucciardi, G.; Nicocia, G.; Morandi, B.; Melioli, G.; Ferlazzo, G. The anti-tumor activity of bacillus Calmette-Guerin in bladder cancer is associated with an increase in the circulating level of interleukin-2. *Immunol. Lett.* **2002**, *81*, 235-238.
- (25) Loddenkemper, R.; Lipman, M.; Zumla, A. Clinical aspects of adult tuberculosis. *Cold Spring Harbor Perspect. Med.* **2016**, *6*, a017848-a017848.
- (26) Narita, M.; Spitters, C. Tuberculosis in Travelers and Immigrants. *J. Korean Med. Assoc.*; **2017**; 356-370.
- (27) Zhu, Q.-Q.; Wu, Q.; Wang, A.-M.; Bao, F.-J.; Zhang, Y.-Z.; Liu, J.; Yan, J.-W.; Fang, X.-H.; Li, L.; Zhang, Z.-K. Epidemiological characteristics of pulmonary tuberculosis in Anhui Province, Eastern China from 2013 to 2018. *PloS one* **2020**, *15*, e0237311-e0237311.
- (28) Ray, S.; Talukdar, A.; Kundu, S.; Khanra, D.; Sonthalia, N. Diagnosis and management of miliary tuberculosis: current state and future perspectives. *Ther. Clin. Risk Manag.* **2013**, *9*, 9-26.
- (29) Namburete, E. Detection of KatG/InhA Mutation to Guide Isoniazid and Ethionamide Use for Drug-resistant Tuberculosis. *Open forum Infect. Dis.* **2017**, *4*, S619-S619.
- (30) Click, E. S.; Kurbatova, E. V.; Alexander, H.; Dalton, T. L.; Chen, M. P.; Posey, J. E.; Ershova, J.; Cegielski, J. P. Isoniazid and Rifampin-Resistance Mutations Associated With Resistance to Second-Line Drugs and With Sputum Culture Conversion. *J. Infect. Dis.* **2020**, *221*, 2072-2082.
- (31) Kundu, M. The role of two-component systems in the physiology of Mycobacterium tuberculosis. *IUBMB life* **2018**, *70*, 710-717.
- (32) Kalscheuer, R.; Palacios, A.; Anso, I.; Cifuentes, J.; Anguita, J.; Jacobs, J. W. R.; Guerin, M. E.; Prados-Rosales, R. The Mycobacterium tuberculosis capsule: a cell structure with key implications in pathogenesis. *Biochem. J.* **2019**, *476*, 1995-2016.
- (33) Abrahams, K. A.; Besra, G. S. Mycobacterial cell wall biosynthesis: a multifaceted antibiotic target. *Int. J. Parasitol.* **2018**, *145*, 116-133.
- (34) Marrakchi, H.; Lanéelle, M.-A.; Daffé, M. Mycolic Acids: Structures, Biosynthesis, and Beyond. *Chem. Biol.* **2014**, *21*, 67-85.
- (35) Indrigo, J.; Hunter, R. L., Jr.; Actor, J. K. Influence of trehalose 6,6'-dimycolate (TDM) during mycobacterial infection of bone marrow macrophages. *Microbiol.* **2002**, *148*, 1991-1998.
- (36) Hsu, F.-F.; Wohlmann, J.; Turk, J.; Haas, A. Structural Definition of Trehalose 6-Monomycolates and Trehalose 6,6'-Dimycolates from the Pathogen Rhodococcus equi by Multiple-Stage Linear Ion-Trap Mass Spectrometry with Electrospray Ionization. *J. Am. Soc. Mass Spectrom.* **2011**, *22*, 2160-2170.
- (37) Vincent, A. T.; Nyongesa, S.; Morneau, I.; Reed, M. B.; Tocheva, E. I.; Veyrier, F. J. The Mycobacterial Cell Envelope: A Relict From the Past or the Result of Recent Evolution? *Front. Microbiol.* **2018**, *9*, 2341-2341.
- (38) Squeglia, F.; Ruggiero, A.; Berisio, R. Chemistry of Peptidoglycan in Mycobacterium tuberculosis Life Cycle: An off-the-wall Balance of Synthesis and Degradation. *Chem. Eur. J.* **2018**, *24*, 2533-2546.
- (39) Maitra, A.; Munshi, T.; Healy, J.; Martin, L. T.; Vollmer, W.; Keep, N. H.; Bhakta, S. Cell wall peptidoglycan in Mycobacterium tuberculosis: An Achilles' heel for the TB-causing pathogen. *FEMS Microbiol. Rev.* **2019**, *43*, 548-575.
- (40) Usha, V.; Lloyd, A. J.; Lovering, A. L.; Besra, G. S. Structure and function of Mycobacterium tuberculosis meso-diaminopimelic acid (DAP) biosynthetic enzymes. *FEMS Microbiol. Rev.* **2012**, *330*, 10-16.
- (41) Harrison, J.; Lloyd, G.; Joe, M.; Lowary, T. L.; Reynolds, E.; Walters-Morgan, H.; Bhatt, A.; Lovering, A.; Besra, G. S.; Alderwick, L. J. Lcp1 Is a Phosphotransferase Responsible for Ligating

- Arabinogalactan to Peptidoglycan in *Mycobacterium tuberculosis*. *MBio. J.* **2016**, *7*, e00972-00916.
- (42) Batt, S. M.; Burke, C. E.; Moorey, A. R.; Besra, G. S. Antibiotics and resistance: the two-sided coin of the mycobacterial cell wall. *Cell Surf.* **2020**, *6*, 100044-100044.
 - (43) Mikusova, K.; Slayden, R. A.; Besra, G. S.; Brennan, P. J. Biogenesis of the mycobacterial cell wall and the site of action of ethambutol. *J. Antimicrob. Agents Chemother.* **1995**, *39*, 2484-2489.
 - (44) Takayama, K.; Wang, C.; Besra, G. S. Pathway to Synthesis and Processing of Mycolic Acids in *Mycobacterium tuberculosis*. *Clin. Microbiol. Rev.* **2005**, *18*, 81-101.
 - (45) Zhao, J.; Siddiqui, S.; Shang, S.; Bian, Y.; Bagchi, S.; He, Y.; Wang, C.-R. Mycolic acid-specific T cells protect against *Mycobacterium tuberculosis* infection in a humanized transgenic mouse model. *eLife* **2015**, *4*.
 - (46) Nataraj, V.; Varela, C.; Javid, A.; Singh, A.; Besra, G. S.; Bhatt, A. Mycolic acids: deciphering and targeting the Achilles' heel of the tubercle bacillus: Mycolic acids and the tubercle bacillus. *Mol. Microbiol. J.* **2015**, *98*, 7-16.
 - (47) Verschoor, J. A.; Baird, M. S.; Grooten, J. Towards understanding the functional diversity of cell wall mycolic acids of *Mycobacterium tuberculosis*. *Prog. Lipid Res.* **2012**, *51*, 325-339.
 - (48) Sridharan, S.; Wang, L.; Brown, A. K.; Dover, L. G.; Kremer, L.; Besra, G. S.; Sacchettini, J. C. X-Ray Crystal Structure of *Mycobacterium tuberculosis* β -Ketoacyl Acyl Carrier Protein Synthase II (mtKasB). *J. Mol. Biol.* **2007**, *366*, 469-480.
 - (49) Qureshi, N.; Takayama, K.; Jordi, H. C.; Schnoes, H. K. Characterization of the purified components of a new homologous series of alpha-mycolic acids from *Mycobacterium tuberculosis* H37Ra. *J. Biol. Chem.* **1978**, *253*, 5411-5417.
 - (50) Dkhar, H. K.; Nanduri, R.; Mahajan, S.; Dave, S.; Saini, A.; Somavarapu, A. K.; Arora, A.; Parkesh, R.; Thakur, K. G.; Mayilraj, S. *Mycobacterium tuberculosis* keto-mycolic acid and macrophage nuclear receptor TR4 modulate foamy biogenesis in granulomas: a case of a heterologous and noncanonical ligand-receptor pair. *J. Immunol.* **2014**, *193*, 295-305.
 - (51) Pawełczyk, J.; Kremer, L. The Molecular Genetics of Mycolic Acid Biosynthesis. *J. Microbiol. spectrum* **2014**, *2*, MGM2-0003-2013.
 - (52) Moody, D. B. How T cells grasp mycobacterial lipid antigens. *Proc. Natl. Acad. Sci. - PNAS* **2017**, *114*, 13312-13314.
 - (53) Yuan, Y.; Zhu, Y.; Crane, D. D.; Barry Iii, C. E. The effect of oxygenated mycolic acid composition on cell wall function and macrophage growth in *Mycobacterium tuberculosis*. *Mol. Microbiol.* **1998**, *29*, 1449-1458.
 - (54) Vilchèze, C. Mycobacterial cell wall: A source of successful targets for old and new drugs. *Appl. Sci.* **2020**, *10*, 2278.
 - (55) Glickman, M. S. The *mmaA2* gene of *Mycobacterium tuberculosis* encodes the distal cyclopropane synthase of the alpha-mycolic acid. *J. Biol. Chem.* **2003**, *278*, 7844-7849.
 - (56) Blomberg, B.; Spinaci, S.; Fourie, B.; Laing, R. The rationale for recommending fixed-dose combination tablets for treatment of tuberculosis. *Bull. World H. Org.* **001**, *79*, 61-68.
 - (57) Hu, Y.-Q.; Zhang, S.; Zhao, F.; Gao, C.; Feng, L.-S.; Lv, Z.-S.; Xu, Z.; Wu, X. Isoniazid derivatives and their anti-tubercular activity. *Eur. J. Med. Chem.* **2017**, *133*, 255-267.
 - (58) Erokhina, M. V.; Kuryina, A. V.; Onishchenko, G. E. Mitochondria are targets for the antituberculosis drug rifampicin in cultured epithelial cells. *Biochem.* **2013**, *78*, 1155-1163.
 - (59) Shi, W.; Zhang, X.; Jiang, X.; Yuan, H.; Lee, J. S.; Barry, r. C. E.; Wang, H.; Zhang, W.; Zhang, Y. Pyrazinamide Inhibits Trans-Translation in *Mycobacterium tuberculosis*. *Sci.* **2011**, *333*, 1630-1632.
 - (60) Zimhony, O.; Vilcheze, C.; Arai, M.; Welch, J. T.; Jacobs, W. R. Pyrazinoic Acid and Its n-Propyl Ester Inhibit Fatty Acid Synthase Type I in Replicating Tubercle Bacilli. *Antimicrob. Agents Chemother.* **2007**, *51*, 752-754.

- (61) Zhang, L.; Zhao, Y.; Gao, Y.; Wu, L.; Gao, R.; Zhang, Q.; Wang, Y.; Wu, C.; Wu, F.; Gurcha, S. S. Structures of cell wall arabinosyltransferases with the anti-tuberculosis drug ethambutol. *Sci.* **2020**, *368*, 1211-1219.
- (62) Korycka-Machata, M.; Rumijowska-Galewicz, A.; Dziadek, J. The effect of ethambutol on mycobacterial cell wall permeability to hydrophobic compounds. *Pol. J. Microbiol.* **2005**, *54*, 5-11.
- (63) Jena, L.; Deshmukh, S.; Waghmare, P.; Kumar, S.; Harinath, B. C. Study of mechanism of interaction of truncated isoniazid–nicotinamide adenine dinucleotide adduct against multiple enzymes of Mycobacterium tuberculosis by a computational approach. *Int. J. Mycobacteriol.* **2015**, *4*, 276-283.
- (64) Scior, T.; Meneses Morales, I.; Garcés Eisele, S. J.; Domeyer, D.; Laufer, S. Antitubercular Isoniazid and Drug Resistance of Mycobacterium tuberculosis - A Review. *Arch. Pharm.* **2002**, *335*, 511-525.
- (65) Martínez-Hoyos, M.; Perez-Herran, E.; Gulten, G.; Encinas, L.; Álvarez-Gómez, D.; Alvarez, E.; Ferrer-Bazaga, S.; García-Pérez, A.; Ortega, F.; Angulo-Barturen, I. Antitubercular drugs for an old target: GSK693 as a promising InhA direct inhibitor. *EBioMed.* **2016**, *8*, 291-301.
- (66) Timmins, G. S.; Deretic, V. Mechanisms of action of isoniazid. *Mol. Microbio.* **2006**, *62*, 1220-1227.
- (67) Vilchèze, C.; Jacobs, J. W. R. Resistance to Isoniazid and Ethionamide in Mycobacterium tuberculosis: Genes, Mutations, and Causalities. *Microbio. spect.* **2014**, *2*, MGM2-0014-2013.
- (68) Seifert, M.; Catanzaro, D.; Catanzaro, A.; Rodwell, T. C. Genetic mutations associated with isoniazid resistance in Mycobacterium tuberculosis: a systematic review. *PloS one* **2015**, *10*, e0119628-e0119628.
- (69) Lempens, P.; Meehan, C. J.; Vandellannoote, K.; Fissette, K.; de Rijk, P.; Van Deun, A.; Rigouts, L.; de Jong, B. C. Isoniazid resistance levels of Mycobacterium tuberculosis can largely be predicted by high-confidence resistance-conferring mutations. *Sci. Rep.* **2018**, *8*, 3246-3249.
- (70) Teixeira, V. H.; Ventura, C.; Leitão, R.; Ràfols, C.; Bosch, E.; Martins, F.; Machuqueiro, M. Molecular Details of INH-C10 Binding to wt KatG and Its S315T Mutant. *Mol. Pharm.* **2015**, *12*, 898-909.
- (71) Quan, D.; Nagalingam, G.; Payne, R.; Triccas, J. A. New tuberculosis drug leads from naturally occurring compounds. *Int. J. Infect. Dis.* **2016**, *56*, 212-220.
- (72) Vosátka, R.; Krátký, M.; Vinšová, J. Triclosan and its derivatives as antimycobacterial active agents. *Eur. J. Pharm. Sci.* **2018**, *114*, 318-331.
- (73) Chetty, S.; Armstrong, T.; Sharma Kharkwal, S.; Drewe, W. C.; De Matteis, C. I.; Evangelopoulos, D.; Bhakta, S.; Thomas, N. R. New InhA Inhibitors Based on Expanded Triclosan and Di - Triclosan Analogues to Develop a New Treatment for Tuberculosis. *Pharm.* **2021**, *14*, 361.
- (74) Armstrong, T.; Lamont, M.; Lanne, A.; Alderwick, L. J.; Thomas, N. R. Inhibition of Mycobacterium tuberculosis InhA: Design, synthesis and evaluation of new di-triclosan derivatives. *Bioorganic Med. Chem.* **2020**, *28*, 115744-115744.
- (75) Parikh, S. L.; Xiao, G.; Tonge, P. J. Inhibition of InhA, the Enoyl Reductase from Mycobacterium tuberculosis, by Triclosan and Isoniazid. *Biochem.* **2000**, *39*, 7645-7650.
- (76) Chhibber, M.; Kumar, G.; Parasuraman, P.; Ramya, T. N. C.; Surolia, N.; Surolia, A. Novel diphenyl ethers: Design, docking studies, synthesis and inhibition of enoyl ACP reductase of Plasmodium falciparum and Escherichia coli. *Bioorganic Med. Chem.* **2006**, *14*, 8086-8098.
- (77) Verma, R.; Boshoff, H. I. M.; Arora, K.; Bairy, I.; Tiwari, M.; Bhat, V. G.; Shenoy, G. G. Synthesis, antitubercular evaluation, molecular docking and molecular dynamics studies of 4,6-disubstituted-2-oxo-dihydropyridine-3-carbonitriles. *J. Mol. Struct.* **2019**, *1197*, 117-133.
- (78) Lindgren, A. E. G.; Öberg, C. T.; Hillgren, J. M.; Elofsson, M. Total Synthesis of the Resveratrol Oligomers (±)-Ampelopsin B and (±)-ε-Viniferin. *Eur. J. Org. Chem.* **2016**, *2016*, 426-429.

- (79) Salem, M. S.; Sakr, S. I.; El-Senousy, W. M.; Madkour, H. M. F. Synthesis, Antibacterial, and Antiviral Evaluation of New Heterocycles Containing the Pyridine Moiety. *Arch. Pharm.* **2013**, *346*, 766-773.
- (80) Marinescu, M.; Popa, C.-V. Pyridine Compounds with Antimicrobial and Antiviral Activities. *Int. J. Mol. Sci.* **2022**, *23*, 5659.

Appendix

Spectroscopic Data:

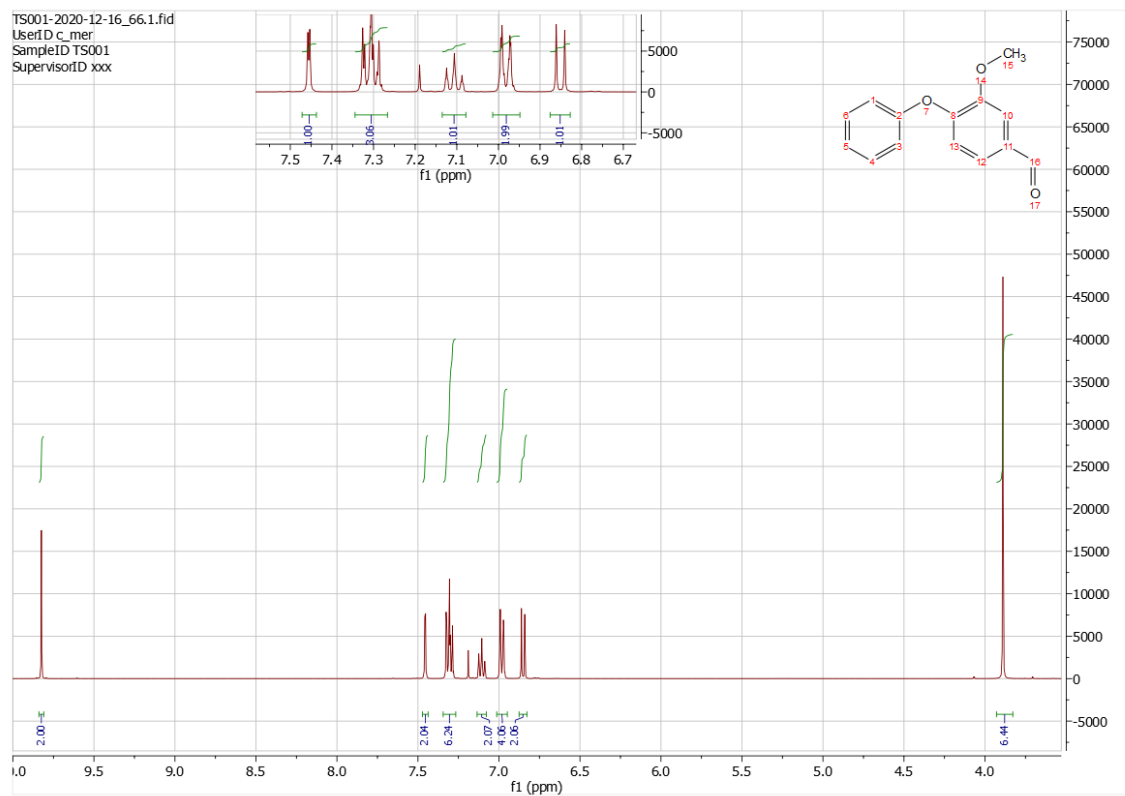


Figure 19: ^1H NMR Spectrum for 3-Methoxy-4-phenoxybenzaldehyde **30**

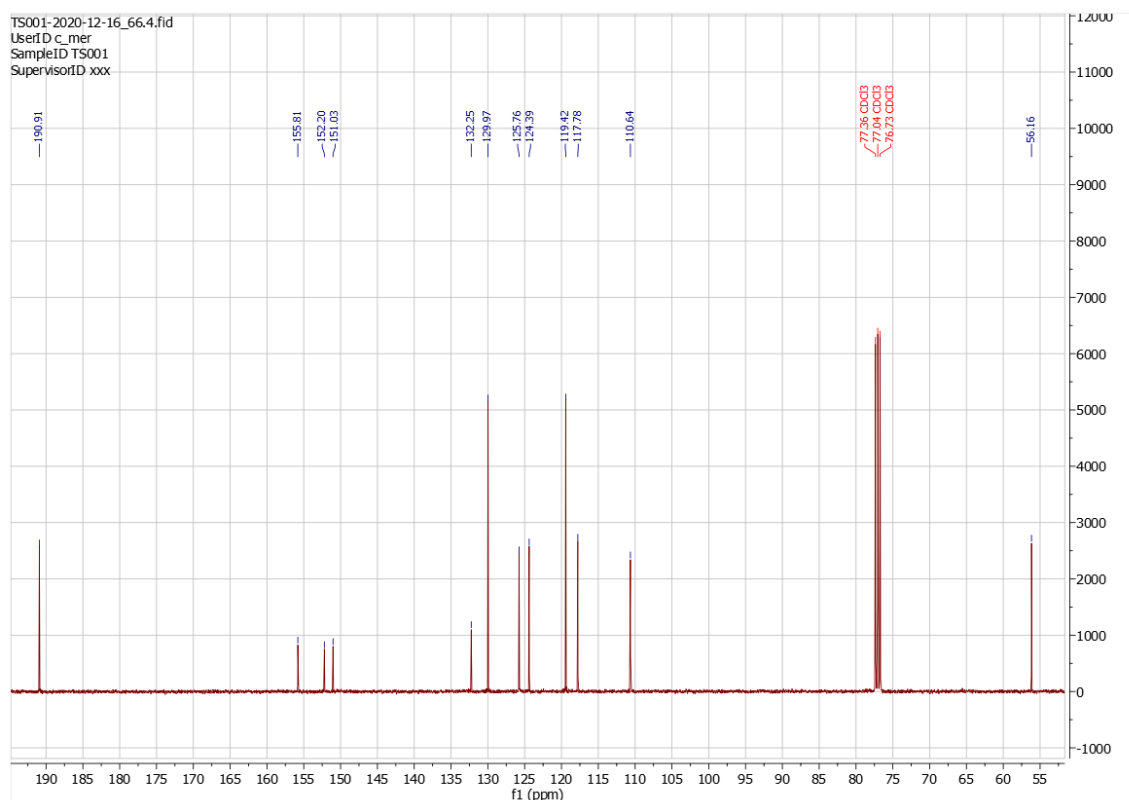


Figure 20: ^{13}C NMR Spectrum for 3-Methoxy-4-phenoxybenzaldehyde **30**

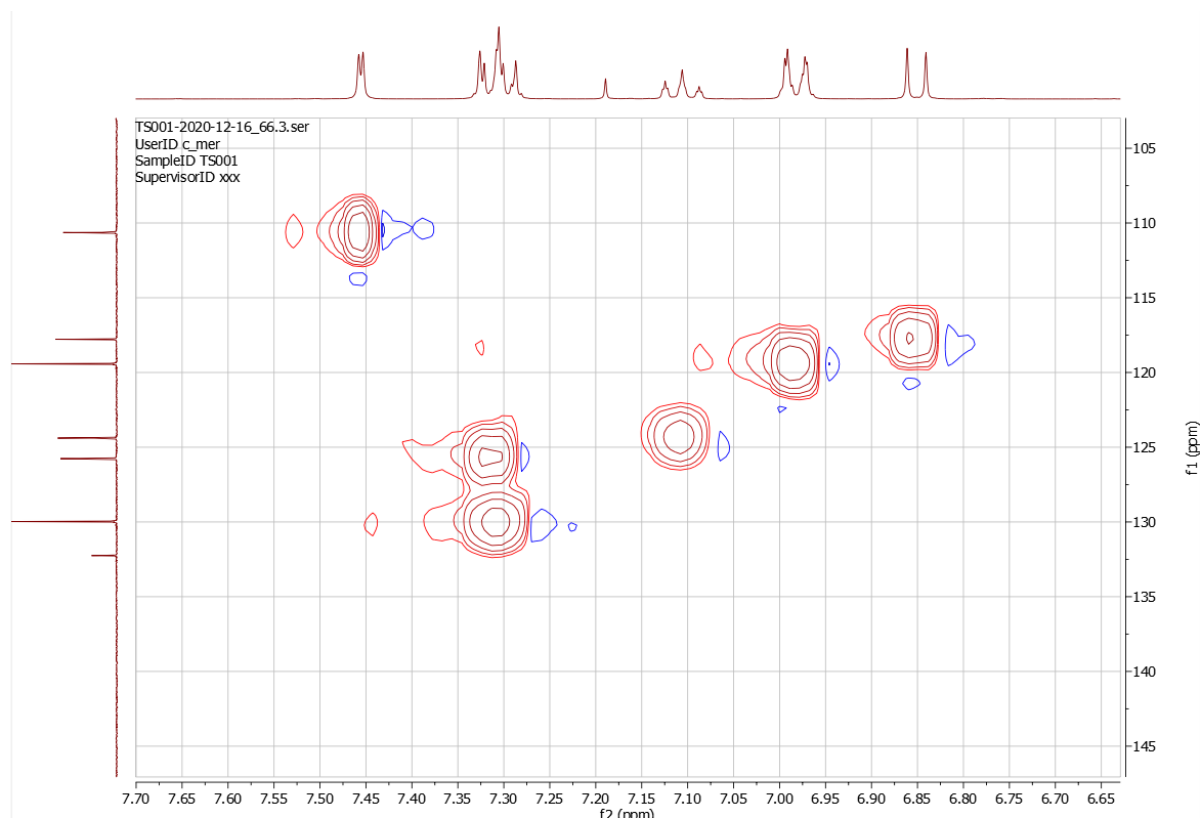


Figure 21: 2D COSY NMR Spectrum for 3-Methoxy-4-phenoxybenzaldehyde **30**

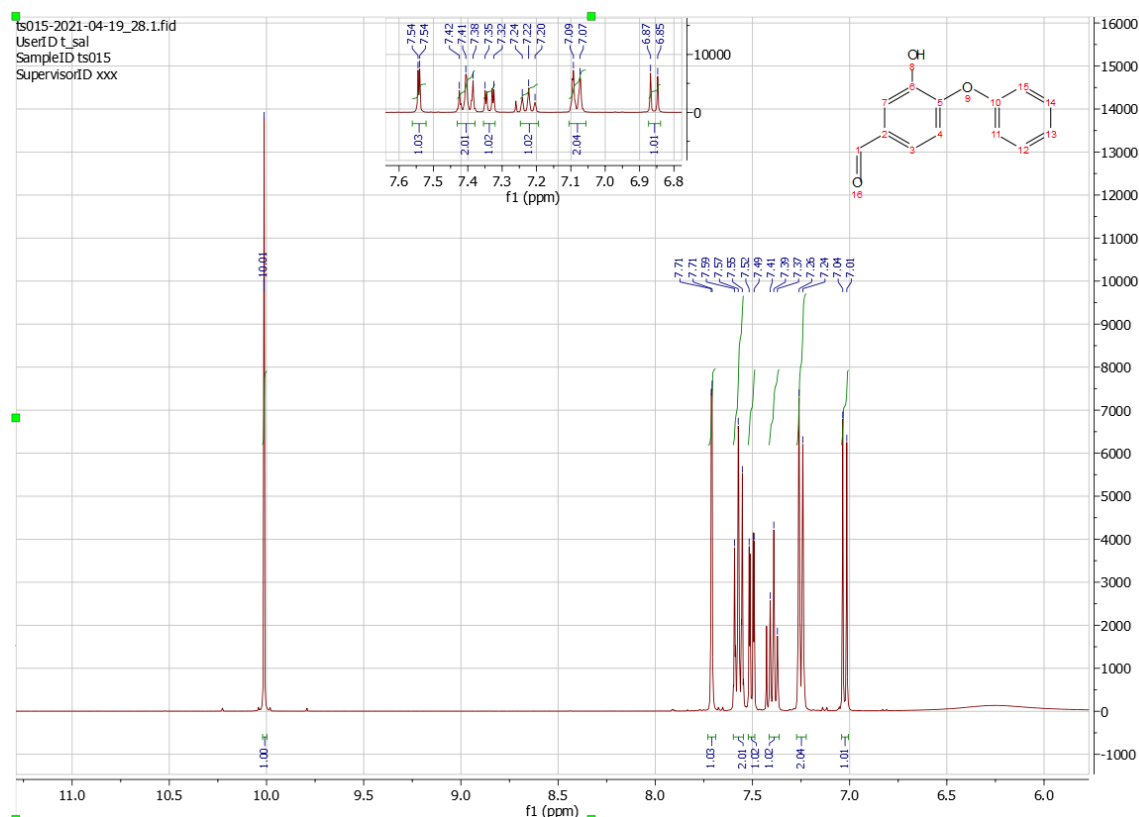


Figure 22: ^1H NMR Spectrum for 3-Hydroxy-4-phenoxybenzaldehyde **31**

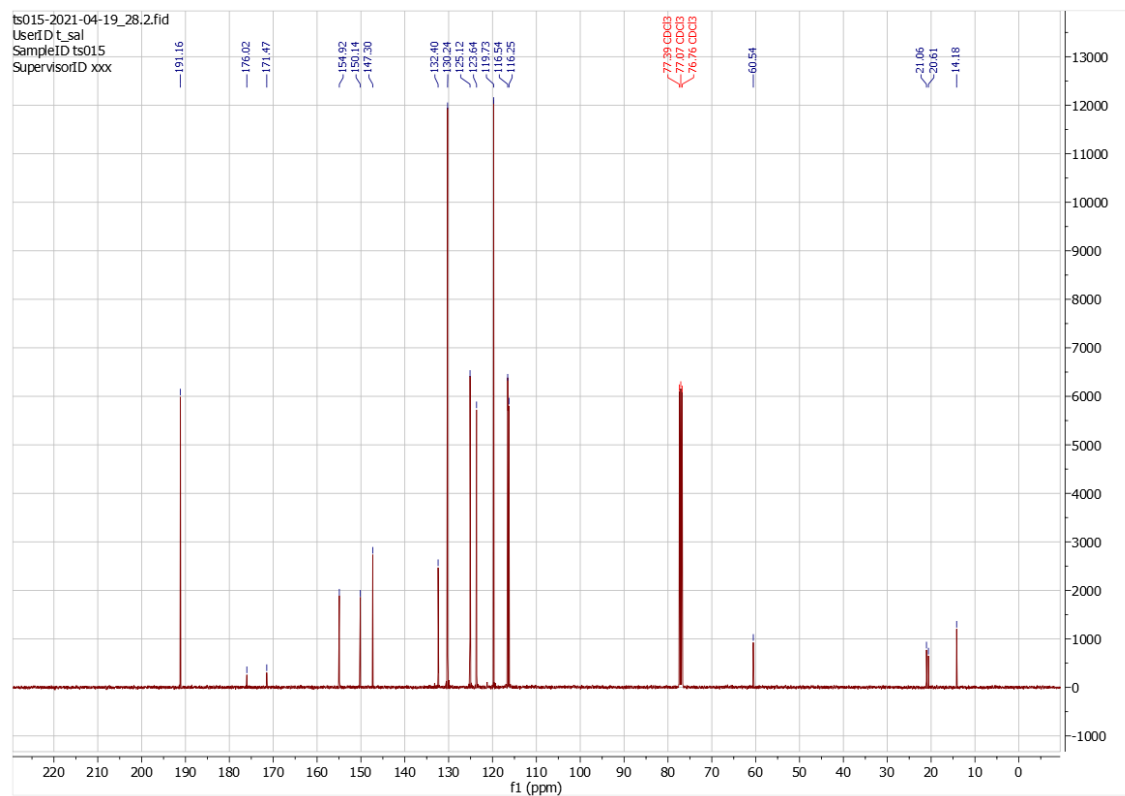


Figure 23: ^{13}C NMR Spectrum for 3-Hydroxy-4-phenoxybenzaldehyde **31**

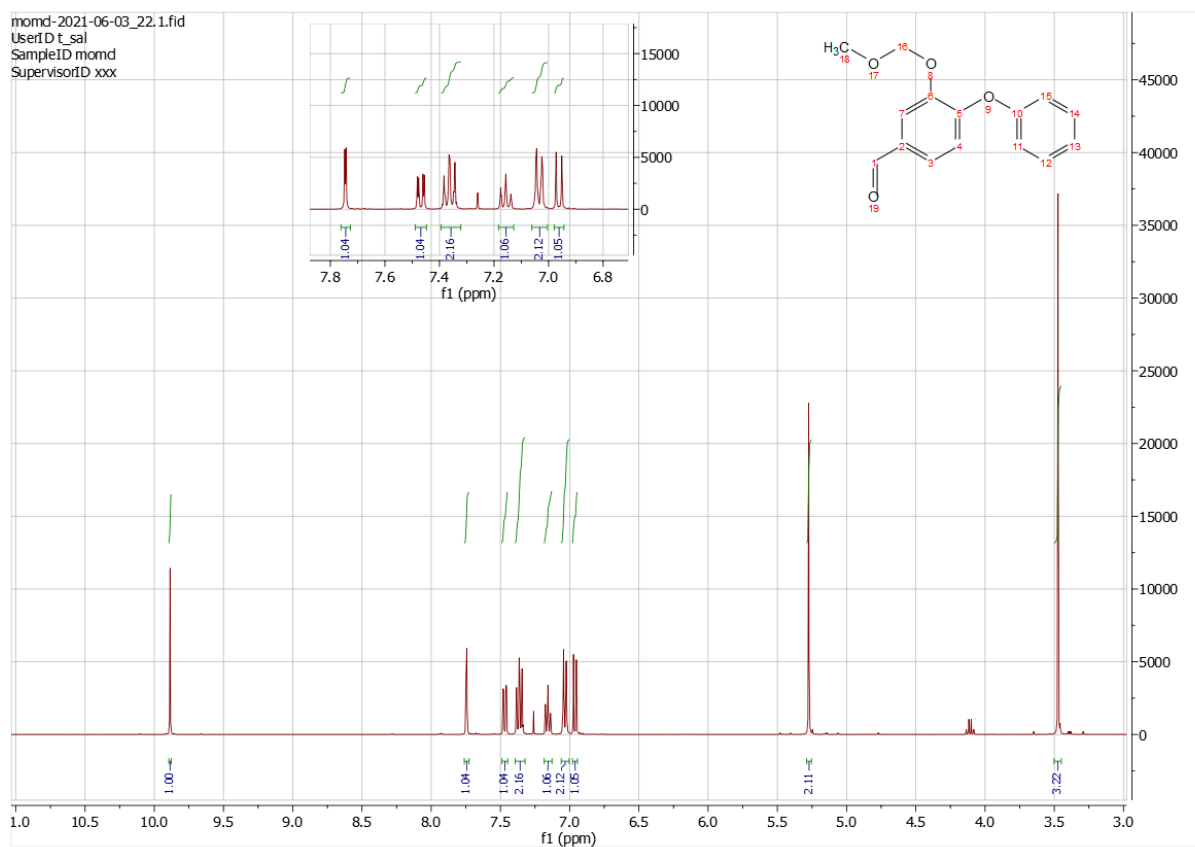


Figure 24: ^1H NMR Spectrum for 3-(Methoxymethoxy)-4-phenoxybenzaldehyde **32**

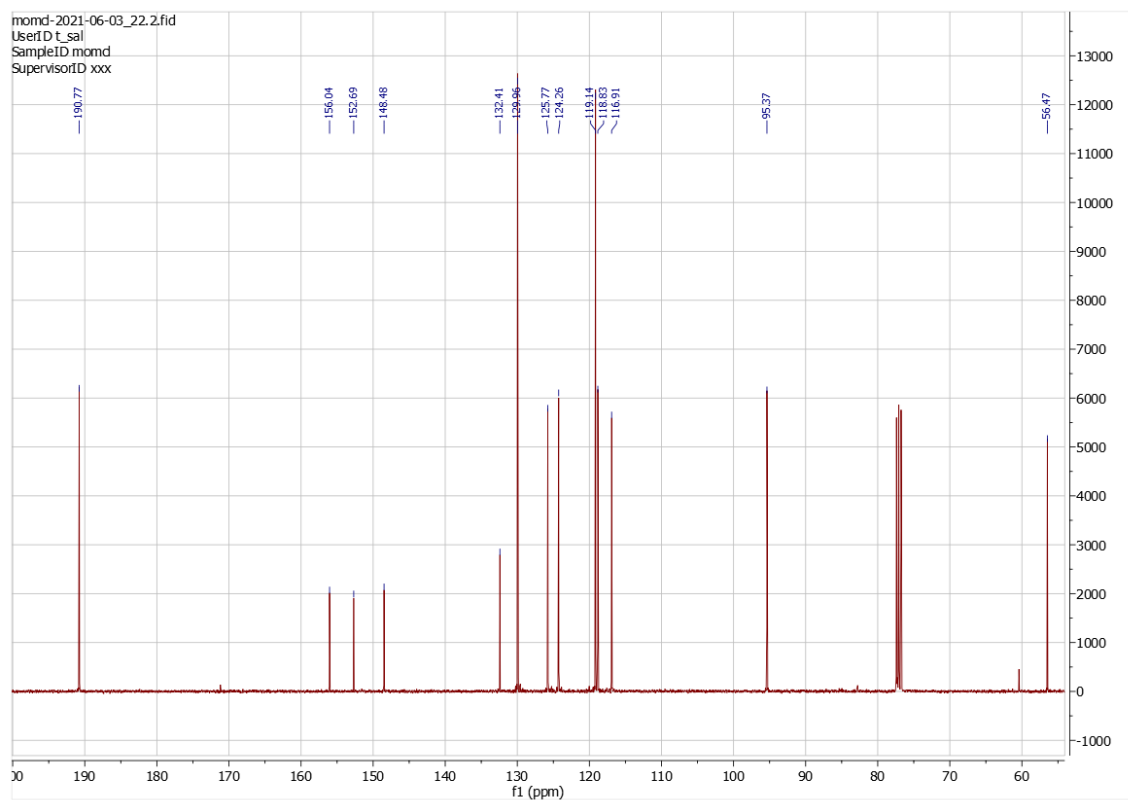


Figure 25: ^{13}C NMR Spectrum for 3-(Methoxymethoxy)-4-phenoxybenzaldehyde **32**

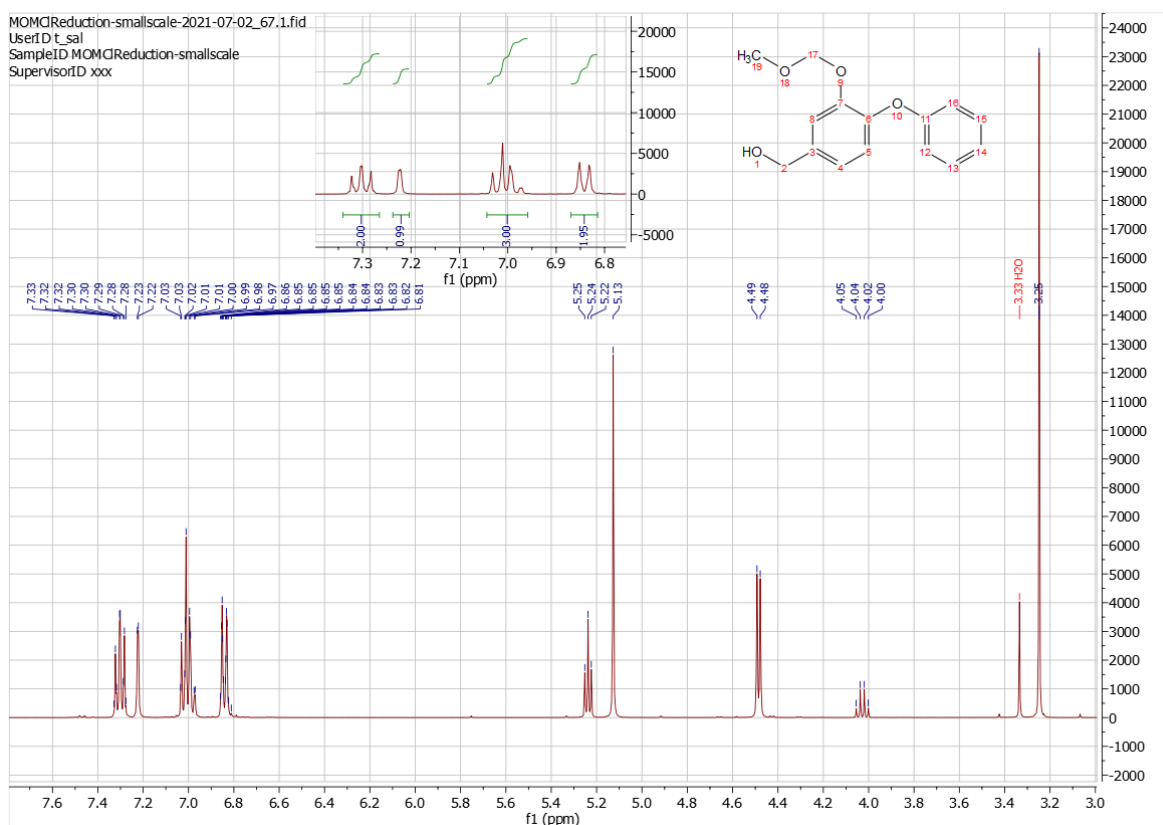


Figure 26: ^1H NMR Spectrum for 3-(Methoxymethoxy)-4-phenoxybenzaldehyde **33**

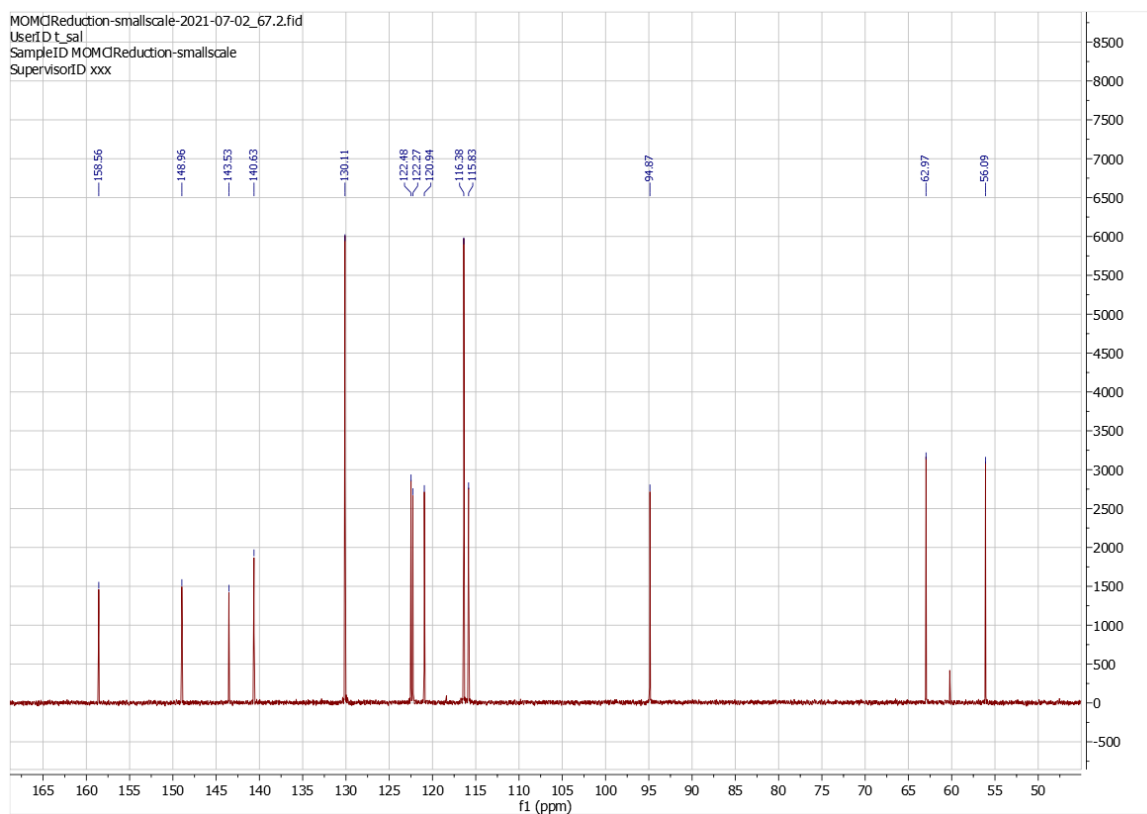


Figure 27: ^{13}C NMR Spectrum for 3-(Methoxymethoxy)-4-phenoxybenzaldehyde **33**

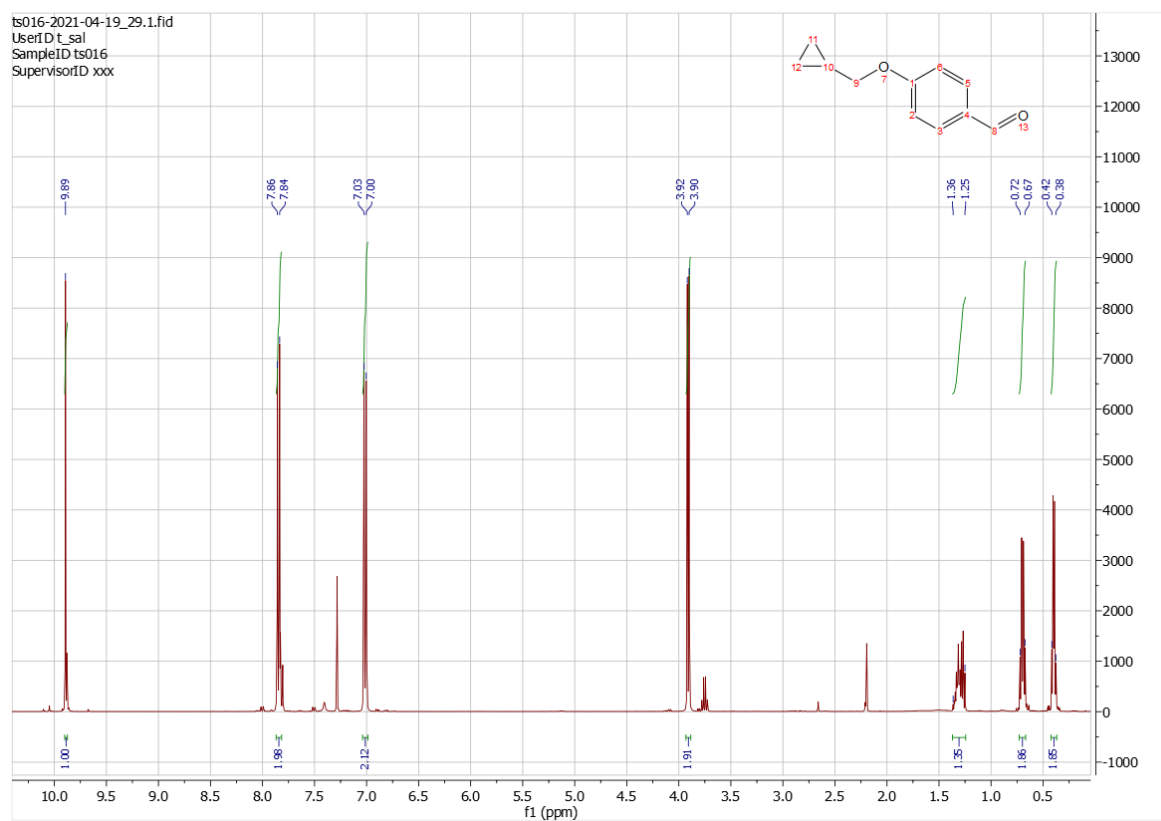


Figure 28: ^1H NMR spectrum for 4-(cyclopropylmethoxy)benzaldehyde, **36**

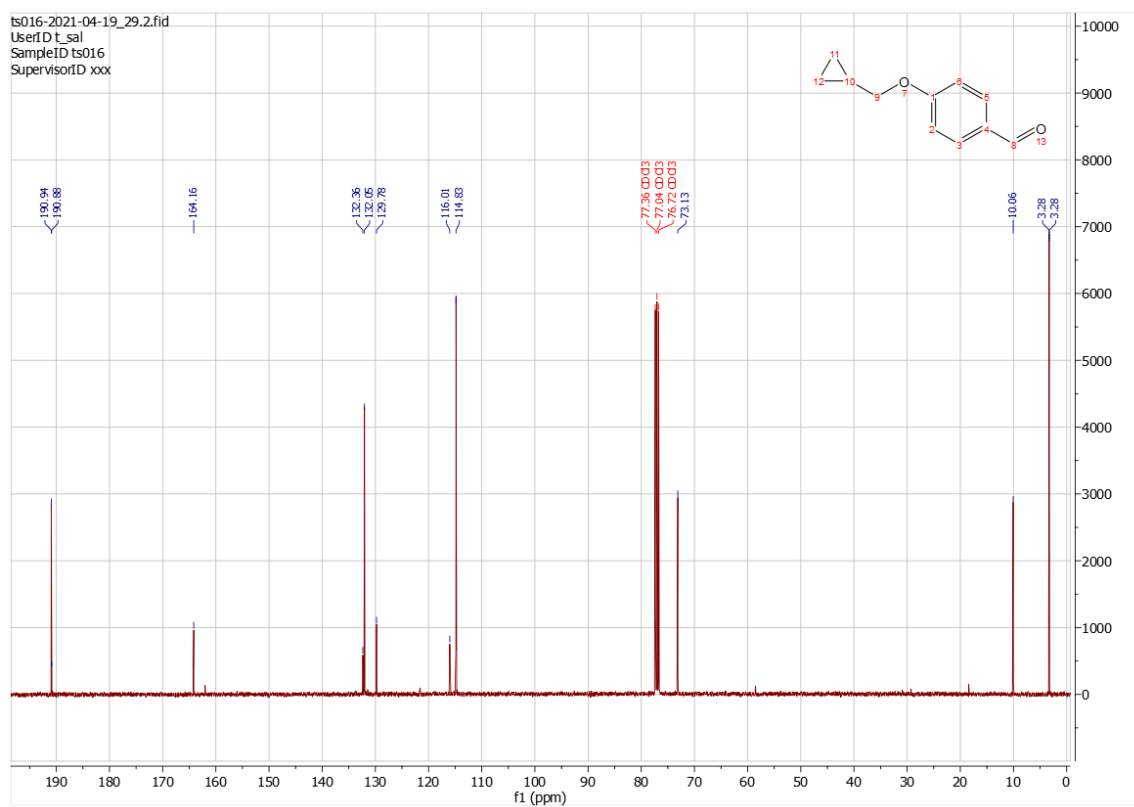
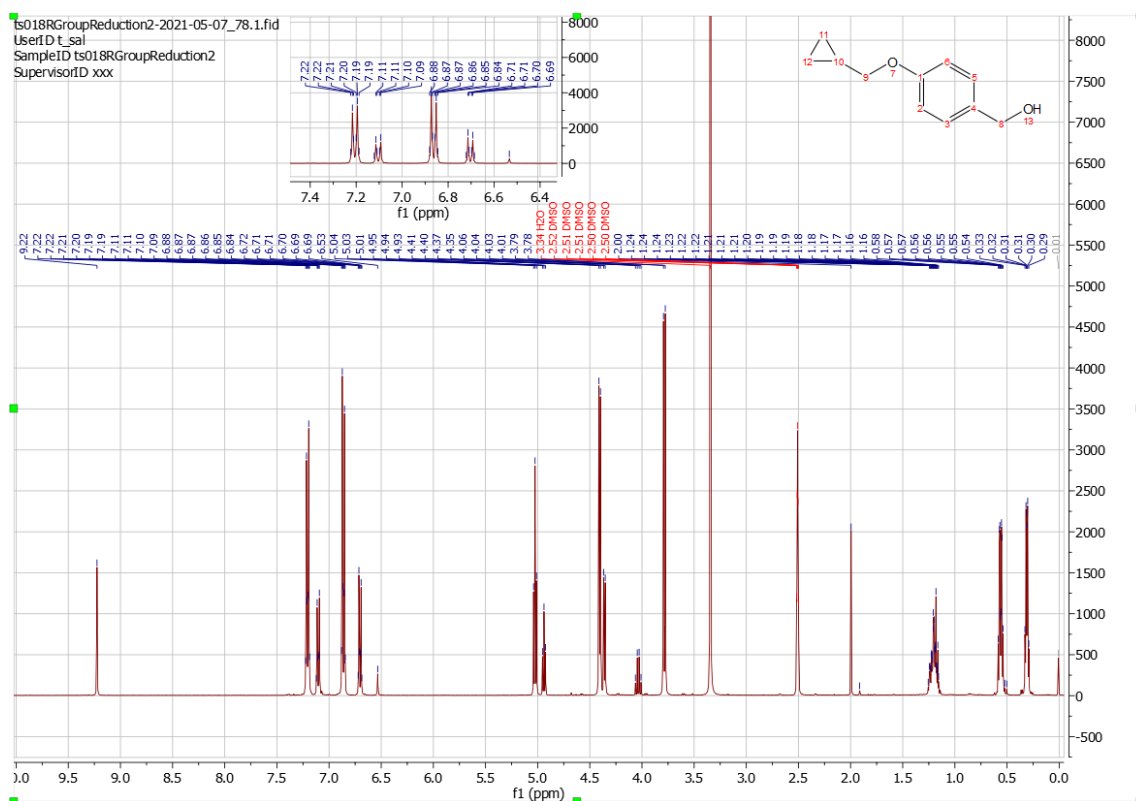


Figure 29: ^{13}C NMR Spectrum for 4-(cyclopropylmethoxy)benzaldehyde, **36**



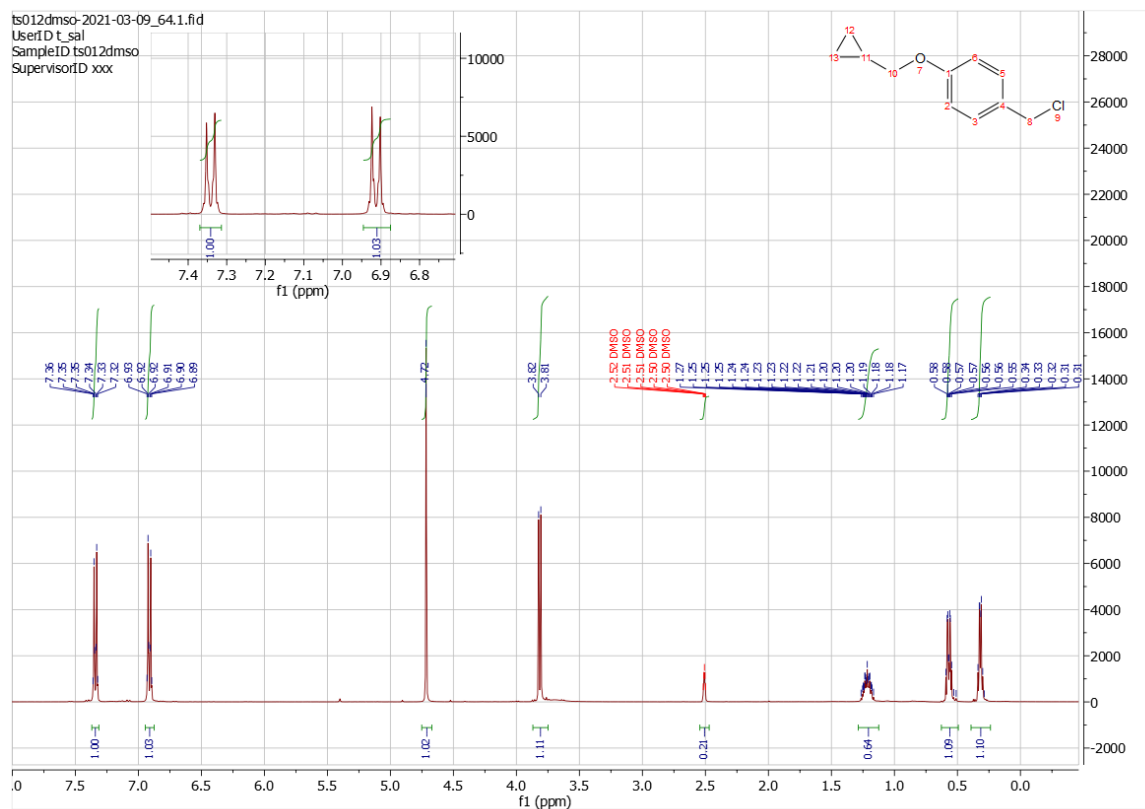


Figure 32: ¹H NMR Spectrum for 4-(cyclopropylmethoxy)benzyl chloride, **38**

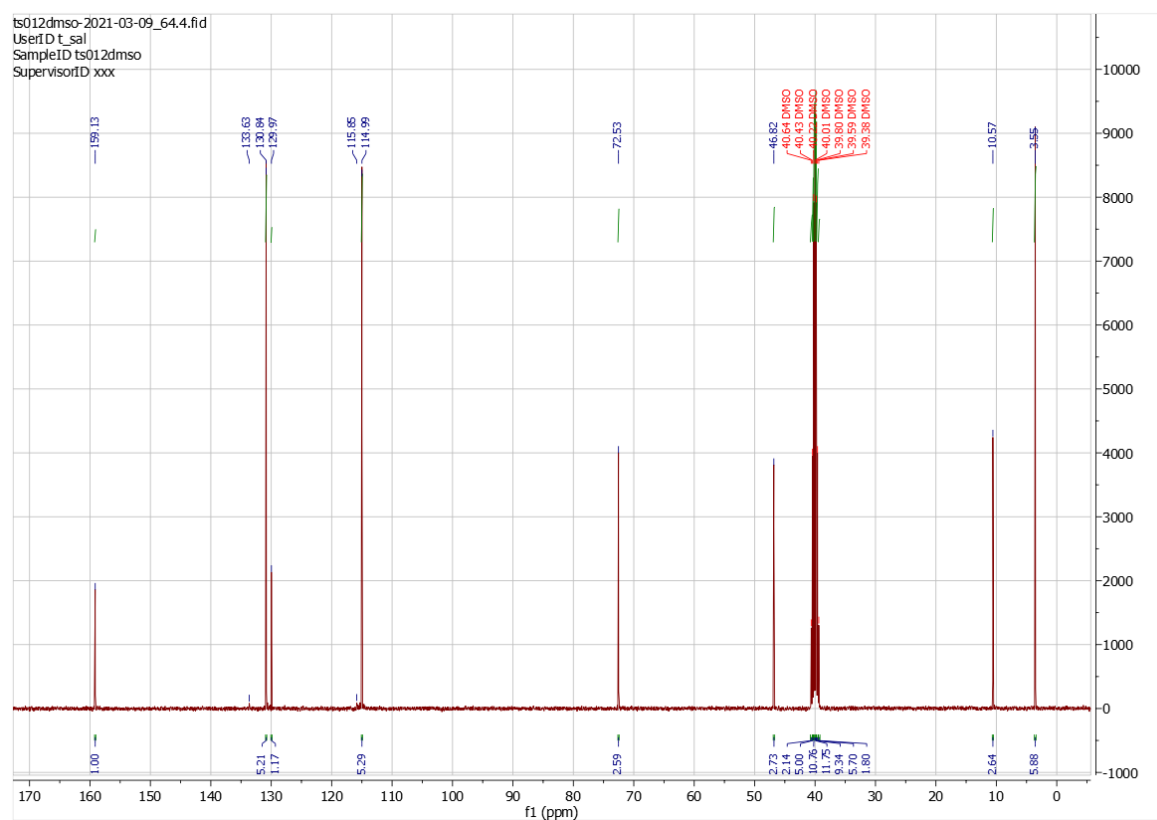


Figure 33: ¹³C NMR Spectrum for 4-(cyclopropylmethoxy)benzyl chloride, **38**

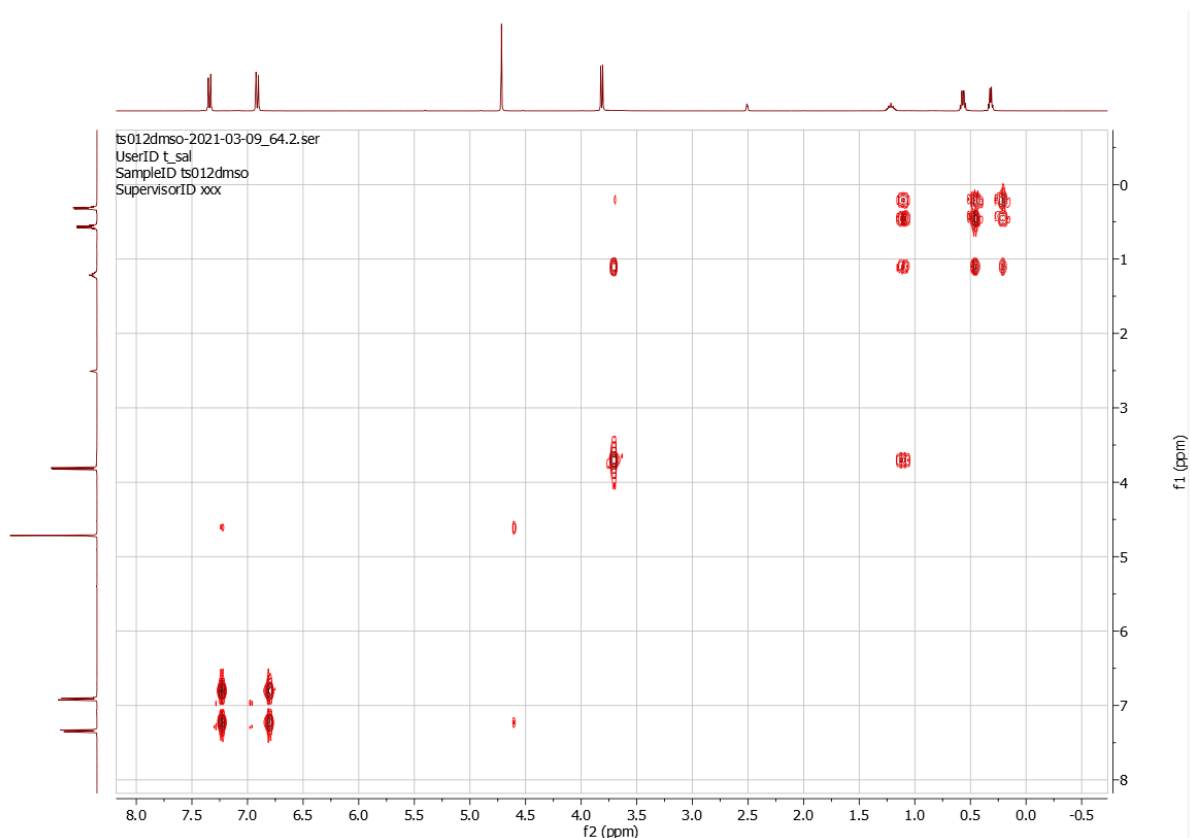


Figure 34: 2D COSY NMR Spectrum for 4-(cyclopropylmethoxy)benzyl chloride, **38**

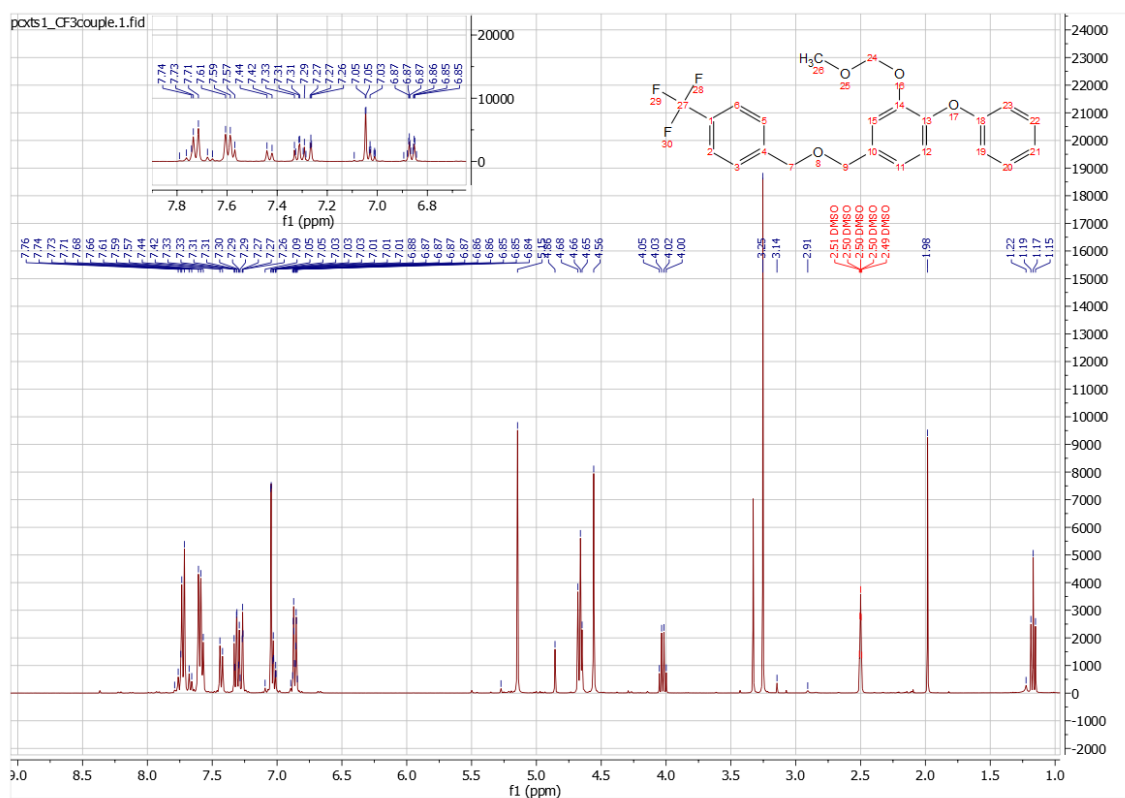


Figure 35: ^1H NMR Spectrum for 2-(Methoxymethoxy)-1-phenoxy-4-(((4-(trifluoromethyl)benzyl)oxy)methyl)benzene **43**

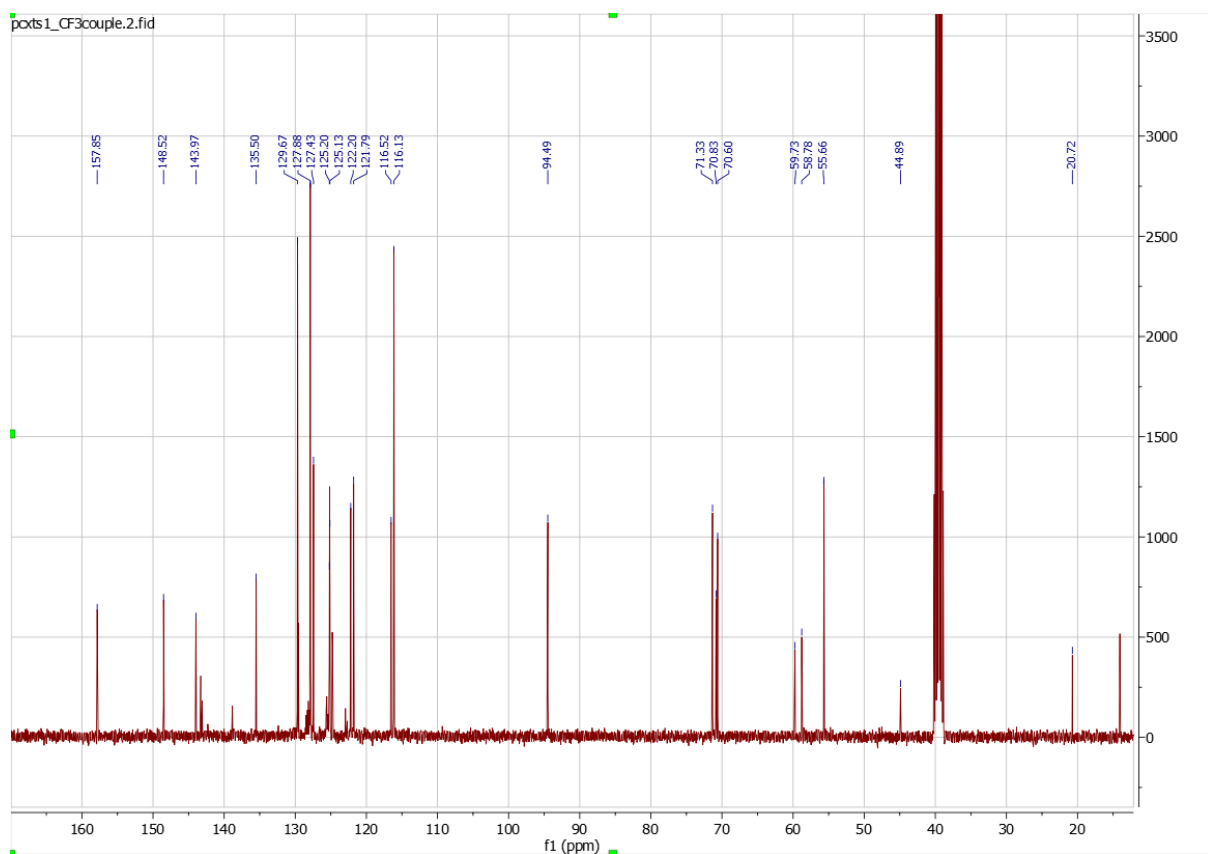


Figure 36: ^{13}C NMR Spectrum for 2-(Methoxymethoxy)-1-phenoxy-4-(((4-(trifluoromethyl)benzyl)oxy)methyl)benzene **43**

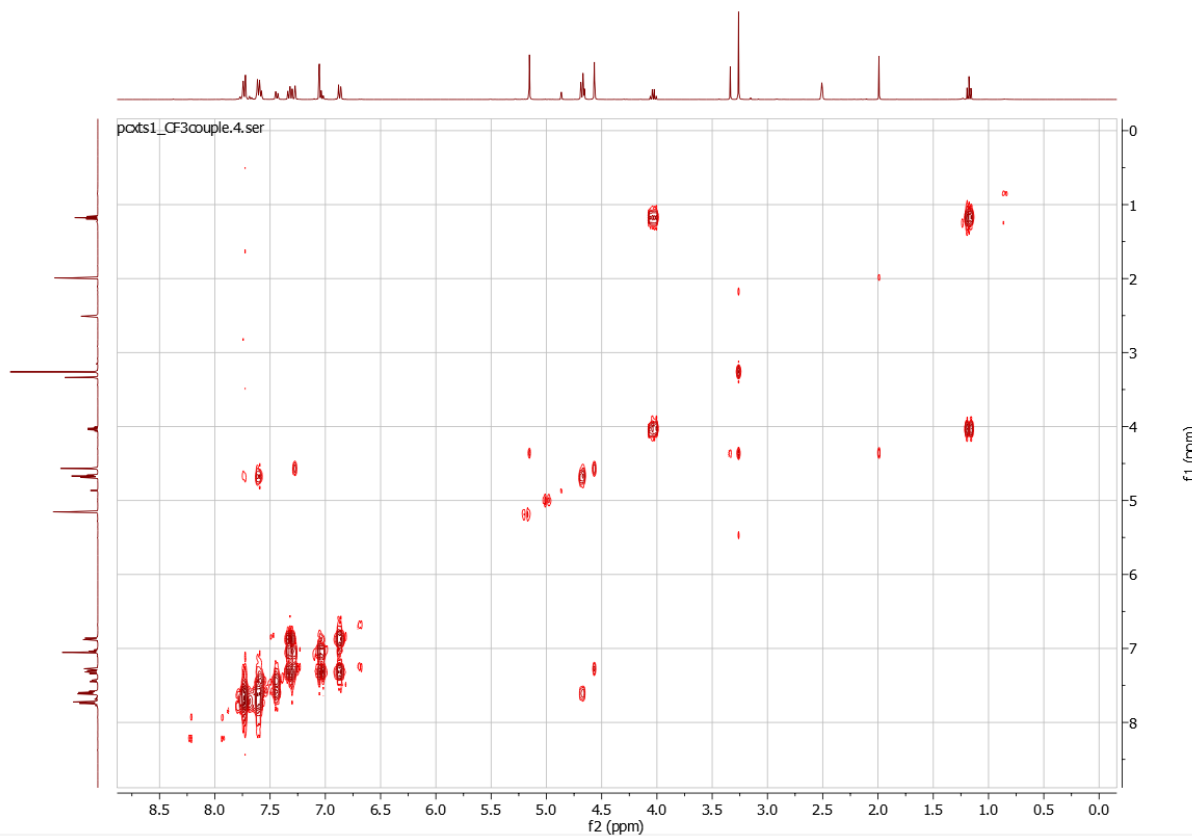


Figure 37: 2D COSY NMR Spectrum for 2-(Methoxymethoxy)-1-phenoxy-4-(((4-(trifluoromethyl)benzyl)oxy)methyl)benzene **43**

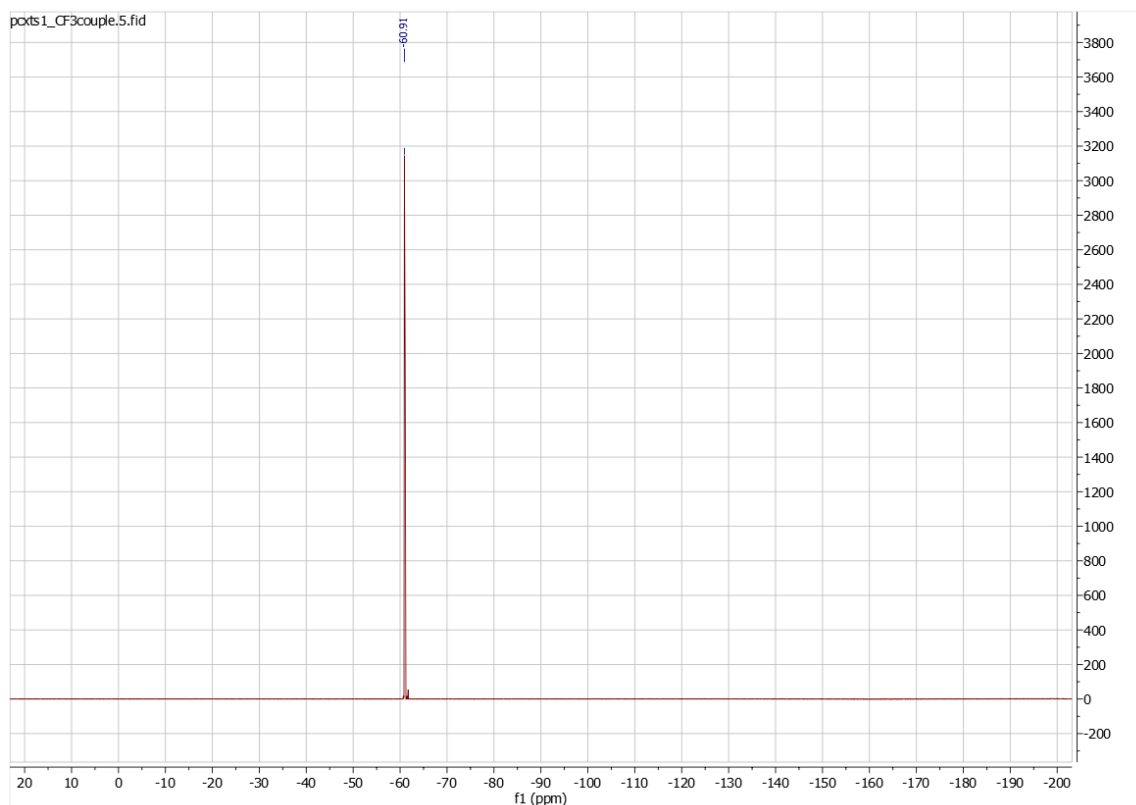


Figure 38: ^{19}F NMR Spectrum for 2-(Methoxymethoxy)-1-phenoxy-4-(((4-(trifluoromethyl)benzyl)oxy)methyl)benzene **43**

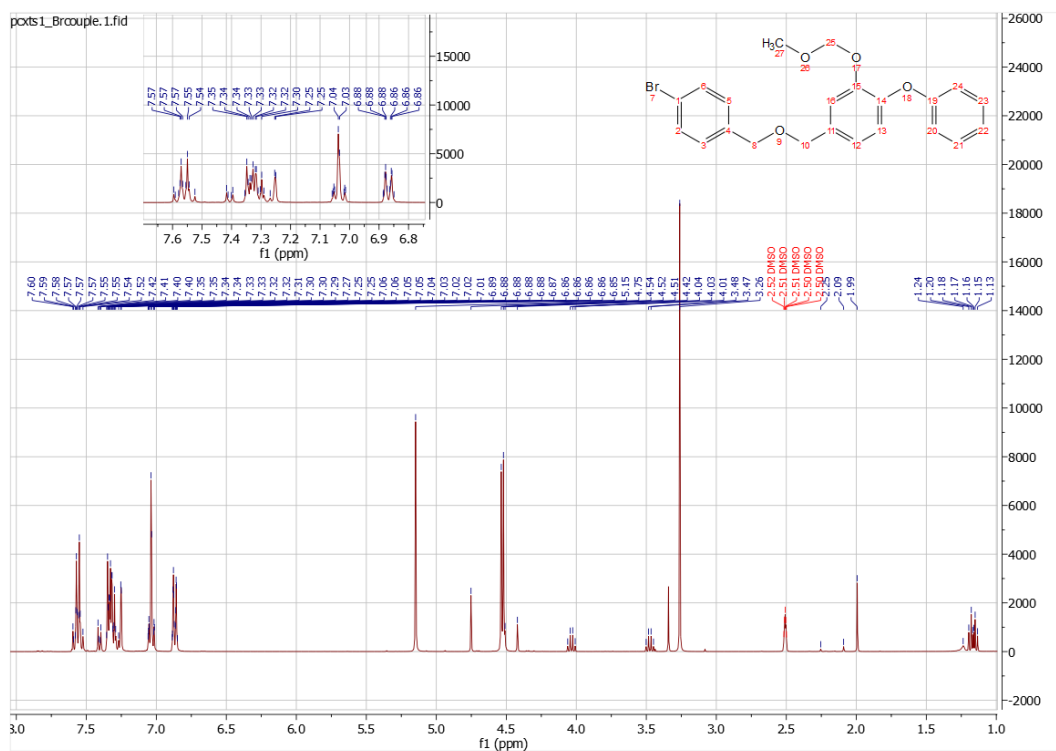


Figure 39: ^1H NMR Spectrum for 4-(((4-Bromobenzyl)oxy)methyl)-2-(methoxymethoxy)-1-phenoxybenzene **45**

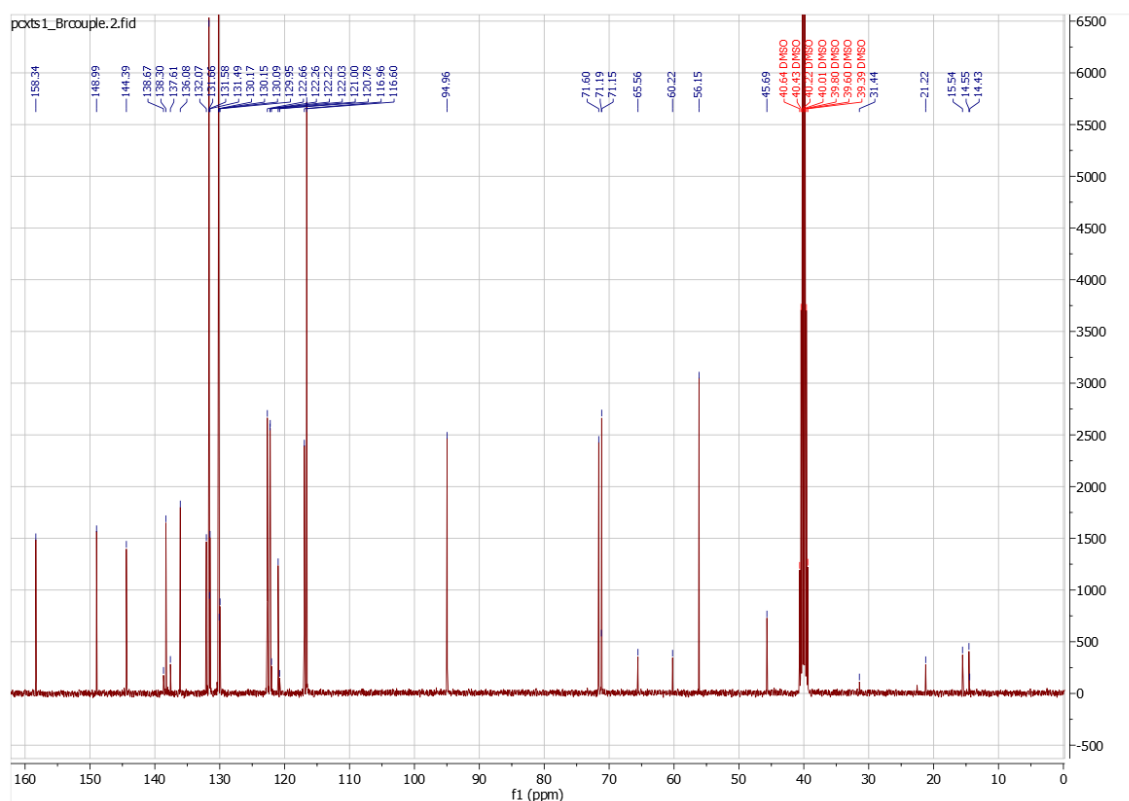


Figure 40: ^{13}C NMR Spectrum for 4-(((4-Bromobenzyl)oxy)methyl)-2-(methoxymethoxy)-1-phenoxybenzene **45**

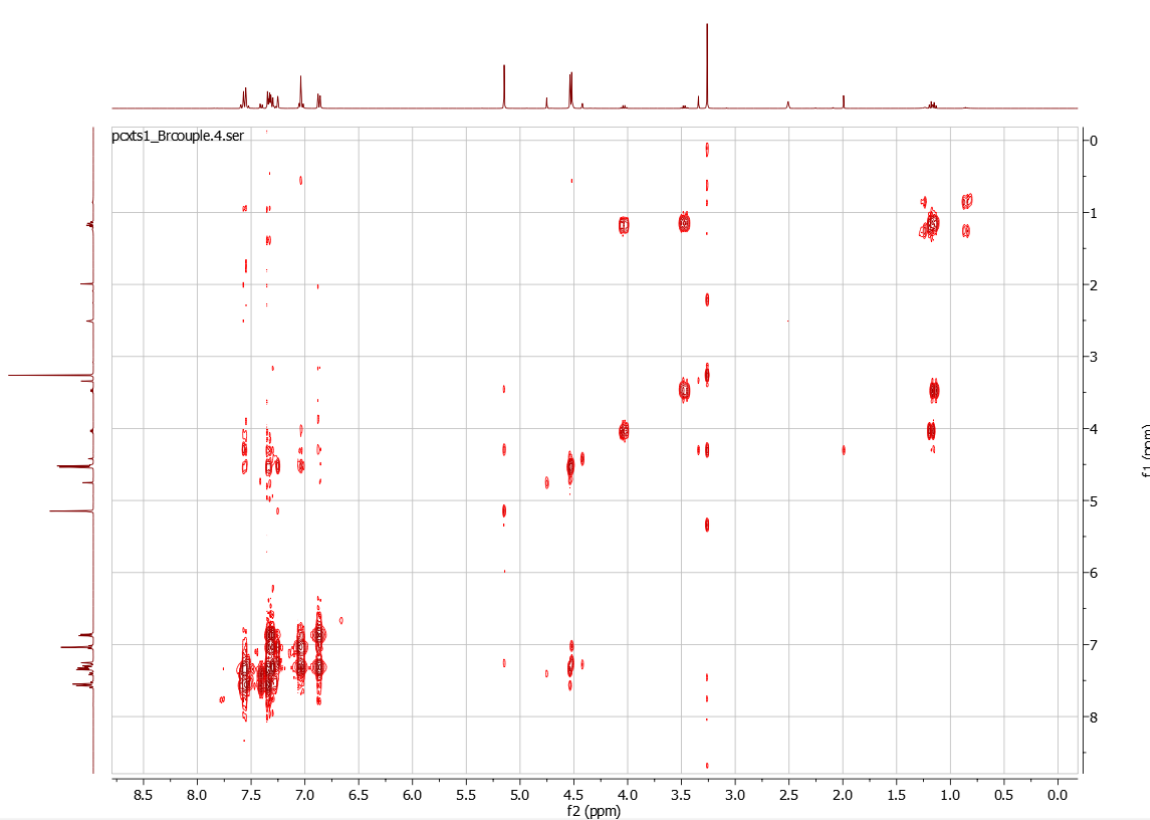


Figure 41: 2D COSY NMR Spectrum for 4-(((4-Bromobenzyl)oxy)methyl)-2-(methoxymethoxy)-1-phenoxybenzene **45**

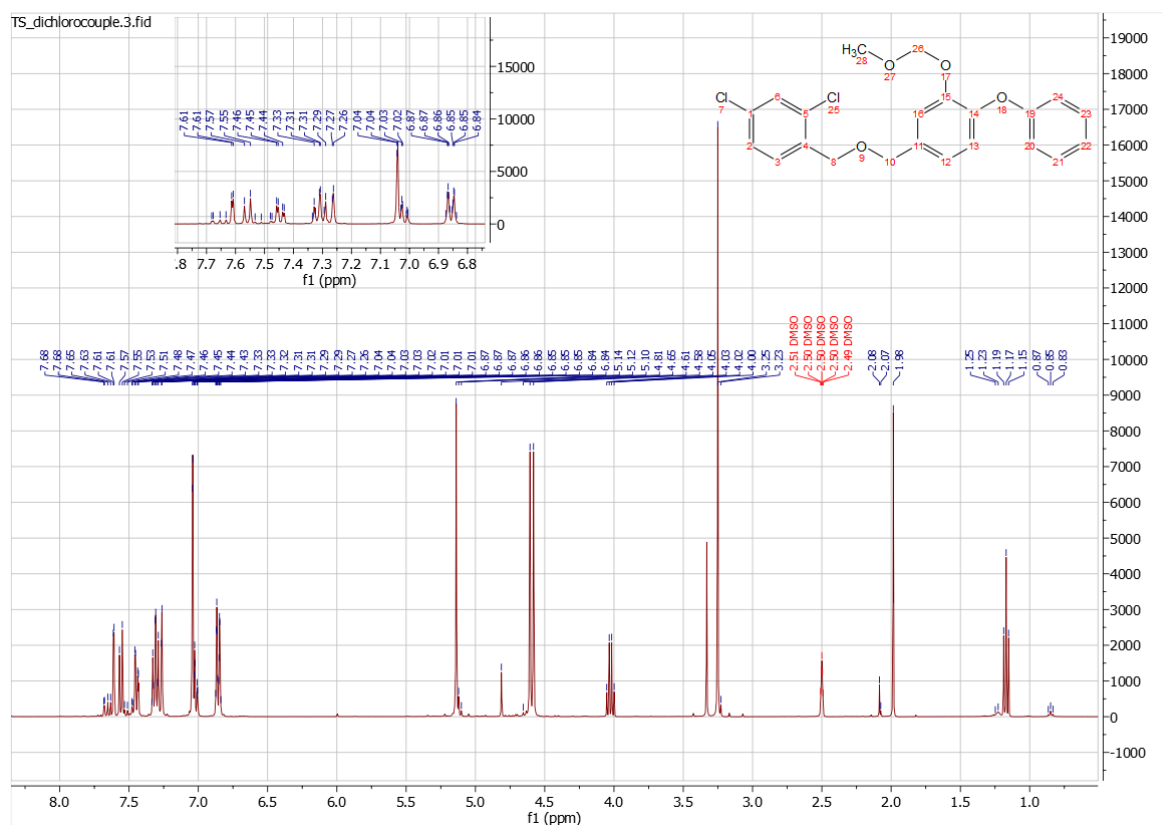


Figure 42: ^1H NMR Spectrum for 2,4-Dichloro-1-(((3-(methoxymethoxy)-4-phenoxybenzyl)oxy)methyl)benzene **46**

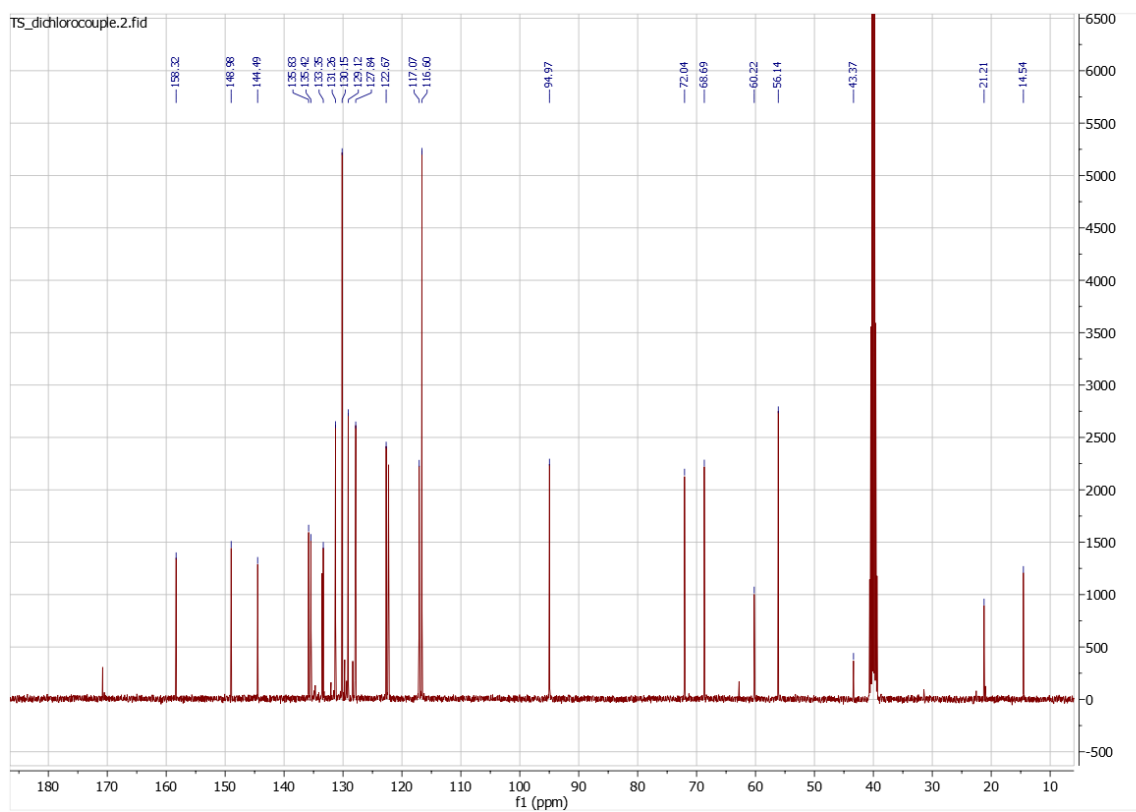


Figure 43: ^{13}C NMR Spectrum for 2,4-Dichloro-1-(((3-(methoxymethoxy)-4-phenoxybenzyl)oxy)methyl)benzene **46**

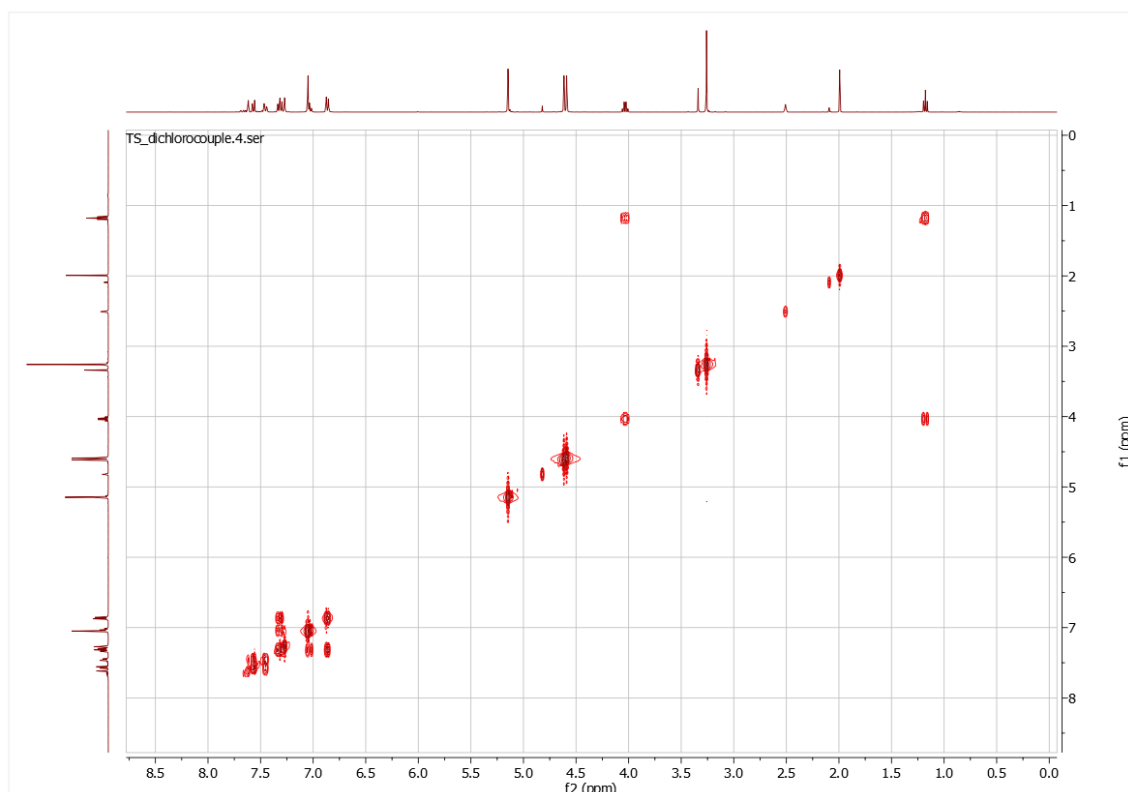


Figure 44: 2D COSY NMR Spectrum for 2,4-Dichloro-1-(((3-(methoxymethoxy)-4-phenoxybenzyl)oxy)methyl)benzene **46**

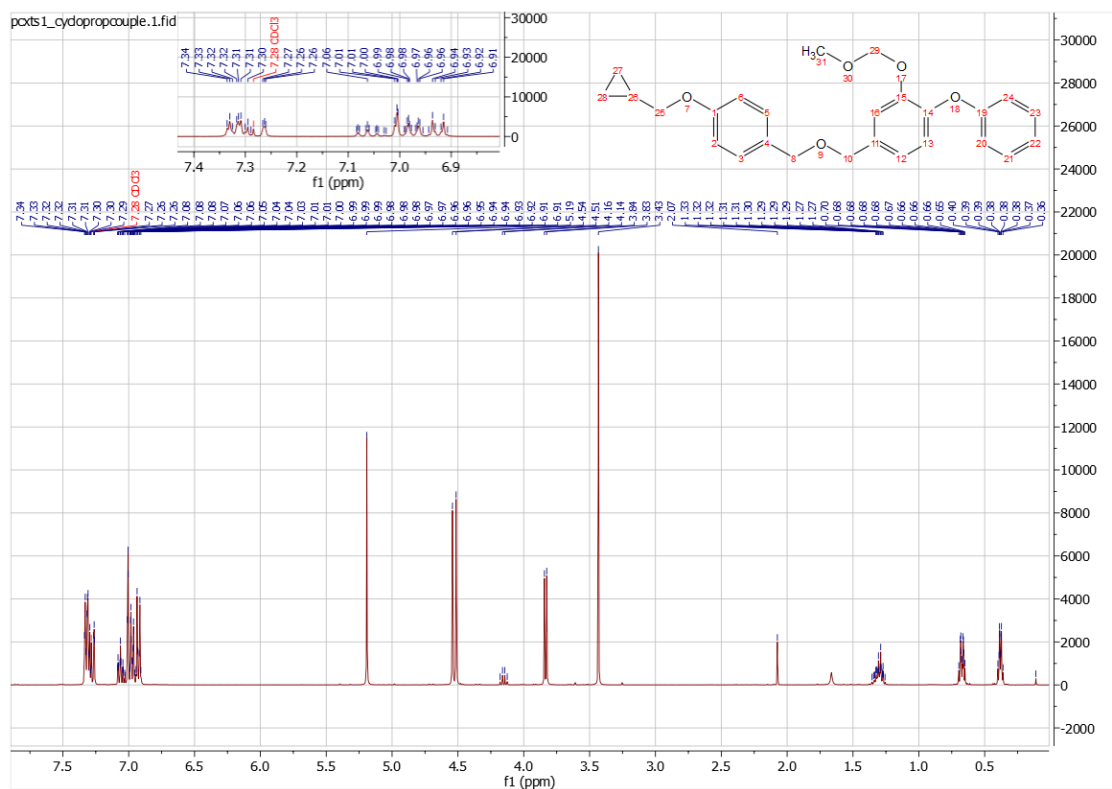


Figure 45: ^1H NMR Spectrum for 4-(((4-(Cyclopropylmethoxy)benzyl)oxy)methyl)-2-(methoxymethoxy)-1-phenoxybenzene **47**

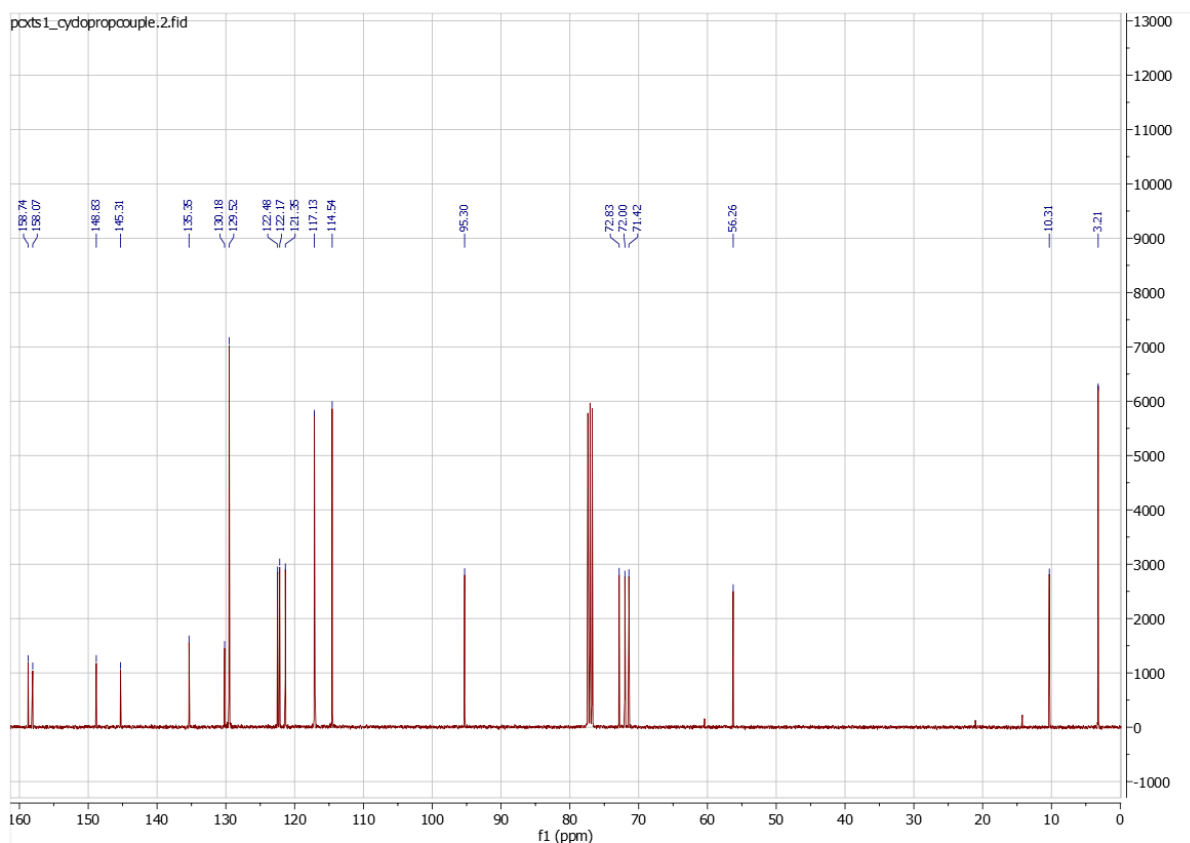


Figure 46: ^{13}C NMR Spectrum for 4-(((4-(Cyclopropylmethoxy)benzyl)oxy)methyl)-2-(methoxymethoxy)-1-phenoxybenzene **47**

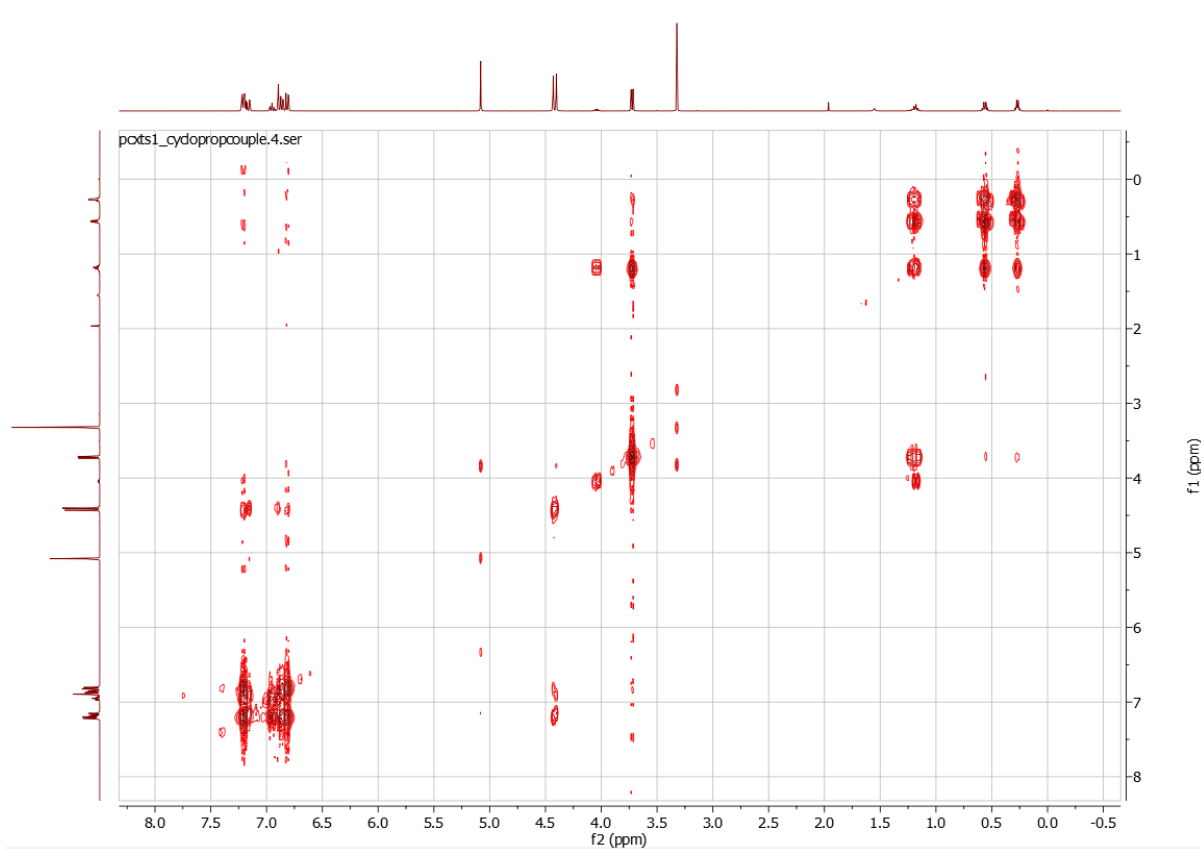


Figure 47: 2D COSY NMR Spectrum for 4-(((4-(Cyclopropylmethoxy)benzyl)oxy)methyl)-2-(methoxymethoxy)-1-phenoxybenzene **47**

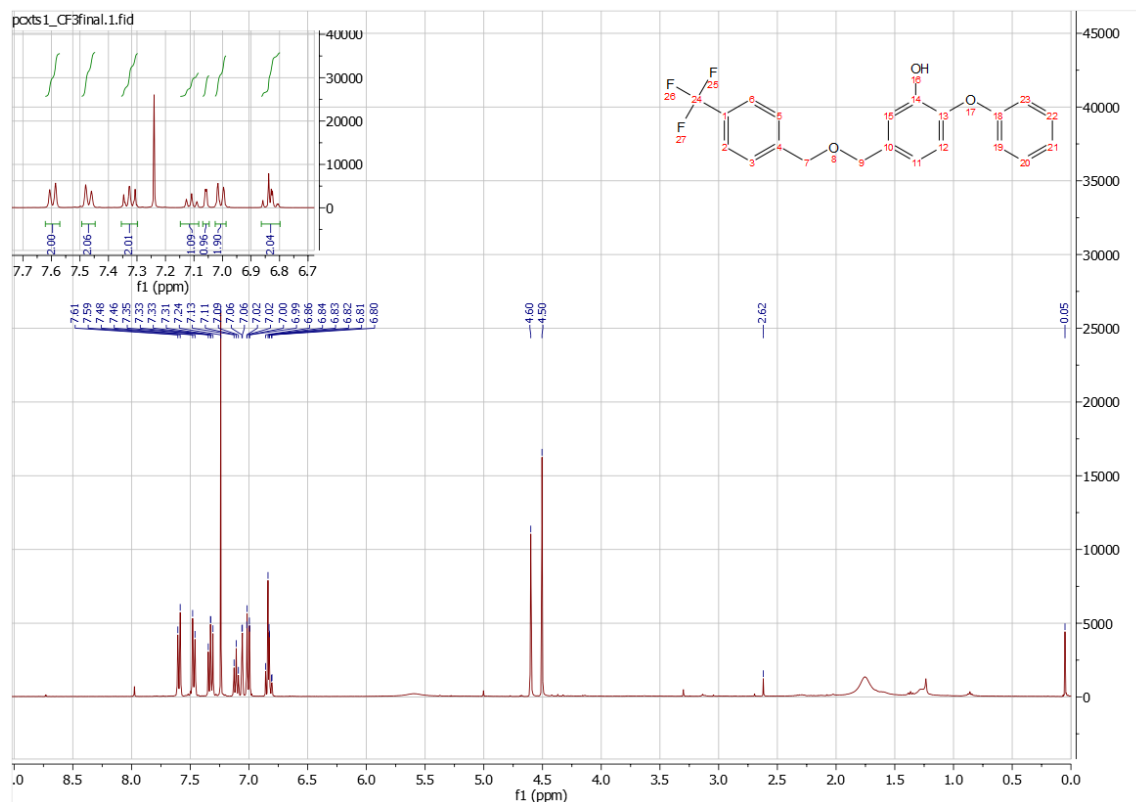


Figure 48: ¹H NMR Spectrum for 2-Phenoxy-5-(((4-(trifluoromethyl)benzyl)oxy)methyl)phenol **48**

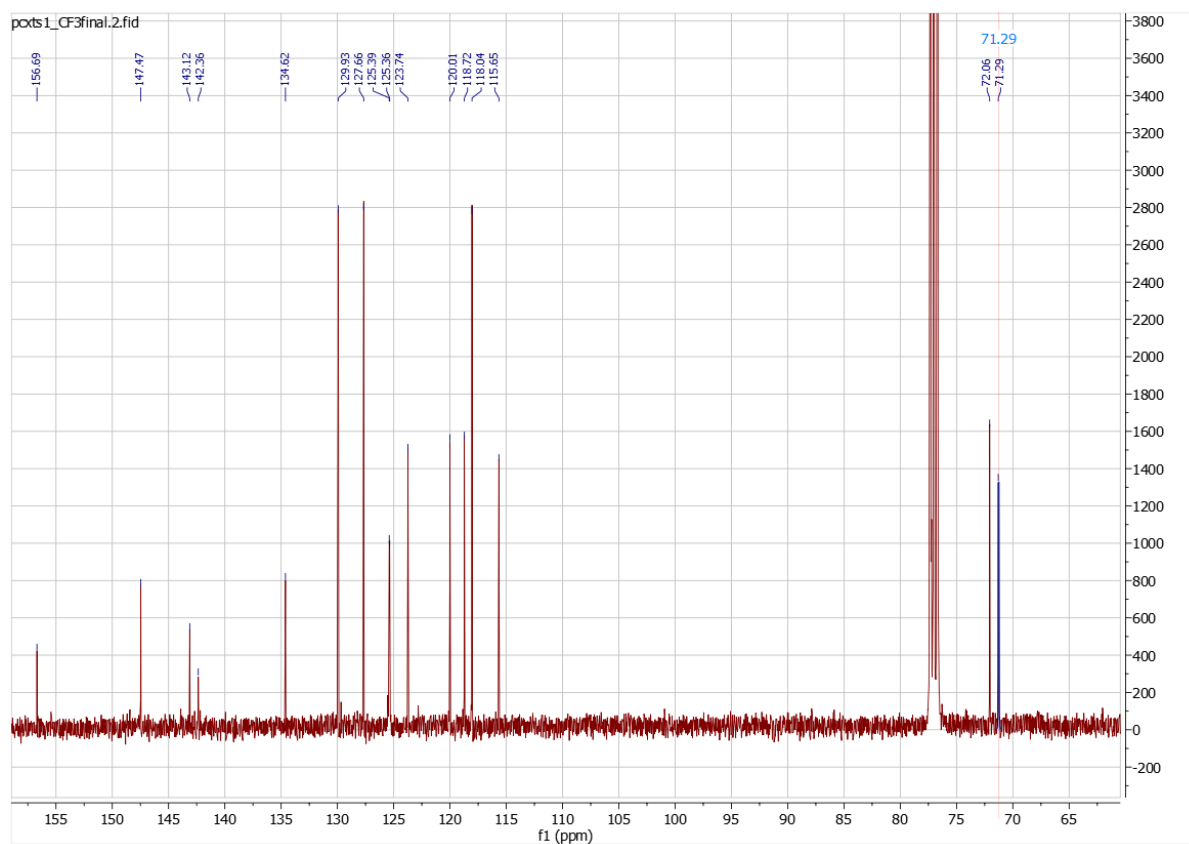


Figure 49: ¹³C NMR Spectrum for 2-Phenoxy-5-(((4-(trifluoromethyl)benzyl)oxy)methyl)phenol **48**

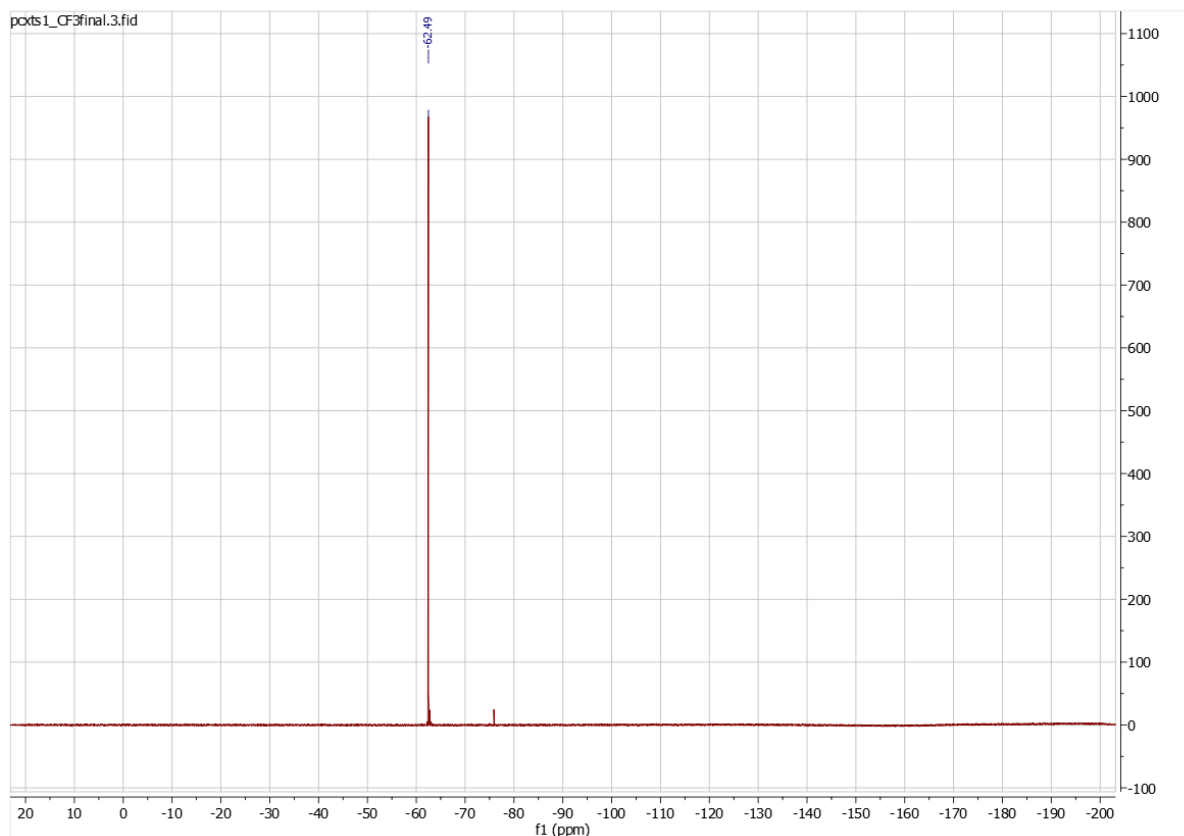


Figure 50: ^{19}F NMR Spectrum for 2-Phenoxy-5-(((4-(trifluoromethyl)benzyl)oxy)methyl)phenol **48**

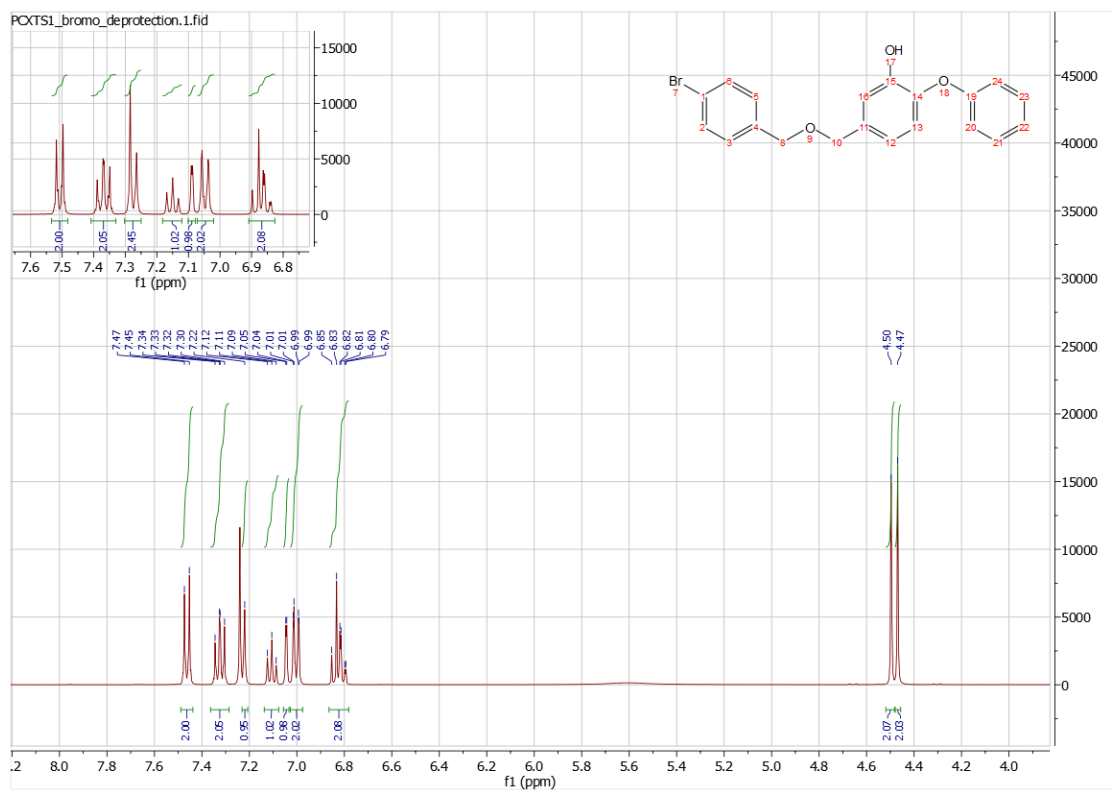


Figure 51: ^1H NMR Spectrum for 5-(((4-bromobenzyl)oxy)methyl)-2-phenoxyphenol **50**

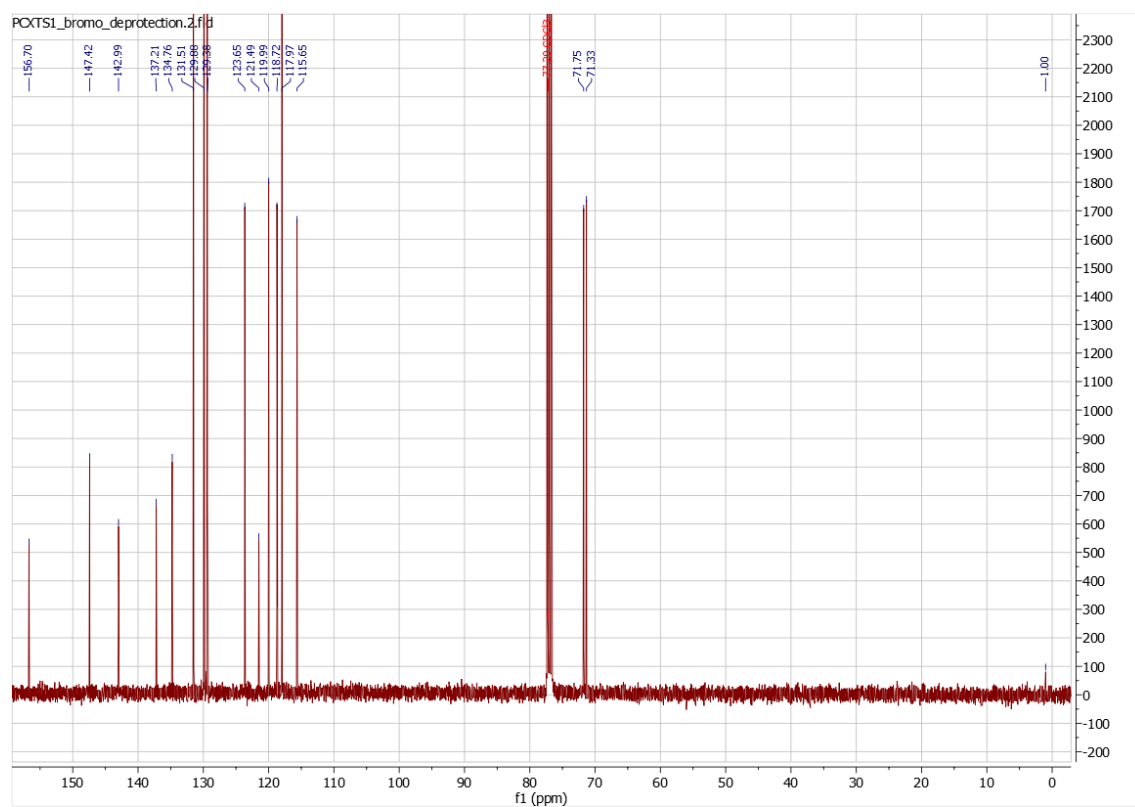


Figure 52: ^{13}C NMR Spectrum for 5-(((4-bromobenzyl)oxy)methyl)-2-phenoxyphenol **50**

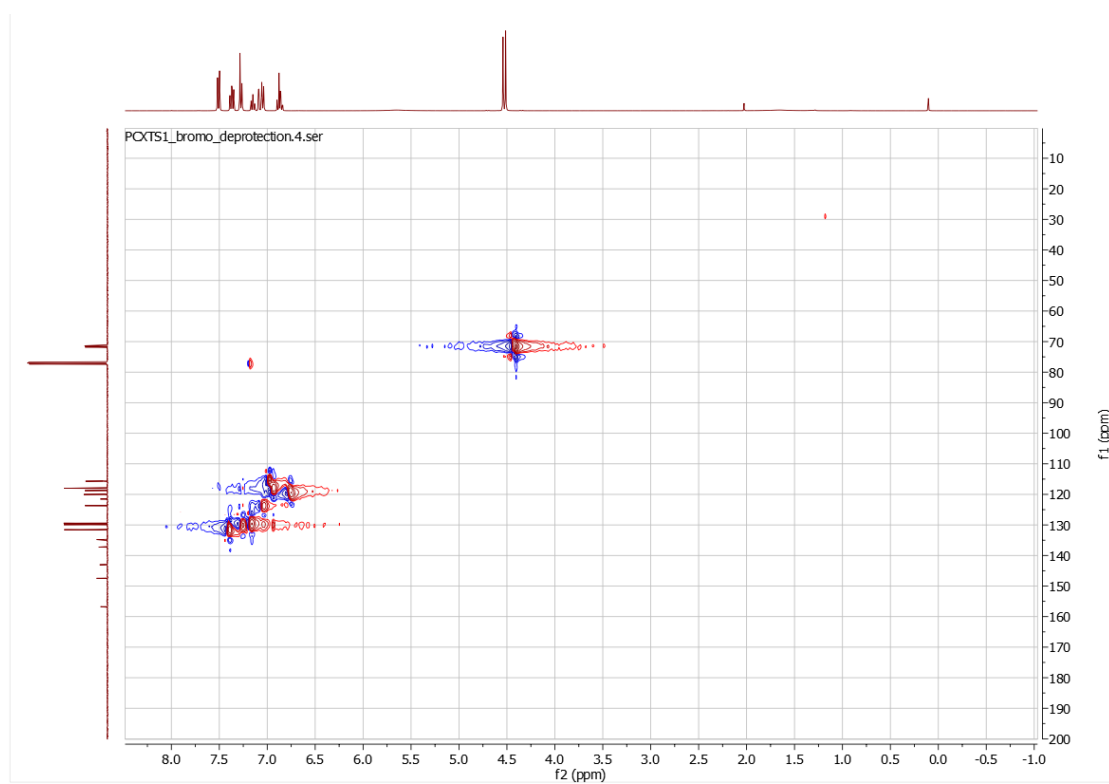


Figure 53: 2D COSY NMR Spectrum for 5-(((4-bromobenzyl)oxy)methyl)-2-phenoxyphenol **50**

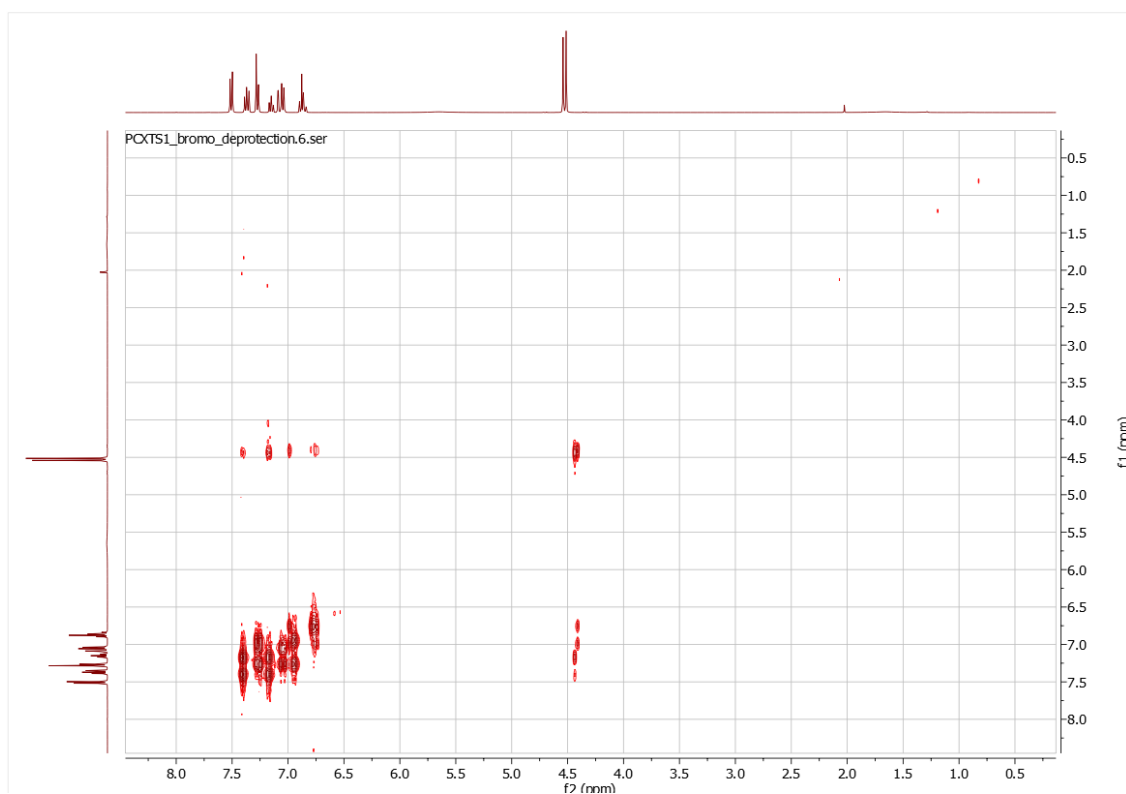


Figure 54: 2nd 2D COSY NMR Spectrum for 5-(((4-bromobenzyl)oxy)methyl)-2-phenoxyphenol **50**

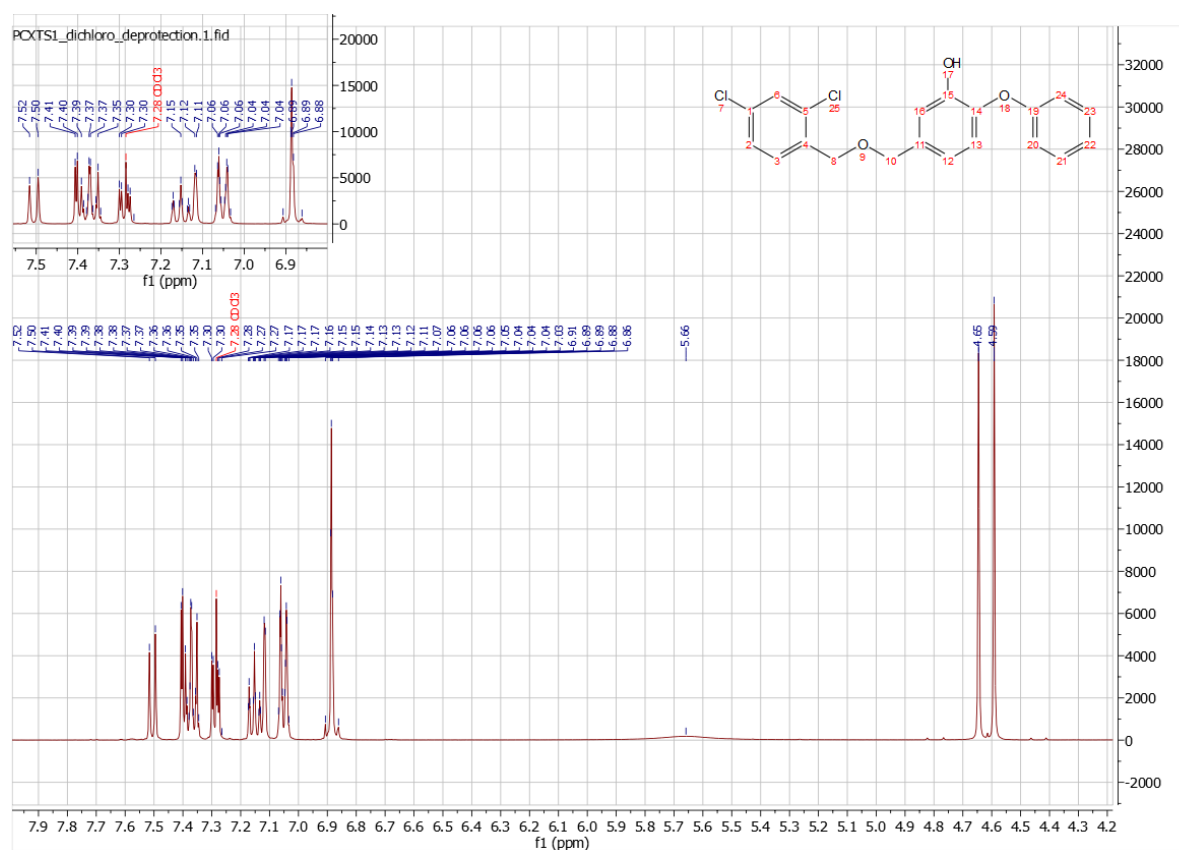


Figure 55: ¹H NMR Spectrum for 2,4-dichloro-1-(((3-(methoxymethoxy)-4-phenoxybenzyl)oxy)methyl)benzene **51**

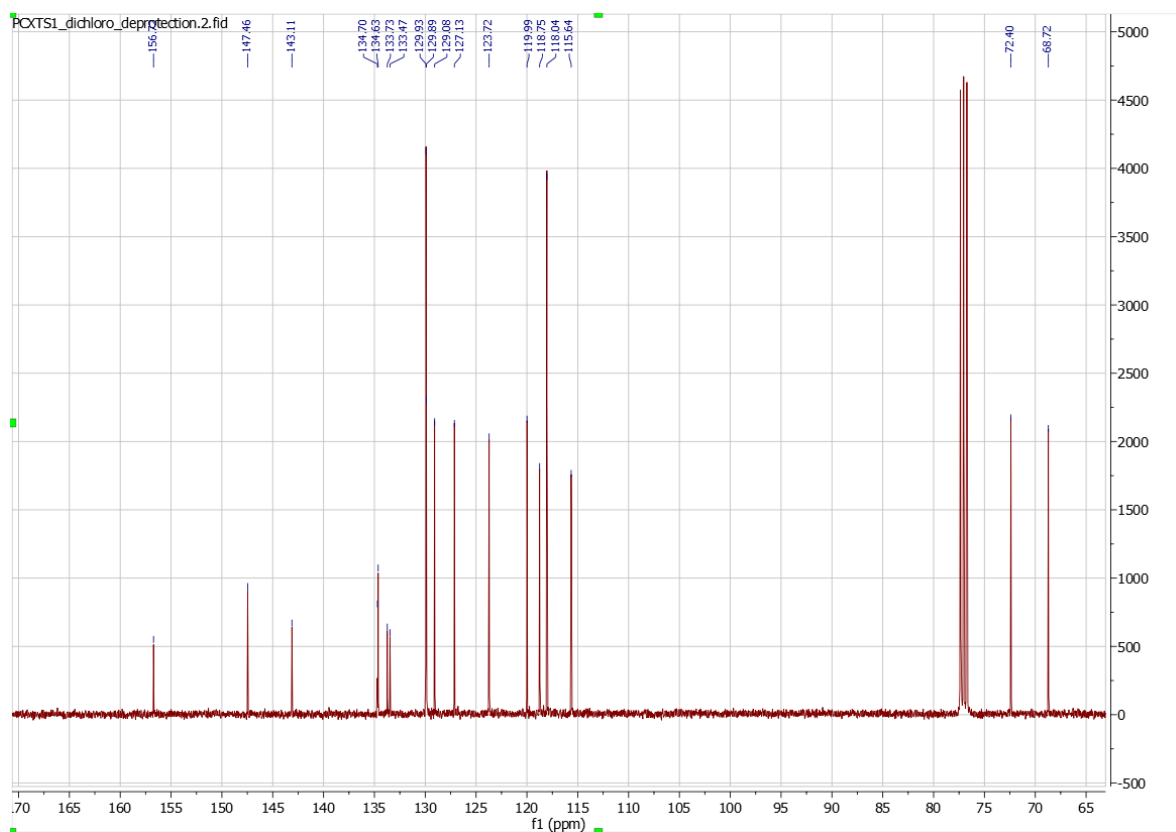


Figure 56: ^{13}C NMR Spectrum for 2,4-dichloro-1-(((3-(methoxymethoxy)-4-phenoxybenzyl)oxy)methyl)benzene **51**

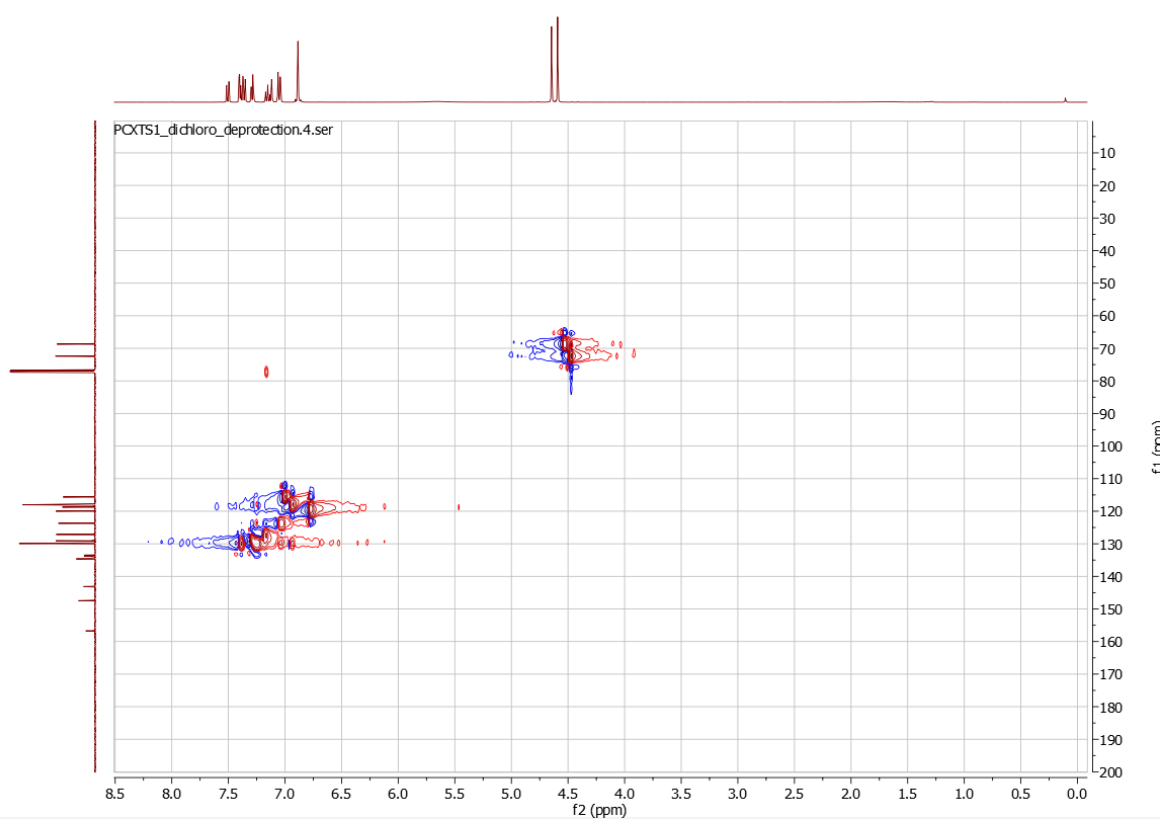


Figure 57: 2D COSY NMR Spectrum for 2,4-dichloro-1-(((3-(methoxymethoxy)-4-phenoxybenzyl)oxy)methyl)benzene **51**

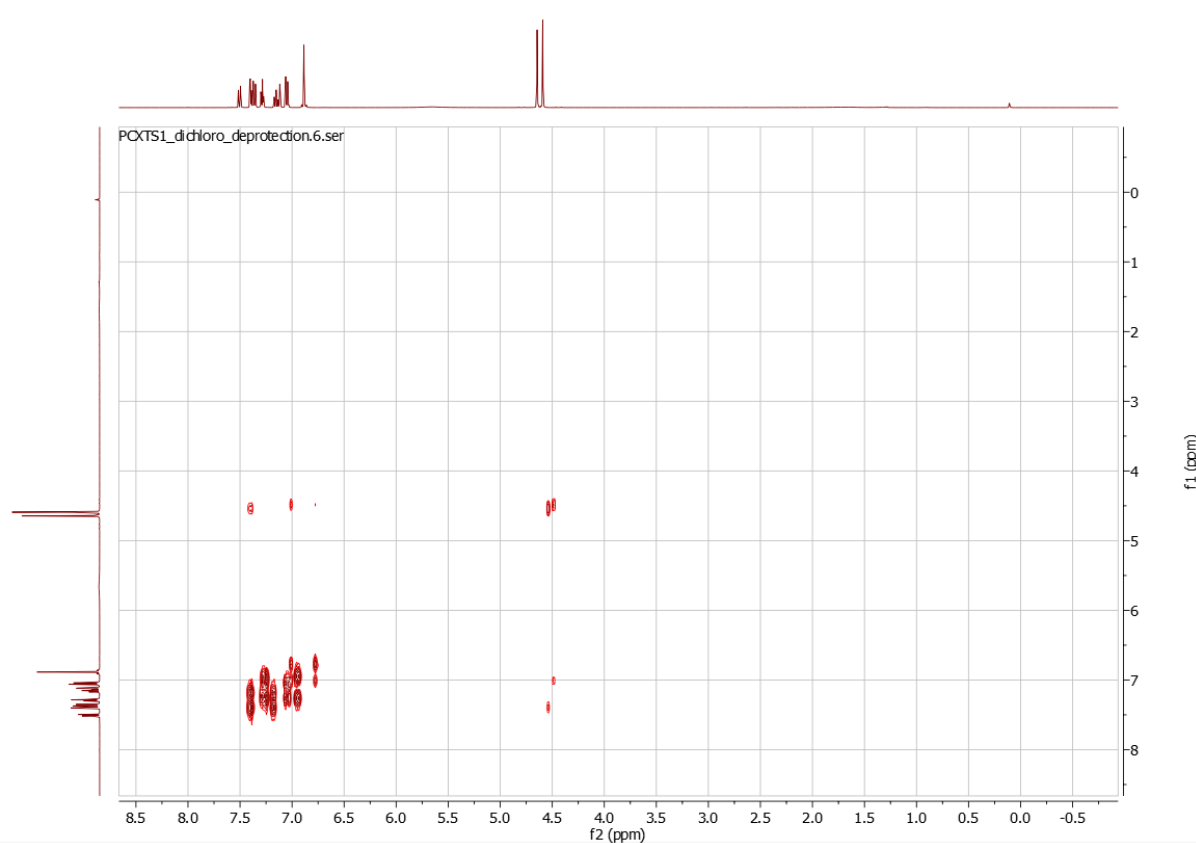


Figure 58: 2nd 2D COSY NMR Spectrum for 2,4-dichloro-1-(((3-(methoxymethoxy)-4-phenoxybenzyl)oxy)methyl)benzene **51**

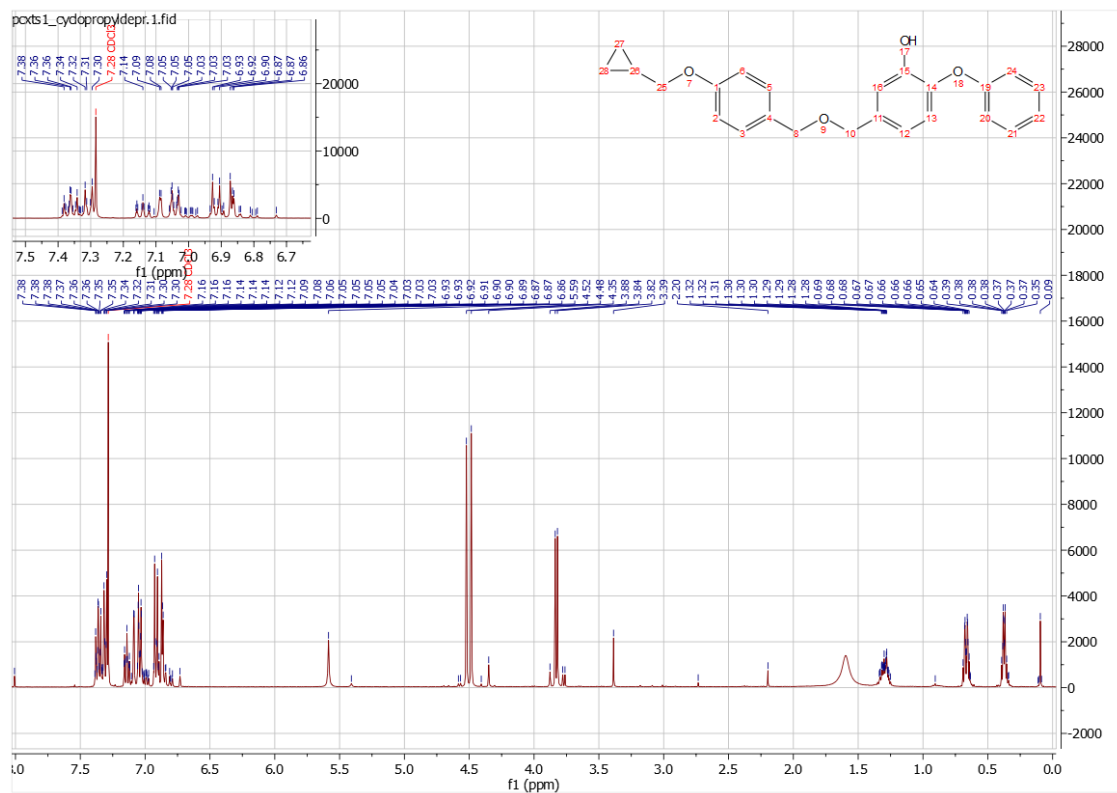


Figure 59: ¹H NMR Spectrum for 4-(((4-(cyclopropylmethoxy)benzyl)oxy)methyl)-2-(methoxymethoxy)-1-phenoxybenzene **52**

IR Data:

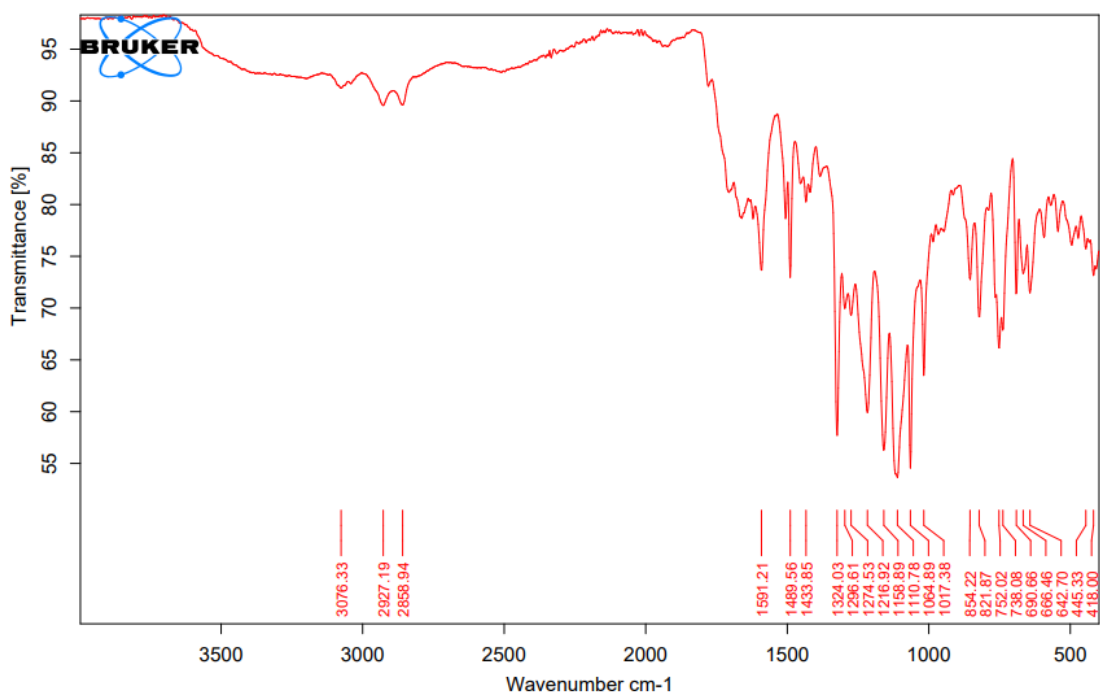


Figure 60: Infra-red Spectrum for 2-Phenoxy-5-(((4-(trifluoromethyl)benzyl)oxy)methyl)phenol **48**

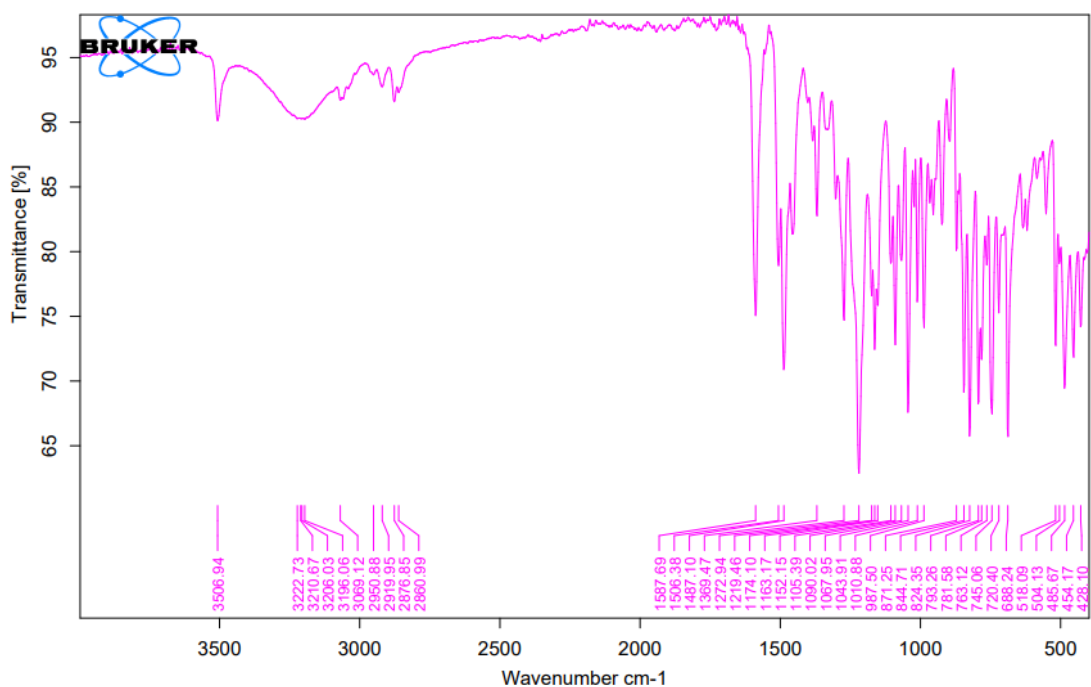


Figure 61: Infra-red Spectrum for 5-(((4-bromobenzyl)oxy)methyl)-2-phenoxyphenol **50**

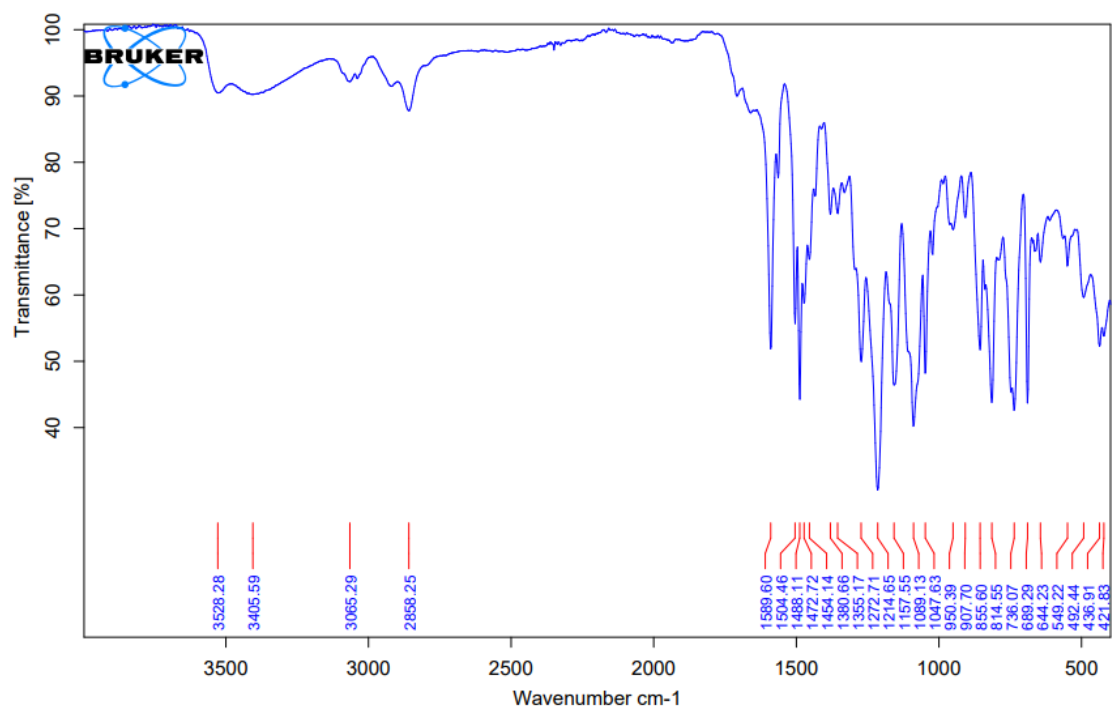


Figure 62: Infra-red Spectrum for 2,4-dichloro-1-(((3-(methoxymethoxy)-4-phenoxybenzyl)oxy)methyl)benzene **51**

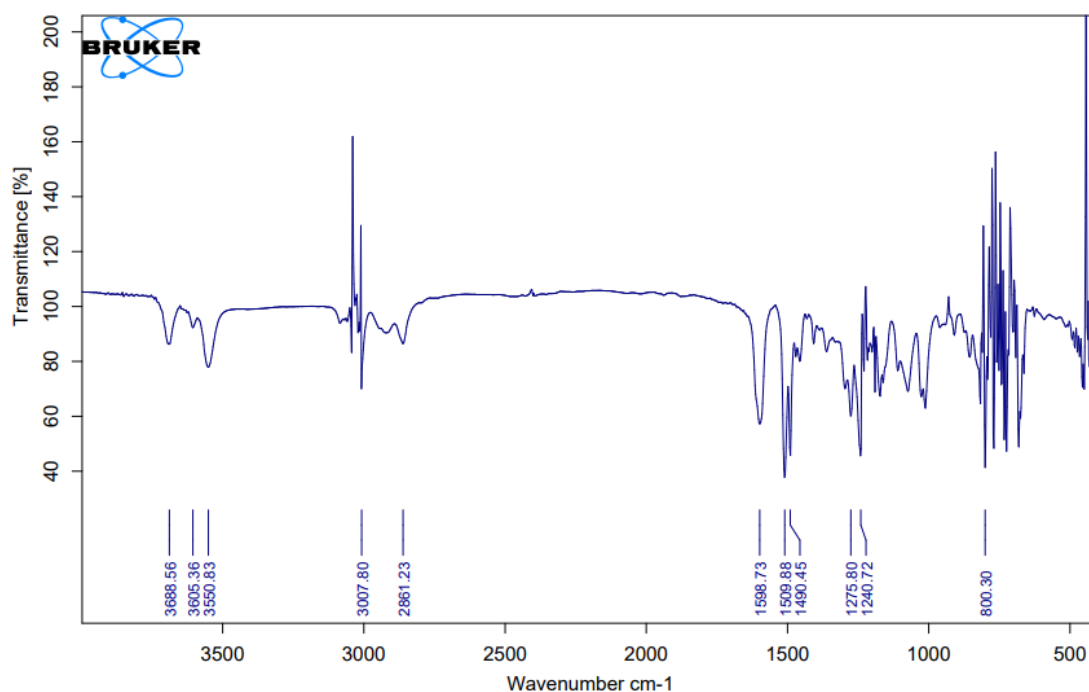


Figure 63: Infra-red Spectrum for 4-(((4-(cyclopropylmethoxy)benzyl)oxy)methyl)-2-(methoxymethoxy)-1-phenoxybenzene **52**